การจำลองการพังทลายของความลาดเอียงของมวลหิน
โดยใช้แบบจำลองทางกายภาพ

นายพงษ์ศักดิ์ แปงเพ็ชร

SIMULATION OF ROCK SLOPE FAILURE

USING PHYSICAL MODELS

Pongsak Pangpetch

A Thesis Submitted in Partial Fulfillment of the Requirements for the

Degree of Master of Engineering in Geotechnology

Suranaree University of Technology

Academic Year 2008

SIMULATION OF ROCK SLOPE FAILURE

USING PHYSICAL MODELS

Suranaree University of Technology has approved this thesis submitted in partial fulfillment of the requirements for a Master's Degree.

Thesis Examining Committee

_____

(Asst. Prof. Thara Lekuthai)

Chairperson

_____

(Assoc. Prof. Dr. Kittitep Fuenkajorn)

Member (Thesis Advisor)

_____

(Assoc. Prof. Ladda Wannakao)

Member

_____   _____

(Prof. Dr. Pairote Sattayatham)   (Assoc. Prof. Dr. Vorapot Khompis)

Vice Rector for Academic Affairs   Dean of Institute of Engineering

พงษ์ศักดิ์ แปงเพ็ชร : การจำลองการพังทลายของความลาดเอียงของมวลหินโดยใช้
แบบจำลองทางกายภาพ (SIMULATION OF ROCK SLOPE FAILURE USING
PHYSICAL MODELS) อาจารย์ที่ปรึกษา : รองศาสตราจารย์ ดร. กิตติเทพ เฟื่องขจร,
176 หน้า

วัตถุประสงค์ของงานวิจัยนี้คือเพื่อประดิษฐ์แท่นทดสอบสำหรับใช้ในการจำลองความลาด
เอียงของมวลหินที่ลดขนาดลงจากความเป็นจริงสำหรับทดสอบในห้องปฏิบัติการภายใต้การ
พังทลายแบบไหลเลื่อนตามแนวระนาบและแบบพลิกคว่ำ และเพื่อเปรียบเทียบผลจากการทดสอบ
กับผลจากการคำนวณด้วยวิธีเชิงทฤษฎี ข้อกำหนดสำหรับการออกแบบแท่นทดสอบคือ แท่นทดสอบ
ต้องสามารถจำลองการพังทลายของความลาดเอียงทั้งแบบไหลเลื่อนและแบบพลิกคว่ำภายใต้
สภาวะแห้งและจมน้ำ และสามารถใส่ผลกระทบของคลื่นไหวสะเทือน (ความเร่งเชิงสถิตจาก
ด้านข้าง) ต่อเสถียรภาพของความลาดเอียง งานวิจัยประกอบด้วย (1) การเลือกตัวอย่างของแท่งหิน
(2) การสร้างแท่นทดสอบ (3) การจำลองแบบจำลองความลาดเอียงที่ลดขนาดลงภายใต้แรงโน้ม
ถ่วงที่แท้จริง (4) การเปรียบเทียบผลของการทดสอบด้วยแบบจำลองกับผลจากการคำนวณด้วยวิธี
เชิงทฤษฎี (5) การประเมินผลกระทบเนื่องจากคลื่นไหวสะเทือน หินทรายหมวดหินภูพานจาก
จังหวัดนครราชสีมาได้ถูกนำมาใช้เป็นหินตัวอย่าง รูปแบบของความลาดเอียงของหินประกอบไป
ด้วย แท่งหินทรายรูปลูกบาศก์ (4×4×4 ซม.) และรูปสี่เหลี่ยมผืนผ้า (4×4×8 ซม. และ 4×4×12
ซม.) ภายใต้การผันแปรมุมของผิวหน้าและความสูงของความลาดเอียง ซึ่งความสูงของความลาด
เอียงสูงสุดคือ 1 ม. แท่งหินทรายถูกจัดเตรียมโดยการตัดด้วยเลื่อยเพื่อให้การจำลองความลาดเอียง
ของหินที่มีรอยแตกสองชุดที่ตั้งฉากกัน การทดสอบมีการผันแปรมุมของผิวหน้าของความลาด
เอียง มุมของระนาบที่ไหลเลื่อน ระดับน้ำ และอัตราเร่งของการสั่นสะเทือน

ความสามารถของการจำลองจะถูกพิสูจน์โดยการจำลองการพังทลายแบบไหลเลื่อนและ
พังทลายแบบพลิกคว่ำของความลาดเอียงของหิน ค่าปัจจัยความปลอดภัยสำหรับการทดสอบ
ความลาดเอียงถูกคำนวณโดยใช้วิธีเชิงทฤษฎีตามวิธีของ Hoek and Bray ผลจากการทดสอบกว่า
สองร้อยชุดแสดงให้เห็นว่าแท่นทดสอบสามารถทำการจำลองลักษณะการพังทลายได้เสมือนจริง
ค่าปัจจัยความปลอดภัยของการไหลเลื่อนตามแนวระนาบมีค่าสูงกว่าผลที่ได้จากการสังเกตการณ์
ประมาณร้อยละ 30 โดยเฉพาะอย่างยิ่งสำหรับความลาดเอียงที่มีมุมของการไหลเลื่อนต่ำและมีก้อนหิน
ขนาดเล็กบนความลาดเอียง การพังทลายแบบพลิกคว่ำสอดคล้องกับวิธีการเชิงทฤษฎีของ Hoek and
Bray เมื่อพิจารณาแรงเสียดทานระหว่างแท่งหินตัวอย่างด้วย

การพังทลายตามแนวระนาบของแบบจำลองความลาดเอียงของหินที่ลดขนาดลง ได้ถูกจำลองภายใต้แรงโน้มถ่วงที่แท้จริงและความเร่งเชิงสถิต ความเร่งเชิงสถิตในแนวราบมีค่าสูงสุดถึง 0.225 g และความสูงของคลื่นอยู่ระหว่าง 24-64 มม. มุมของการไหลเลื่อนจากการทดสอบภายใต้คลื่นไหวสะเทือนค่อนข้างต่ำกว่ามุมที่ได้จากการคำนวณ ความแตกต่างนี้จะเพิ่มขึ้นสำหรับความลาดเอียงที่มีตัวอย่างหินขนาดเล็กและอยู่ภายใต้ความเร่งที่สูงขึ้น ผลจากการจำลองด้วยแบบจำลองเชิงกายภาพภายใต้สภาวะแห้งและจมน้ำนั้นสอดคล้องกับการวิเคราะห์เชิงตัวเลขโดยใช้โปรแกรม FLAC โดยการทดสอบได้จำลองรอยแตกที่มีผิวเรียบ เปิดเผยอและมีค่าการยึดเกาะต่ำ ผลจากงานวิจัยนี้ระบุว่าการประเมินเสถียรภาพของความลาดเอียงของหินภายใต้แรงดันสถิตและคลื่นไหวสะเทือนโดยใช้วิธีเชิงทฤษฎีเพียงอย่างเดียวจะไม่เป็นไปในเชิงอนุรักษ์ โดยเฉพาะอย่างยิ่งมวลของความลาดเอียงที่ประกอบไปด้วยรอยแตกที่มีระยะห่างน้อย

PONGSAK PANGPETCH : SIMULATION OF ROCK SLOPE FAILURE

USING PHYSICAL MODELS. THESIS ADVISOR : ASSOC. PROF.

KITTITEP FUENKAJORN, Ph.D., PE., 176 PP.

ROCK SLOPE/SLIDING/TOPPLING/MODEL/SANDSTONE

The objectives of this research are to invent a test platform for use in the laboratory simulation of scaled-down rock slope models under plane sliding and toppling failures and to compare the observed results with those calculated by the deterministic methods. The design objectives for the test platform are that it must be capable of simulating sliding and toppling failures under both dry and submerged conditions, and should allow assessing the effects of dynamic load (lateral static acceleration) on the slope stability. The research effort mainly involves (1) collection of rock block samples, (2) construction of a test platform, (3) simulation of scaled-down slopes model under real gravitational force, (4) comparison of the test results with those from the deterministic method, and (5) assessing the effect of seismic loads. Phu Phan sandstone from Nakhon Ratchasima province has been selected for use as rock samples. Rock slopes are formed by cubical (4×4×4 cm) and rectangular (4×4×8 cm and 4×4×12 cm) blocks of sandstone, under various slope face angles with the maximum slope height up to 1 m. The sandstone blocks prepared by saw-cutting are arranged to simulate rock slopes with two mutually perpendicular joint sets. The test variables include slope face angle, sliding plane angle, water height, and horizontal pseudo-static accelerations.

The model capability is demonstrated by simulating two-dimensional plane sliding and toppling failures of rock slopes. Factors of safety for the tested slopes are calculated using the deterministic method given by Hoek and Bray. Results from over 200 tests suggest that the test platform can realistically simulate the modes of failure. The calculated factor of safety over-estimates the actual observations of plane sliding by as much as 30%, particularly for slopes with low angled sliding planes and comprising short blocks. The observed toppling failures agree well with those determined by Hoek and Bray solution when the friction between the rock blocks is considered in the calculation.

Plane failures of scaled-down rock slope models have been simulated under real gravitational force and pseudo-static accelerations of up to 0.225 g with amplitudes between 24 and 64 mm. The observed sliding angles under dynamic loading are considerably lower than those calculated by the deterministic method. The discrepancy becomes larger for slope models formed by shorter sandstone blocks and under a higher acceleration. The results from the physical model simulations under dry and submerged conditions agree well with those obtained from finite difference analyses using FLAC code. The findings imply that for the smooth, open and low-cohesion joints as simulated here, assessment of rock slope stability under static and dynamic loading by using the deterministic method alone may not be conservative, particularly for the slope mass comprising joints with small spacing.

School of Geotechnology   Student's Signature_____

Academic Year 2008   Advisor's Signature_____

ACKNOWLEDGMENTS

TABLE OF CONTENTS

<div align="right">**Page**</div>

TABLE OF CONTENTS (Continued)

TABLE OF CONTENTS (Continued)

LIST OF TABLE

LIST OF TABLE (Continued)

LIST OF FIGURES

LIST OF FIGURES (Continued)

LIST OF FIGURES (Continued)

LIST OF FIGURES (Continued)

LIST OF FIGURES (Continued)

LIST OF FIGURES (Continued)

LIST OF FIGURES (Continued)

Figure **Page**

LIST OF SYMBOLS AND ABBREVIATIONS

c	=	cohesive strength
ϕ	=	angle of friction
γ	=	unit weight of rock
γ_w	=	unit weight of water
A	=	area of face
H	=	slope height
W	=	weight of the sliding block
U	=	uplift water force
V	=	horizontal water force
Ψ_f	=	slope face angle
Ψ_p	=	sliding plane angle
Z_w	=	water depth
Z	=	tension crack depth
P_{n-1}	=	force preventing toppling of the nth block
P_n	=	force inducing toppling of the nth block
$P_{n,t}$	=	force resisting toppling of nth block
P_R	=	accumulate resisting force
W_n	=	weight of nth block
M_n	=	distance between block base and the point where P_n applies
L_n	=	distance between block base and the point where P_{n-1} apples

LIST OF SYMBOLS AND ABBREVIATIONS (Continued)

Δx	=	width of each block
y_n	=	height of the nth block
l_{ab}	=	the length of the failure plane
F_h	=	horizontal inertial forces which act through the centroid of the failure mass
F_v	=	vertical inertial forces which act through the centroid of the failure mass
a_h	=	horizontal pseudo-static accelerations
a_v	=	vertical pseudo-static accelerations
k_h	=	dimensionless horizontal pseudo-static coefficients
k_v	=	dimensionless vertical pseudo-static coefficients
g	=	gravitational acceleration
R	=	radius of wheel
y	=	length of crack arm
ω	=	angular velocity
T	=	duration of flywheel rotation
h	=	distance between base and top of slope model
ψ_{p0}	=	initial sliding plane angle
ψ_{f0}	=	initial slope face angle
α	=	angle of the back of slope model
t	=	thickness of rock

CHAPTER I

INTRODUCTION

1.1   Background of problems and significance of the study

Physical models or scaled-down models have long been used to simulate the failure behavior of rock slope in the laboratory. They have been used as teaching and research tools to reveal the two-dimensional failure process of rock slopes under various geological characteristics.   They are sometimes employed to gain an understanding of a unique failure process under site-specific conditions. Perhaps the most popular and widely used model is the Goodman's friction table (Goodman, 1976).   Bray and Goodman (1981) discuss the base friction principle that it is commonly used to reproduce the effects of gravity in two-dimensional physical models of excavations in rock. They develop mathematical principles upon which analogy between gravity and base friction can be examined. The friction table has been evolved into several versions. Cement mixed with sand, plaster or wooden blocks are commonly used to form the slope models.   Teme (1987) has used inclinable base-friction table as a tool in modeling of excavations. It is similar to that described by Goodman (1981), Hoek and Bray (1981), and Hittinger (1978). Teme's machine can however be inclined to simulate various dip angles in the field, and can test rigid and non-rigid model materials. Recently numerical analyses, primarily with distinct element and finite element methods, have been employed to simulate the plane sliding and toppling failures observed from the slope models (e.g. Kim and

Lee, 1992; Lanoro et al., 1997). Comparisons of the results from the computations and observations are made to verify the representative capability of the computer modeling and to improve an understanding of the actual behavior of rock slope failure.

The friction table poses some disadvantages. The driving force inducing sliding or failure is not from true gravitational force. Instead it largely depends on the friction and velocity of the moving belt, and hence additional calibration or correction is required to reveal the actual slope behavior. A stick-slip behavior between the belt and testing materials is common problem particularly under low speeds, making the driving force by belt moving unrealistic. In addition, since the friction table is in horizontal or gently inclined, assessment of the true effect of water can not be made.

1.2   Research objectives

The objectives of this research are to invent a test platform for use in the laboratory simulation of scaled-down rock slope models under plane sliding and toppling failures and to compare the observed results with those calculated by the deterministic methods. The main tasks involve fabrication of the test platform to meet the requirements, preparation of rock blocks for using in slope simulation, demonstration of the physical model performance, and calculation of the slope model stability using deterministic methods.

1.3   Research methodology

The research effort is divided into six tasks including the literature review, sample collection and preparation, construction of the physical model, physical model testing, comparisons, and thesis writing and presentation.

1.3.1   Literature review

Literature review has been carried out to study the rock slope failure from case studies in Thailand and abroad, rock slope failure criterion, and the results and factors of rock slope failure in particularly effects from earthquake vibration. The sources of information are from journals, technical reports and conference papers. A summary of the literature review will be given in the thesis.

1.3.2   Sample collection and preparation

Rock with uniform texture and properties will be selected for model testing. The block specimen dimensions primarily are 4×4×4 cm, 4×4×8 cm, and 4×4×12 cm. Up to about 1,000 blocks are prepared.

1.3.3   Construction of the physical model

The test platform for physical model test will be constructed in Geomechanical Laboratory in Suranaree University of Technology. The testing space (area) is about 1×1 m.

1.3.4   Physical model experiments

Plane sliding and toppling failure of slope models will be simulated for various slope heights and face angles. Video of the slope movement will be recorded for further analysis and comparisons.

1.3.5 Comparison

Results obtained from the simulations will be compared with the solutions from the deterministic methods and with the computer simulations.

1.3.6 Thesis writing and presentation

All research activities, methods, and results will be documented and compiled in the thesis. The contents or findings will be published in the conference, proceedings or journals.

1.4 Scope and limitations of the study

Scaled-down slope models are simulated in two dimensions. The slope models have a maximum height of up to 1.5 m under various slope angles. Failure of slope model is induced by the gravitational force. Continuous monitoring of the failure process will be made during the test. The effect of submerging condition will be studied. The effect of earthquake will be studied in the horizontal direction normal to strike of the slope model. One type of rock will be selected for this research. Both plane sliding and toppling failure will be simulated.

1.5 Thesis contents

Chapter I introduces the thesis by briefly describing the background of problems and significance of the study. The research objectives, methodology, scope and limitations are identified. Chapter II summarizes results of the literature review. Chapter III describes the design procedure for physical model. Chapter IV describes the results obtained from the laboratory testing. The experiments are divided into 3 tests, including 1) plane sliding and toppling failure tests under dry condition 2) plane sliding failure tests under submerged condition, and 3) plane sliding failure under

dynamic loading. Chapter V describes the results obtained from finite difference analysis. Chapter VI concludes the research results, and provides recommendations for future research studies.

CHAPTER II

LITERATURE REVIEW

2.1   Introduction

This chapter summarizes the results of literature review carried out to improve an understanding of simulation of rock slope failure using physical model. The topics reviewed here include the rock slope stability, effect of seismic loading, and previous studies on physical models.

2.2   Rock slope stability

Kamutchat (2004) described the problem of evaluating the stability of slopes in jointed and weathered rock masses which remains as a major challenge in the practice of rock engineering. The stability of structures depend on the strength and deformability of the rock masses. The rock masses are typically heterogeneous and anisotropic (unpredictable) because of the different rock types and properties. The most universally occurring anisotropic characteristic of all rock masses is the presence of distinct breaks, or discontinuities, in the physical continuity of the rock. These include bedding surfaces, joints, and faults, etc. The water can reduce rock strength from pervasive chemical weathering. The presence of discontinuities in rock mass is the primary controlling factor of rock mass strength and deformability. Discontinuities also have a dominant role in defining rock mass properties. The slope geometries have become important on stability evaluation. Hoek and Bray (1981) and

Goodman (1989) have classified the modes of slope failure into four types; plane and wedge sliding, toppling and circular failure.

A plane slide forms under gravity alone when a rock block tests on an incline weakness plane that "daylights" into free space. The inclination of the plane of slip must be greater than the friction angle of that plane. The conditions for failure reside dormantly in the slope until excavation or rock movement removes the barrier to block translation. Movement of a block supposes that the restraint to sliding has been overcome not only along the surface of sliding but along the lateral margins of the slide. In soft rocks, like shale, the side restraint can be released by rupture of the rock itself if the base of sliding is inclined considerably steeper than the friction angle. In hard rocks, plane sliding can occur only if there are other discontinuities or valleys transverse to the crest of the slope releasing the sides of the block (Hoek and Bray, 1981).

Wedge slides can occur when two planes of weakness intersect to define a tetrahedral block. Slip can occur without any topographic or structural release features if the line of intersection of two discontinuities daylights into the excavation.

Toppling failure involves overturning of rock layers like a series of cantilever beams in slates, schists, and thin-bedded sediments inclined steeply into the hillside. Each layer tending to bend downhill under its own weight transfers force downslope. If the toe of the slope is allowed to slide or overturn, flexural cracks will form in the layers above, liberating a large mass of rock. If there are frequent cross-joints, the layers can overturn as rigid columns rather than having to fail in flexure. In either event, destructive slope movements must be prefaced by interlayer slip of a normal faults type.

For a circular failure, rock body is divided into a discontinuous mass. The failure path is normally defined by one or more discontinuity. In case of soil slope, the individual particles are very small compared with the size of the slope, and a strongly defined structural no longer existed. Then the failure paths are in the circular form.

Using the shear strength parameters c and ϕ, the factor of safety of plane sliding given by the total force resisting sliding to the total force tending to induce sliding, is (Hoek and Bray, 1981)

$$FS = \frac{cA + (W \cos \psi_p - U - V \sin \psi_p) Tan\phi}{W \sin \psi_p + V \cos \psi_p} \qquad (2.1)$$

where

$$A = (H - Z) \cos ec\psi_p \qquad (2.2)$$

$$U = \frac{1}{2} \gamma_w Z_w (H - Z) \cos ec\psi_p \qquad (2.3)$$

$$V = \frac{1}{2} \gamma_w Z_w^2 \qquad (2.4)$$

for tension crack in the upper slope surface

$$W = \frac{1}{2} \gamma H^2 \left[\left(1 - (Z/H)^2 \right) \cot \psi_p - \cot \psi_f \right] \qquad (2.5)$$

and, for the tension crack in the slope face

$$W = \frac{1}{2}\gamma H^2 \left[(1 - Z/H)^2 \cot \psi_p (\cot \psi_p \tan \psi_f - 1)\right] \tag{2.6}$$

where c is cohesive strength, ϕ is angle of friction, γ is unit weight of rock, γ_w is unit weight of water, A is area of face, H is slope height, W is weight of the sliding block, U is uplift water force, V is horizontal water force, Ψ_f is slope face angle, Ψ_p is sliding plane angle, Z_w is water depth, and Z is tension crack depth.

When the tension crack is not vertical the above equations cannot be used and it is often easier to determine A, W, Z, and Z_w using a scale drawing on graph paper.

When the geometry of the slope and the depth of water in the tension crack are known, the calculation of a factor of safety is straightforward. In some cases, however, it may be necessary to compare a range of slope geometries, water depths and the influence of different shear strengths. In such cases a spreadsheet may be used to carry out the analysis and create graphs showing the sensitivity of the factor of safety to these changes (Simons et al., 2000).

A procedure for the toppling and sliding of a regular system of blocks has been proposed by Goodman and Bray (1976). Giani (1992) explained the purpose of the analysis is to assess the limit equilibrium condition of overall blocky system and to determine external forces, such as a cable force, required to stabilize the slope made up by the blocky system. The procedure considers the equilibrium of the forces of each block starting from the uppermost block and determining the interaction force with the adjacent block down to the slope toe. When the lower force obtained on the toe block is positive (downward directed) the slope is unstable, when it is zero, the limiting equilibrium condition is reached.

Limit equilibrium analysis of toppling on a stepped base proposed by Hoek and Bray (1981) can be written as:

$$P_{n-1} = \frac{P_n (M_n - \Delta x \tan \phi) + (W_n / 2)(y_n \sin \alpha - \Delta x \cos \alpha)}{L_n} \qquad (2.7)$$

where P_{n-1} is force preventing toppling of the nth block, P_n is force inducing toppling of the nth block, W_n is weight of nth block, M_n is distance between block base and the point where P_n applies, L_n is distance between block base and the point where P_{n-1} apples, Δx is width of each block, y_n is height of the nth block, and α is plane angle.

Giani (1992) states that since the geometry of the blocky system and the friction angle of the block sides and bases are known (or assumed to be known) the equilibrium of each block can be solved by establishing if the toppling or the sliding mode is critical. The method is suitable for only particular geometries of the blocky system, which consider the system rigid and use the statical equilibrium equations.

2.3   Effect of seismic load

The previously described procedures for static slope stability analysis have been used for many years and calibrated against many actual slope failures. The database against which seismic slope stability analyses can be calibrated is much smaller. Kramer (1996) explained the analysis of the seismic stability of slopes is further complicated by the need to consider the effects of (1) dynamic stresses induced by earthquake shaking, and (2) the effects of those stresses on the strength and stress-strain behavior of the slope materials.

Siad (2003) considered gravity and inertial forces developed in the rock mass by the passage of seismic waves are the external forces. The rock mass is crossed by two sets of fractures which are considered to be planar and persistent. The stability factor is very sensitive to variations of horizontal seismic coefficient. It is reduced due to seismic effect. However, the value flattens as friction angle of fracture increases.

Sepulveda et al. (2005) conducted field investigations and slope stability back analyses to confirm the impact of topographic amplification on the triggering of landslides during the 1994 earthquake. Their results suggest that the observed extensive rock sliding and falling would have not been possible under unamplified seismic conditions, which would have generated a significantly lower number of areas affected by landslides. In contrast, modeling slope stability using amplified ground shaking predicts slope failure distributions matching what occurred in 1994. This observation confirms a significant role for topographic amplification on the triggering of landslides at the site and emphasizes the need to select carefully the inputs for seismic slope stability analyses.

Beginning in the 1920s, the seismic stability of earth structures has been analyzed by a pseudostatic approach in which the effects of an earthquake are represented by constant horizontal and/or vertical accelerations (Kramer, 1996). The first explicit application of the pseudostatic approach to the analysis of seismic slope stability has been attributed to Terzaghi (1950). Giani (1992) discussed that a pseudostatic analysis can be carried out by using the limit equilibrium method and by schematizing the dynamic loading occurrence with a time constant force which is proportional to the mass of the potentially unstable volume of rock, according to the seismic coefficient.

Kramer (1996) states that the magnitudes of the pseudostatic acceleration should be related to the severity of the anticipated ground motion as selection of pseudostatic accelerations for design is not a simple matter. The horizontal pseudostatic force clearly decreases the factor of safety. It reduces the resisting force (forϕ>0) and increases the driving force. The vertical pseudostatic force typically has less influence on the factor of safety since it reduces (or increases, depending on its direction) both the driving force and the resisting force. As a result, the effects of vertical accelerations are frequently neglected in pseudostatic analyses resolving the forces on the potential failure mass in a direction parallel to the failure surface,

$$FS = \frac{\text{resisting force}}{\text{driving force}} = \frac{cl_{ab} + \left[(W - F_v)\cos\beta - F_h \sin\beta\right]\tan\phi}{(W - F_v)\sin\beta + F_h \cos\beta} \qquad (2.8)$$

where c and ϕ are the Mohr-Coulomb strength parameters that describe the shear strength on the failure plane, l_{ab} is the length of the failure plane, W is the weight of the failure mass, and F_h and F_v are the horizontal and vertical inertial forces which act through the centroid of the failure mass. The magnitudes of the pseudostatic forces are

$$F_h = \frac{a_h W}{g} = k_h W \qquad (2.9)$$

$$F_v = \frac{a_v W}{g} = k_v W \qquad (2.10)$$

where a_h and a_v are horizontal and vertical pseudostatic accelerations, k_h and k_v are dimensionless horizontal and vertical pseudostatic coefficients. Pseudostatic analyses

can be unreliable for soils that build up large pore pressures or show more than about 15% degradation of strength due to earthquake shaking. The pseudostatic approach can be used to evaluate pseudostatic factors of safety for planar, circular, and noncircular failure surfaces. Many commercially available computer programs for limit equilibrium slope stability analysis have the option of performing pseudostatic analyses.

Kramer (1996) described that earthquake magnitude is a quantitative measure of the size of an earthquake. Most magnitude scales are based on measured ground motion characteristics. The common magnitudes are shown in Table 2.1.

The example of earthquake magnitude such as: Both the 1906 San Francisco and 1960 Chile earthquakes produced ground shaking that led to surface wave magnitudes (M_s) of 8.3, however, reflected in the moment magnitudes (M_w) of the earthquake as 7.9 for San Francisco and 9.5 for Chile (Kramer, 1996). The 1994 Northridge earthquake ($M_w = 6.7$) triggered extensive rock slope failures in Pacoima Canyon, immediately north of Los Angeles, California (Sepulveda et al., 2005). The 1995 Nuweiba earthquake measured ML = 6.2 on the local magnitude scale based on coda duration and Mw = 7.2 on the moment magnitude scale. The overall distribution of 177 aftershocks of the Nuweiba earthquake in the magnitude range $3.5 \leq Mw \leq 7.2$ (Shamir, et al., 2003). The 1995, October 1, Dinar, Turkey, earthquake (Ms = 6.1) determined from inversion of teleseismic P and SH waveforms (Utkucu et al., 2002). The large magnitude (Mw = 7.7) Bhuj earthquake which occurred on January 26th, 2001, within the Kachch peninsula in Gujarat (Sarkar and Chander, 2003).

Table 2.1 Magnitudes commonly used by seismic networks (USGS, 2008).

Magnitude type	Applicable magnitude range	Distance range	Comments
Duration (M_d)	<4	0-400 km	Based on the duration of shaking as measured by the time decay of the amplitude of the seismogram. Often used to compute magnitude from seismograms with "clipped" waveforms due to limited dynamic recording range of analog instrumentation, which makes it impossible to measure peak amplitudes.
Local (ML)	2-6	0-400 km	The original magnitude relationship defined by Richter and Gutenberg for local earthquakes in 1935. It is based on the maximum amplitude of a seismogram recorded on a Wood-Anderson torsion seismograph. Although these instruments are no longer widely in use, ML values are calculated using modern instrumentation with appropriate adjustments.
Surface wave (M_s)	5-8	20-180 degrees	A magnitude for distant earthquakes based on the amplitude of Rayleigh surface waves measured at a period near 20 sec.
Moment (M_w)	>3.5	all	Based on the moment of the earthquake, which is equal to the rigidity of the earth times the average amount of slip on the fault times the amount of fault area that slipped.
Energy (M_e)	>3.5	all	Based on the amount of recorded seismic energy radiated by the earthquake.
Moment (M_i)	5-8	all	Based on the integral of the first few seconds of P wave on broadband instruments (Tsuboi method).

Table 2.1 Magnitudes commonly used by seismic networks (USGS, 2008). (Cont.)

Magnitude type	Applicable magnitude range	Distance range	Comments
Body (M_b)	4-7	16-100 degrees (only deep earthquakes)	Based on the amplitude of P body-waves. This scale is most appropriate for deep-focus earthquakes.
Surface wave (ML_g)	5-8	all	A magnitude for distant earthquakes based on the amplitude of the Lg surface waves.

Hatzor et al. (2004) analyzed dynamic stability of jointed rock slopes using the DDA method. Comparison of predicted damage with actual slope performance over a historic time span of 2000 years allows they concluded that introduction of 2% kinetic damping should suffice for realistic damage predictions. The peak horizontal ground acceleration (PGA) for DDA computation varied from 0.06g to 0.2g. The acceleration levels of 1g blocks at upper row in terrace may be expected to lift in the air for very short time spans when the scaled accelerations attain a level of 1g. It should be noted that the frequency content was not altered in the scaled records as all acceleration components were multiplied by a scalar only. It is not possible to check the validity of this result of DDA. The effect of bolting is apparent with the dense bolting pattern the terrace remains virtually intact after 10s of shaking with PGA = 0.6g.

Maugeri et al. (2000) tested the failure of a shallow foundation subjected to an eccentric load by shaking table. To achieve the experimental critical acceleration k_h (horizontal acceleration coefficients) of foundation-soil system, the test was performed by means of different shakes during which the peak acceleration of the sine dwell motion was gradually increased up from ±0.10 to ±0.35g.

The example of horizontal ground acceleration such as the Dead Sea valley and Mount Masada bedrock have been classified as a region in which earthquake-induced peak horizontal ground acceleration (PGA) exceeding 0.2g. Two thousand years ago the Masada cliff top was marked by construction. The mountain was later shaken by several major earthquakes, with deep bedrock accelerations certainly exceeding 0.1g and probably even exceeding 0.2g (Hatzor et al., 2004).

For historical earthquakes with no seismograph records, seismologists can estimate the intensity of ground motion from the Mercalli scale (Table 2.2), using the

information as a kind of crude seismograph. If intensity information is available for enough different places, a rough estimate of the earthquake magnitude can be made (Gendzwill, 2008).

2.4   Previous physical models

Crawford and Curran (1982) investigated the potential practical importance of rate- and displacement- dependent frictional resistance of discontinuities on the stability of rock structure with the aid of a rigid sliding block slope stability model. Constitutive relationships for rate-dependent frictional resistance, based on experimental observations, have been utilized. It is shown that the existence of a rate effect may be an important consideration in the design structures in jointed rock masses.

The kinematics of a model restrained so that friction at its base from the moving belt creates a gravity effect, are described by Goodman (1976). The base friction principle is used widely to reproduce the effects of gravity in two-dimensional physical models of excavation in rock. The body force of gravity is simulated by the drag of a belt moving along the underside of the model. They developed the mathematical principles upon which analogy between gravity and base friction can be examined. It is shown that equations of motion in the realm of the model are obtainable from those of the real world by replacing any linear or angular acceleration term by corresponding linear or angular velocity term. For limiting equilibrium analysis,   in   which   motion   incipient,   the   analogy   is   flawless.

Table 2.2 The intensity of ground motion is estimated from the Mercalli scale (Adapted from Richter, 1958 and Wald et al., 1999).

Modified Mercalli Intensity	Acceleration (g)	Description of Intensity Level
I	<0.0017	Not felt except by a very few under especially favorable circumstances.
II	0.0017	Felt only by a few persons at rest, especially on upper floors of buildings. Delicately suspended objects may swing.
III	0.014	Felt quite noticeably by persons indoors, especially on upper floors of buildings. Many people do not recognize it as an earthquake. Standing motor cars may rock slightly. Vibration similar to the passing of a truck. Duration estimated.
IV	0.014 – 0.039	Felt indoors by many, outdoors by few during the day. At night, some awakened. Dishes, windows, doors disturbed; walls make cracking sound. Sensation like heavy truck striking building. Standing motor cars rocked noticeably.
V	0.039 – 0.092	Felt by nearly everyone; many awakened. Some dishes, windows broken. Unstable objects overturned. Pendulum clocks may stop.
VI	0.092 – 0.18	Felt by all; many frightened. Some heavy furniture moved; a few instances of fallen plaster. Damage slight.
VII	0.18 – 0.34	Damage negligible in building of good design and construction; slight to moderate in well-built ordinary structures; considerable damage in poorly built or badly designed structures; some chimneys broken. Noticed by persons driving motorcars.
VIII	0.34 – 0.65	Damage slight in specially designed structures; considerable in ordinary substantial buildings with partial collapse. Damage great in poorly built structures. Fall of chimneys, factory stacks, columns, monuments, walls. Heavy furniture overturned.
IX	0.65 – 1.24	Damage considerable in specially designed structures; well-designed frame structures thrown out of plumb. Damage great in substantial buildings, with partial collapse. Buildings shifted off foundations.
X	> 1.24	Some well-built wooden structures destroyed; most masonry and frame structures destroyed with foundations. Rails bent.
XI	> 1.24	Few, if any (masonry) structures remain standing. Bridges destroyed. Rails bent greatly.
XII	> 1.24	Damage total. Lines of sight and level distorted. Objects thrown into the air.

Teme (1987) has used inclinable base-friction table as a tool in modeling of excavation (Figure 2.1). He found that the advantages of the inclinable base-friction table include (1) it has the ability to used rigid and/or non-rigid model materials, (2) it is suitable for both teaching and research, (3) strict adherence to the recommended testing methodology will provide reproducible results, (4) the design of the machine is simple enough to be easily reproduced, and (5) it is relatively inexpensive to construct. However, limitations of the machine include (1) there is a stick-slip and wobbling of the friction belt especially when high gear ratios are used to drive the belt system and (2) there is a limit to the weight and volume of model materials that can be carried by the inclinable base plate of the machine during routine testing.

Kokusho and Ishizawa (2005) studied the energy approach for earthquake induced slope failure evaluation by used shaking table. They proposed that the earthquake energy used for the slope failure can be successfully quantified in the test and its contribution to displacement is discussed in the light of the energy balance established for the block model.

Recently numerical analyses, primarily with distinct element methods, have been employed to simulate the plane sliding and toppling failures observed from the slope models. Lanaro et al. (1997) used the Distinct Element Method (D.E.M) modeling to studied block toppling (Figures 2.2 and 2.3). The model consisted of an arrangement of blocks of artificial material which toppled when its base was tilted. The model geometry, block interfaces, material properties and dynamic loading sequence influence the numerical results. The friction angle, rotation velocity and the sharpness of block corners, which are the principal factors governing the model response,
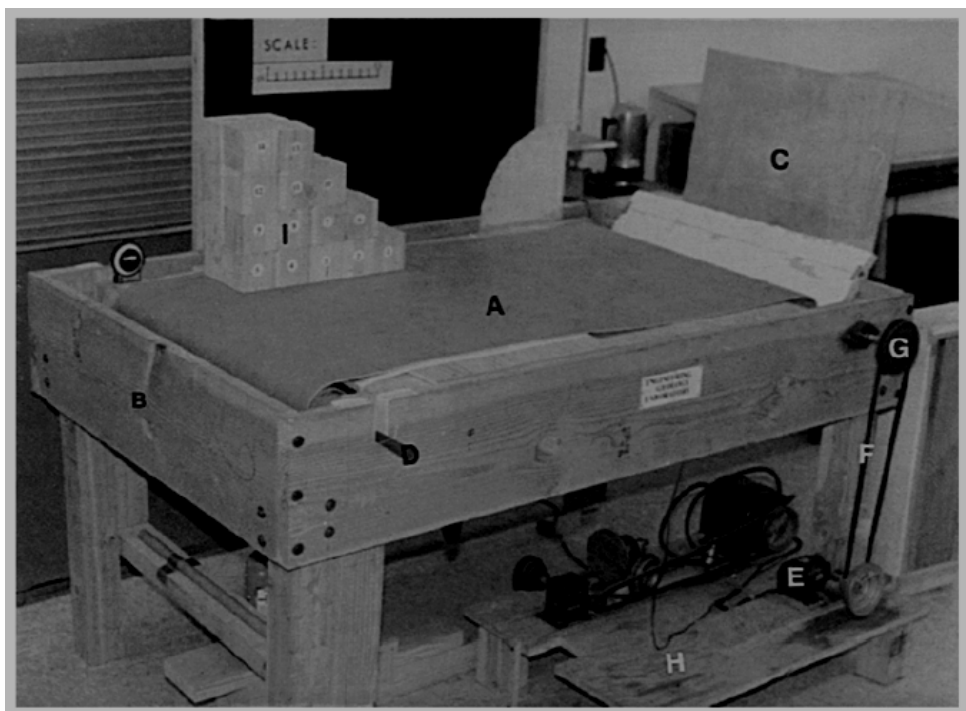
Figure 2.1 General view of the modelling machine. (A) Friction belt. (B) Main supporting frame. (C) Blocking system. (D) Rear axle. (E) Motor. (F) V-belt. (G) Pulleys. (H) Motor support frame. (I) Model block. (Teme, 1987).
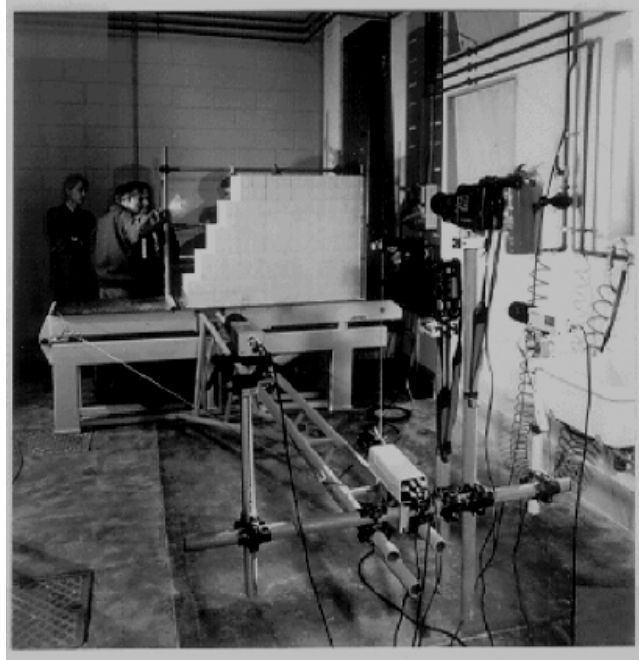
Figure 2.2 A view of the tilt table and the video recording sets (Lanaro, 1997).
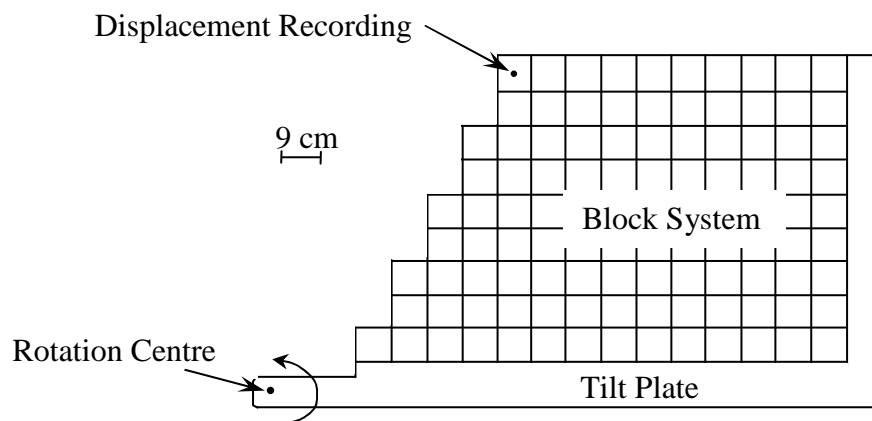
Figure 2.3 Geometry of the model and location of the monitoring point (Lanaro, 1997).

have been investigated. They studied a valuable validation test of the Distinct Element Method against experimental results.

Li et al. (2007) analyzed critical excavation depth for a jointed rock slope using a Face-to-Face Discrete Element Method (DEM). The DEM is based on the discontinuity analysis which can consider anisotropic and discontinuous deformations due to joints and their orientations. They compared the effect of joints on the failure modes between DEM simulations and experimental observations. It is found that the DEM predicts a lower critical excavation depth than the LEM (limit equilibrium method) of the joint structures in the rock mass are not ignored.

Bhasin and Kaynia (2004) studied the static and dynamic rock simulation of a 700 m high rock slope in western Norway. They used numerical modeling to estimate the volume of the rock mass that could potentially slide under static and dynamic forces. This estimation was required to assess the run-up heights (tsunami) in a fjord that could potentially be caused by the rock slide. The results indicate that, due to variations in the inclination of discontinuities, the entire slope does not become unstable and that down-slope sliding and rotation of blocks occur mainly on the top layers of the slope. This model has helped not only to better understand the dynamics of the rock slide but also to estimate the potential rock volume that can become unstable when subjected to static and dynamic loads.

CHAPTER III

TEST PLATFORM

3.1   Introduction

A physical test platform has been built for use in the simulation of failure of scaled-down rock slopes under real gravitational force. This chapter describes the design requirements and components of the test platform, calculation of the horizontal pseudo-static accelerations, and calculation of slope height at failure.

3.2   Design requirements and components

The functional requirements for the test platform are (1) to test slope models with a maximum height of up to 1.5 m under varied slope face angles, (2) to induce failure of slope model using real gravitational force, (3) to allow continuous monitoring of the failure process during testing, (4) to assess the effect of submerging condition on the slope failure, and (5) to allow incorporating the effect of earthquake on the stability condition.

To meet these requirements the test platform comprises two main components: a 2.2×2.2 m test frame supported by a movable stand. The frame is hinged through steel rods in the middle to the stand (Figure 3.1 and 3.2) allowing frame rotation from horizontal position (during arranging and loading block samples) to vertical position (for testing under true gravitational force). The frame is made of four 5-cm wide C-shaped steel bars at each side linked with a steel plate at each corner.
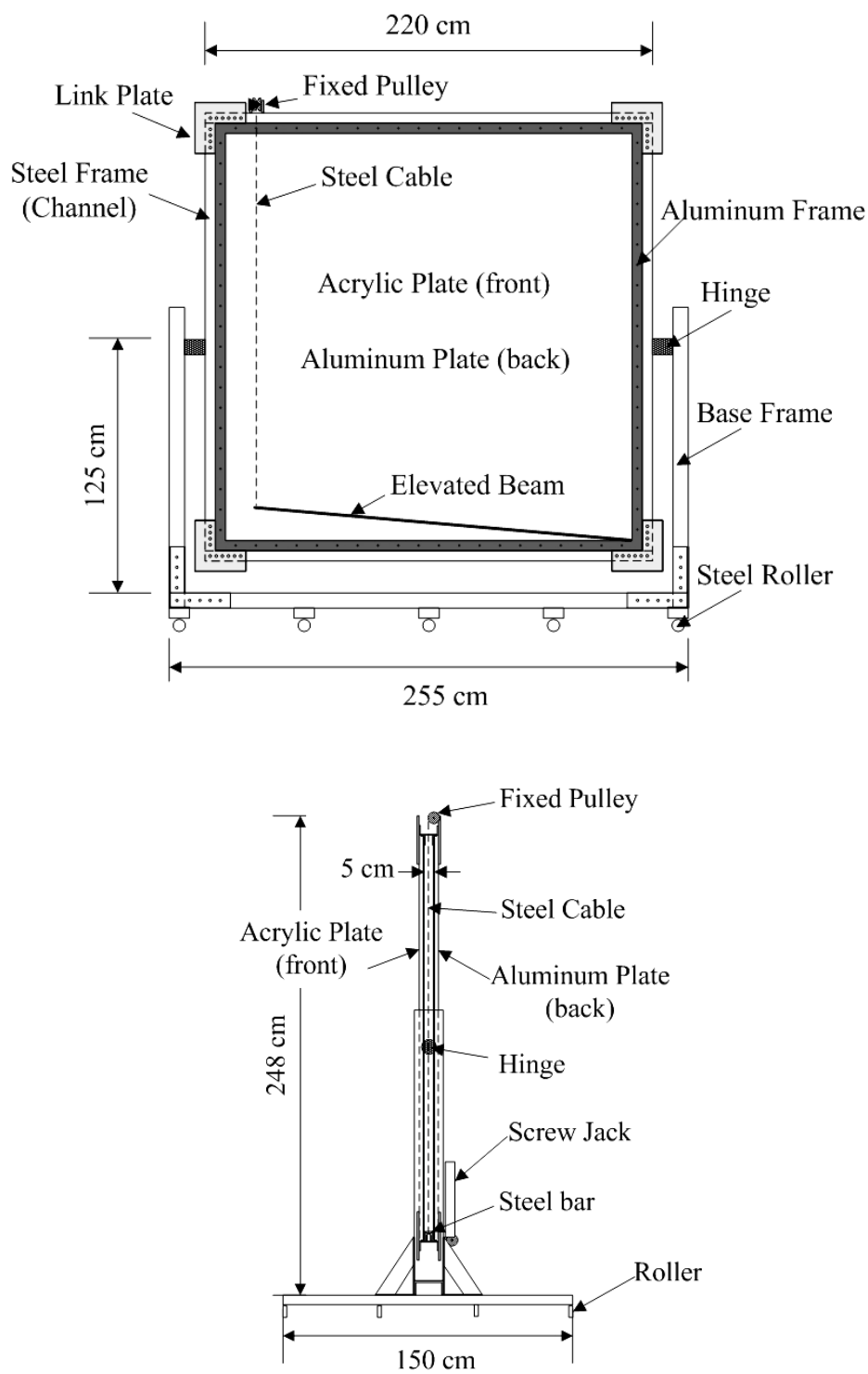
Figure 3.1 Schematic drawing of test platform for physical model.

220 cm

Fixed Pulley

Aluminum Frame

Link Plate

Steel Cable

Motor

Acrylic Sheet (front)

Steel Frame
(Channel)

Aluminum Plate (Black)

Hinge

Tilting Beam

Roller

255 cm
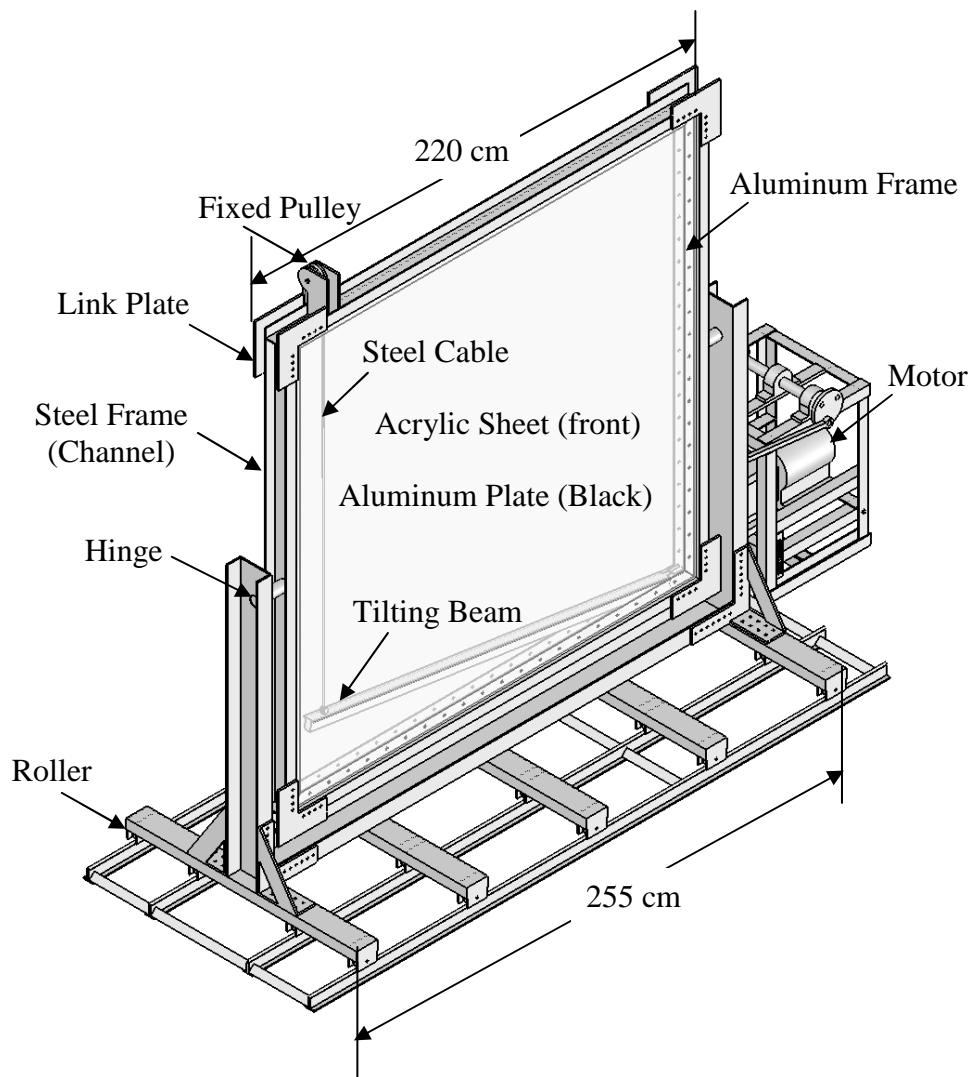
Figure 3.2 Perspective view of schematic drawing of test platform for physical

model tests.

A custom-made 2×2 m clear acrylic sheet with 10 mm thick is placed in the front of the frame, while an aluminum plate with the same size is in the back. The spacing between the acrylic sheet and the steel plate is 5 cm. All gaps and connections are water-tight. They are sealed with quick-dried silicone gel. When the frame is in horizontal position, the aluminum plate becomes a flat bed supporting the rock blocks during loading. The clear and removable acrylic sheet is installed before rotating the frame to the upright position to prevent the block samples from tipping over. It also allows visual inspection and monitoring of slope movement during the test. The test frame can accommodate 4 cm thick rock blocks arranged with a maximum height up to 1.5 m. A minimum clearance of 0.5 cm is maintained between the front acrylic sheet and rock blocks and between the rear aluminum plate and the rock to ensure that no friction is induced at these interfaces (equivalent to the release surface assumption used in Hoek and Bray solution)

Steel grooved rollers mounted underneath the stand are used for testing under dynamic loading. The rollers will be placed on a set of steel rails equipped with a high torque motor and piston to induce a cyclic motion of the entire test platform. The lateral static acceleration can be created and controlled by adjusting the frequencies and amplitudes of the piston and speed of the motor. Note that the rails and dynamic components are being built, and hence not included in the Figure.

During the test a screw jack connecting with steel cable placing on a pulley lifts one end of a steel beam pre-installed underneath and along the slope model. Since the beam is securely hinged at the bottom near the slope toe, the entire slope model can be slowly tilted sideway toward the slope face, and eventually inducing

failure. Figure 3.3 shows the test platform with block samples loaded inside the test frame.

Figure 3.4 shows the crank arm components used to generate the horizontal acceleration to the test frame. The acceleration at point B, represented by a, can be calculated using a set of equations given by Riley & Sturges (1993).

$$a = R\omega_{OA}^2 \cos\theta + y\omega_{AB}^2 \cos\phi - y\alpha_{AB} \sin\phi \qquad (3.1)$$

where R = radius of wheel, y = length of crack arm, ω_{OA} and ω_{AB} = angular velocity of OA and AB, θ = angle between AO and OB, α_{AB} = relationship between the acceleration of points A and B, and T = duration of flywheel rotation. The angle ϕ can be obtained from:

$$\phi = \sin^{-1}\left[\frac{R\sin\theta}{y}\right] \qquad (3.2)$$

The angular velocity of OA and AB can be calculated by:

$$\omega_{OA} = \frac{2\pi}{T}; \quad \omega_{AB} = \frac{R\omega_{OA} \cos\theta}{y\cos\phi} \qquad (3.3)$$

The relationship between point A and B, and α_{AB}, is calculated by:
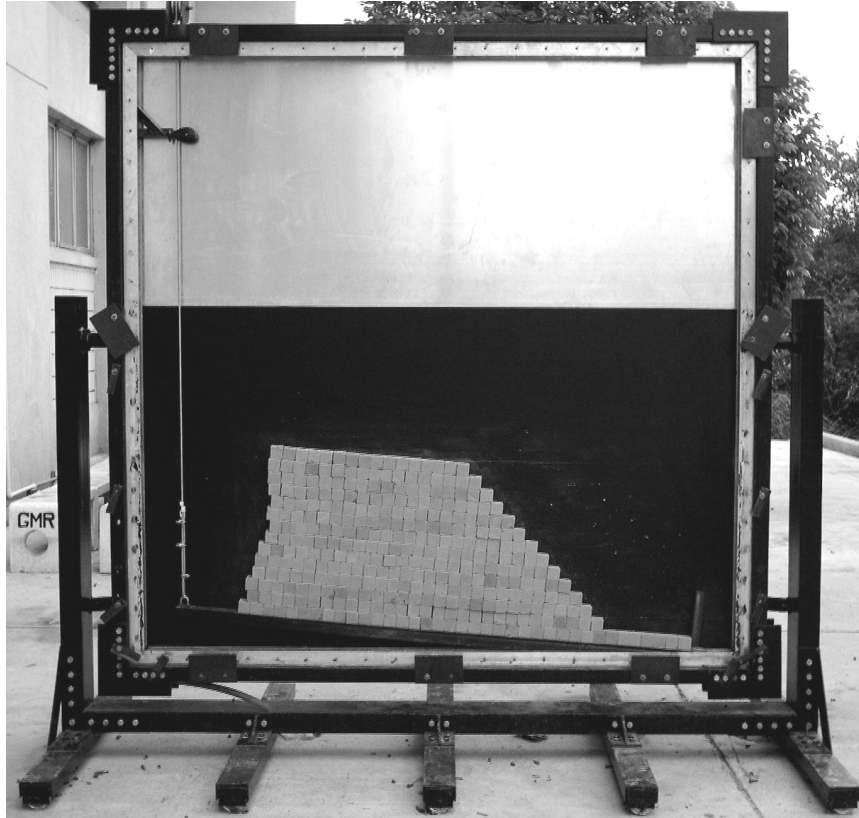
Figure 3.3 Example of test arrangement: Cubical blocks of Phu Phan sandstone

placed in test platform.
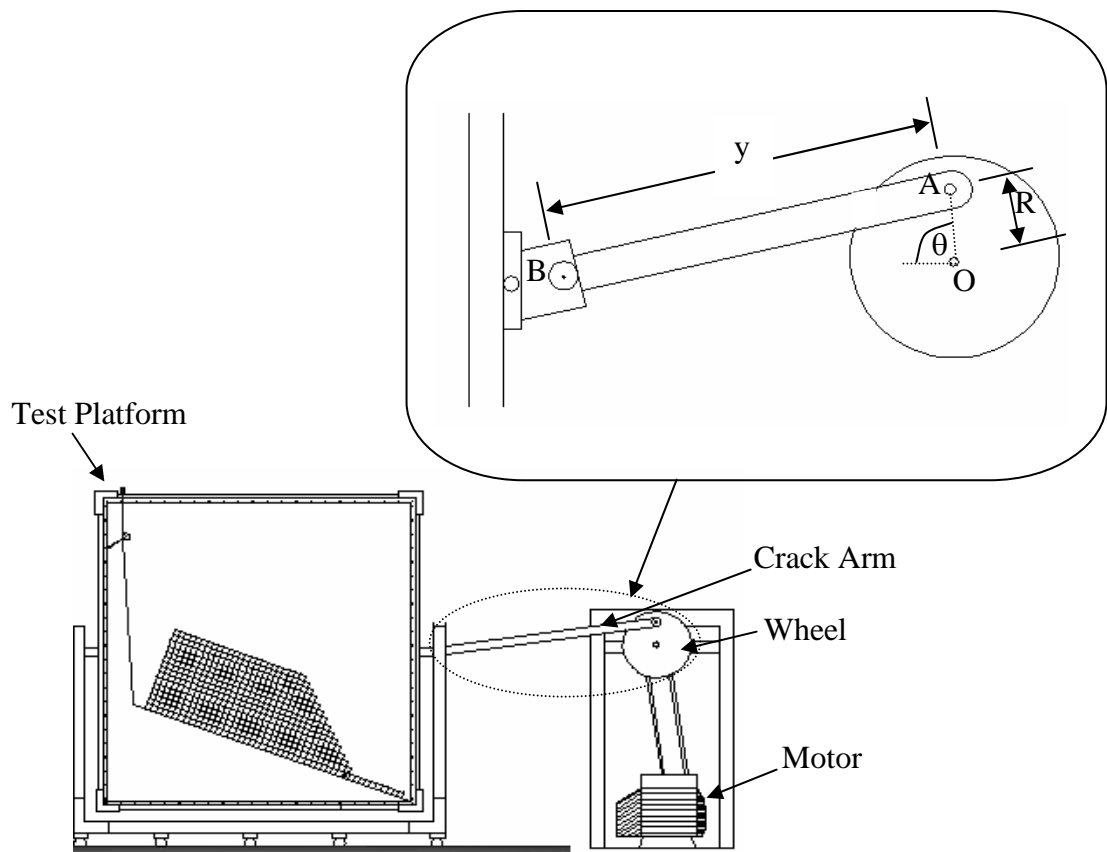
Figure 3.4 Crank arm and flywheel used to induce dynamic loading to the test platform.

$$\alpha_{AB} = \frac{R\omega_{OA}^2 \sin\theta - y\omega_{AB}^2 \sin\phi}{y\cos\phi} \tag{3.4}$$

The actual rotational duration (T) is monitored for each slope model because different slope geometry and slope mass yield different weights, and hence change the speed of the test platform and the flywheel rotation.

3.3   Calculation of slope height

Before testing the initial angles of tilting beam, slope face and upper slope face are measured to the nearest 1 degree. After the failure is observed, the screw jack is secured to hold the tilting beam in-placed. The final angle of the tilting beam is re-measured. The slope height (H) and slope face (ψ_f) at failure can therefore be calculated (Figure 3.5).

$$H = \frac{h\sin(\psi_{f0} + (\psi_p - \psi_{p0}))}{\sin(\psi_{f0} - \psi_{p0})} \tag{3.5}$$

$$\psi_f = \psi_{fO} + (\psi_p - \psi_{pO}) \tag{3.6}$$

where: h   = distance between base and top of slope model

  H   = height of slope at failure

  ψ_{f0} = initial slope face angle

  ψ_f = slope face angle at failure

  ψ_{p0} = initial sliding plane angle

  ψ_p = sliding plane angle at failure

Figure 3.5 Parameters used for calculating slope height of slope model at failure.

Video camera continuously records the slope movement and hence obtaining redundant measurements of the slope angle and height immediately before failure. The video playbacks are also very useful to identify the location where the failure was initiated, and how it progressed.

CHAPTER IV

SLOPE MODEL TESTING

4.1 Introduction

This chapter describes the method and results of the slope model testing. The simulations are made under dry and submerged conditions. The effects of dynamic loading are assessed.

4.2 Sample preparation

Phu Phan sandstone from Nakhon Ratchasima province has been selected for use as rock samples primarily because it has highly uniform texture, density and strength. It is classified as fine-grained quartz sandstone with 72% Quartz (0.2-0.8 mm), 20% feldspar (0.1-0.8 mm), 3% mica (0.1-0.3 mm), 3% rock fragments (0.5-2mm), and 2% others (0.5-1 mm). The average density is 2.27 g/cc. To form slope models with two mutually perpendicular joint sets, cubical (4x4x4 cm) and rectangular (4×4×8 cm and 4×4×12 cm) shaped sandstone blocks have been prepared. The cubical blocks are used to simulate joint sets with equal spacing, while the rectangular blocks simulate joint sets with different spacings. Quality control has been carried out to ensure that the geometry of each block meets the specifications. A total of nearly 1000 blocks of Phu Phan sandstone has been prepared (Figure 4.1).

Tilt testing is performed on the sandstone blocks to determine shear strength of the saw-cut surfaces. Size of the upper (sliding) block is varied. Its weight is measured and taken into the calculation of normal load. The tests are repeated 4 times
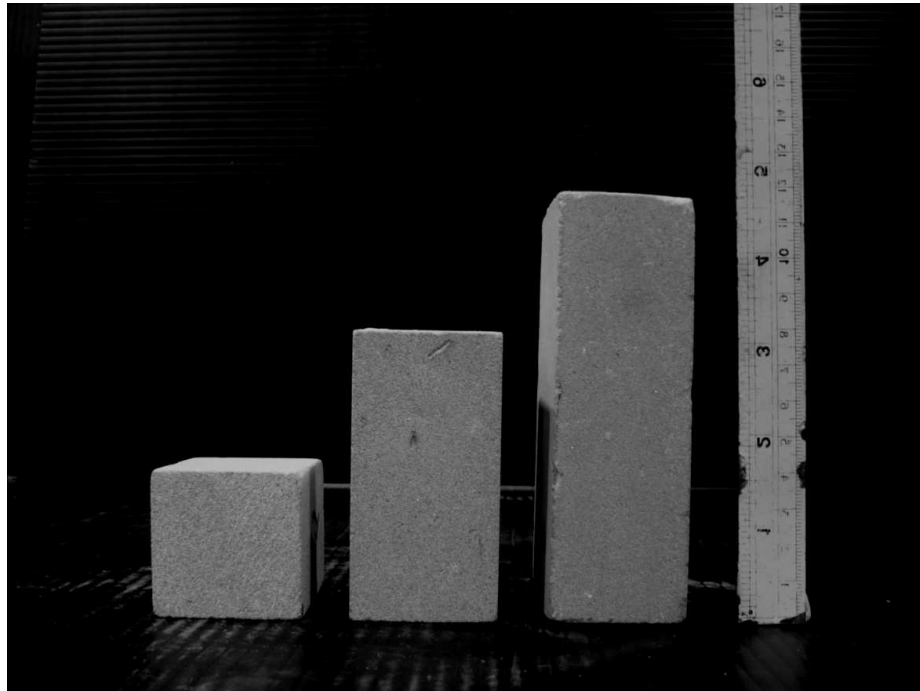
Figure 4.1. Nearly 1000 blocks of Phu Phan sandstone prepared for testing.

for each block size. Table 4.1 shows the test results. The basic friction angle is about 26 degrees and cohesion is 0.053 kPa (Figure 4.2). The measured cohesion is extremely low which agrees with the results obtained by Kemthong (2006). He reports that the basic friction angle for smooth (saw-cut) surfaces of Phu Phan sandstone is averaged as 32 degrees with virtually zero cohesion. The discrepancy of the friction angles is probably due to the intrinsic variability of the rock and the difference in the ranges of normal loads used in the tests. The uniaxial compressive strength of the tested sandstone is 72.37 ± 8.53 MPa and elastic modulus equals to 18.43 ± 1.08 GPa (Kemthong, 2006).

4.3   Simulation of plane sliding failure under dry condition

The simulations involve two-dimensional plane sliding of rock slope form by cubical (4×4×4 cm) and rectangular (4×4×8 cm and 4×4×12 cm) blocks of sandstone, under various slope face angles with the maximum slope height up to 1 m.

Thirty-eight plane sliding failures has been simulated for dry slope models with heights varying from 16 to 77 cm and slope face angles from 41 to 73 degrees (Appendix A). Each set of slope geometry comprises sandstone blocks with the same dimension, and is simulated at least 3 times to ensure the repeatability of the results. Table 4.2 summarizes the test parameters and results for modeling under dry condition. Figure 4.3 shows an example of the plane sliding failure for a slope model formed by 4×4×12 cm sandstone blocks. Figure 4.4 shows simulation results by presenting the slope height at failure as a function of sliding plane angle. Since the measured cohesion is very low and negligible, the deterministic method simply yields the sliding plane angle equal to the friction angle of the block surfaces.

Table 4.1 Tilt test results of Phu Phan sandstone.

Sample No.	Width (mm)	Length (mm)	Area (mm^2)	Weight (g)				ϕ_b (degrees)			
				1	2	3	avg.	1	2	3	avg.
1	43.35	43.50	1885.7	170.2	170.6	170.6	170.5	27	30	30	30
2	40.35	42.00	1694.7	177.1	177.2	177.4	177.2	25	27	24	25
3	41.85	41.85	1751.4	172.9	172.9	172.3	172.7	29	31	28	29
4	41.80	41.85	1749.3	167.7	167.9	168.3	168.0	30	30	29	30
5	41.15	41.20	1695.3	162	160.8	161.4	161.4	30	27	30	30
6	41.20	82.15	3384.6	500.6	500.7	500.6	500.6	29	32	29	29
7	40.75	82.10	3345.6	497.6	497.6	497.3	497.5	29	27	29	29
8	41.95	81.50	3418.9	496.2	495.8	495.9	496.0	29	26	26	26
9	42.70	82.15	3507.8	514.9	515.5	515.1	515.2	26	29	26	26
10	41.45	82.75	3430.0	489.9	490.2	490.7	490.3	30	29	27	29
11	40.25	81.30	3272.3	684.3	684.1	683.6	684.0	29	29	28	29
12	40.25	79.80	3212.0	656.7	657.1	657.1	657.0	27	25	26	26
13	38.80	80.00	3104.0	651.5	651.6	651.7	651.6	28	30	29	29
14	38.45	79.45	3054.9	662.5	662.2	662.7	662.5	29	27	27	27
15	38.40	80.80	3102.7	663.6	663.4	663.6	663.5	27	25	27	27
16	41.65	82.15	3421.6	999.3	999.2	999.3	999.3	29	28	29	29
17	40.70	82.30	3349.6	982.1	982.2	982.3	982.2	26	26	26	26
18	42.70	82.35	3516.4	994.6	994.1	994.2	994.3	28	27	26	27
19	42.30	81.25	3436.9	1007.2	1007.2	1007.1	1007.2	27	27	26	27
20	41.15	84.85	3491.6	1035.1	1035.2	1034.9	1035.1	27	26	25	26
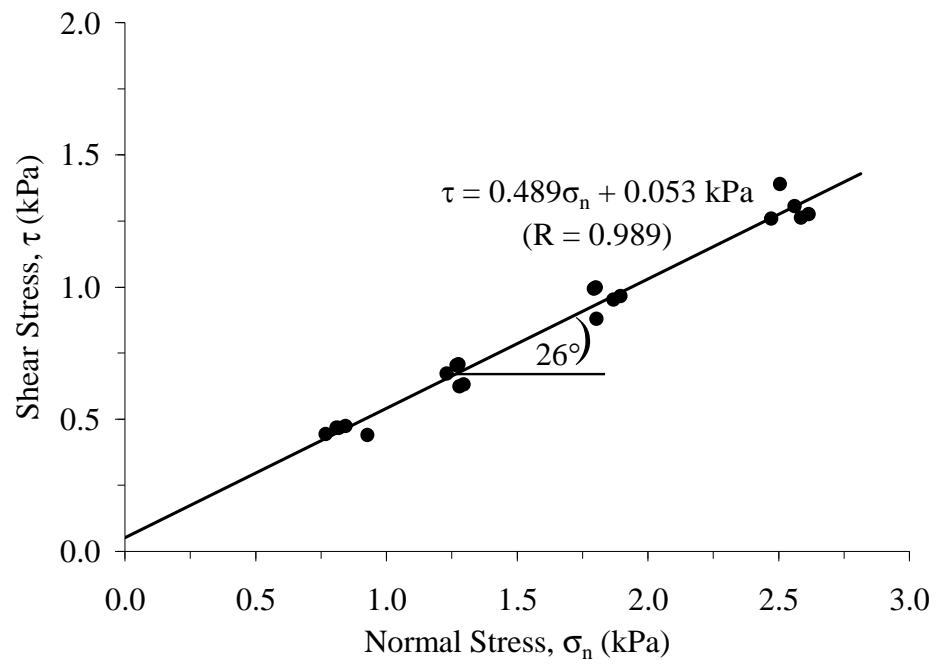
Figure 4.2 Results of tilt testing on bocks of Phu Phan sandstone size; 4×4×4 cm,

4×4×8 cm and 4×4×12 cm.

Table 4.2 Test parameters and results of slope model simulations under dry conditions.

Block Size	No. of Testing	H (cm)	ψ_f (degrees)	ψ_p (degrees)
4×4 cm	43	20-68	40-52	21-25
8×4 cm	53	16-77	49-75	23-27
12×4 cm	49	16-93	44-72	25-26
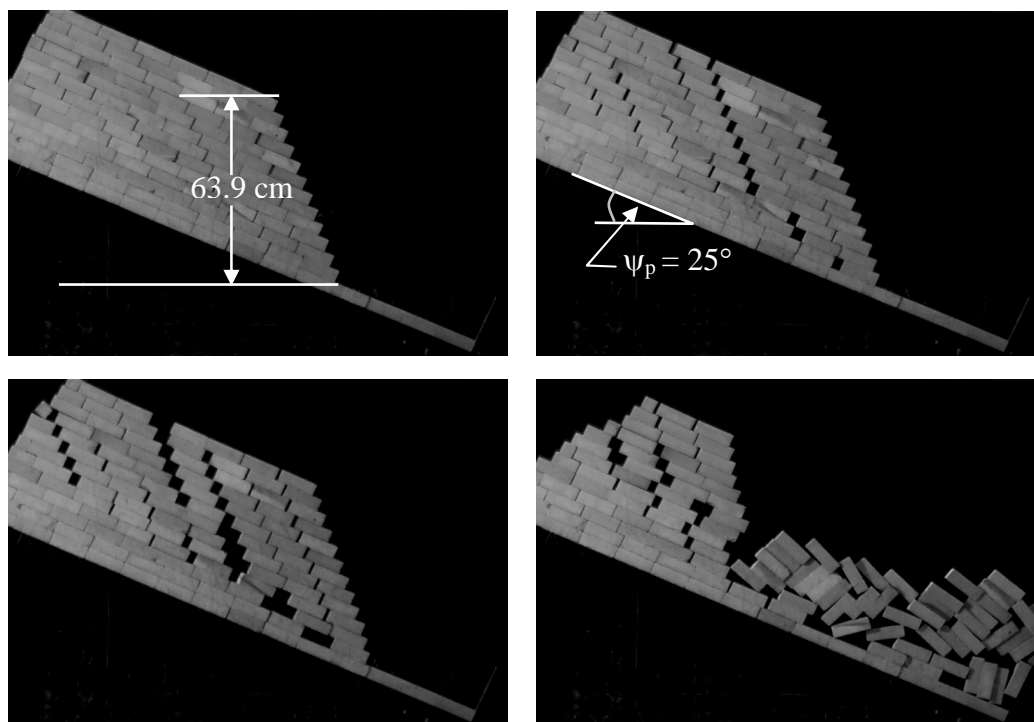
Figure 4.3 Simulation of sliding failure of rock slope formed by 12×4 cm blocks of sandstone under dry condition. Failure occurred at ψ_f=71°, ψ_p=25°, and H=63.9 cm.
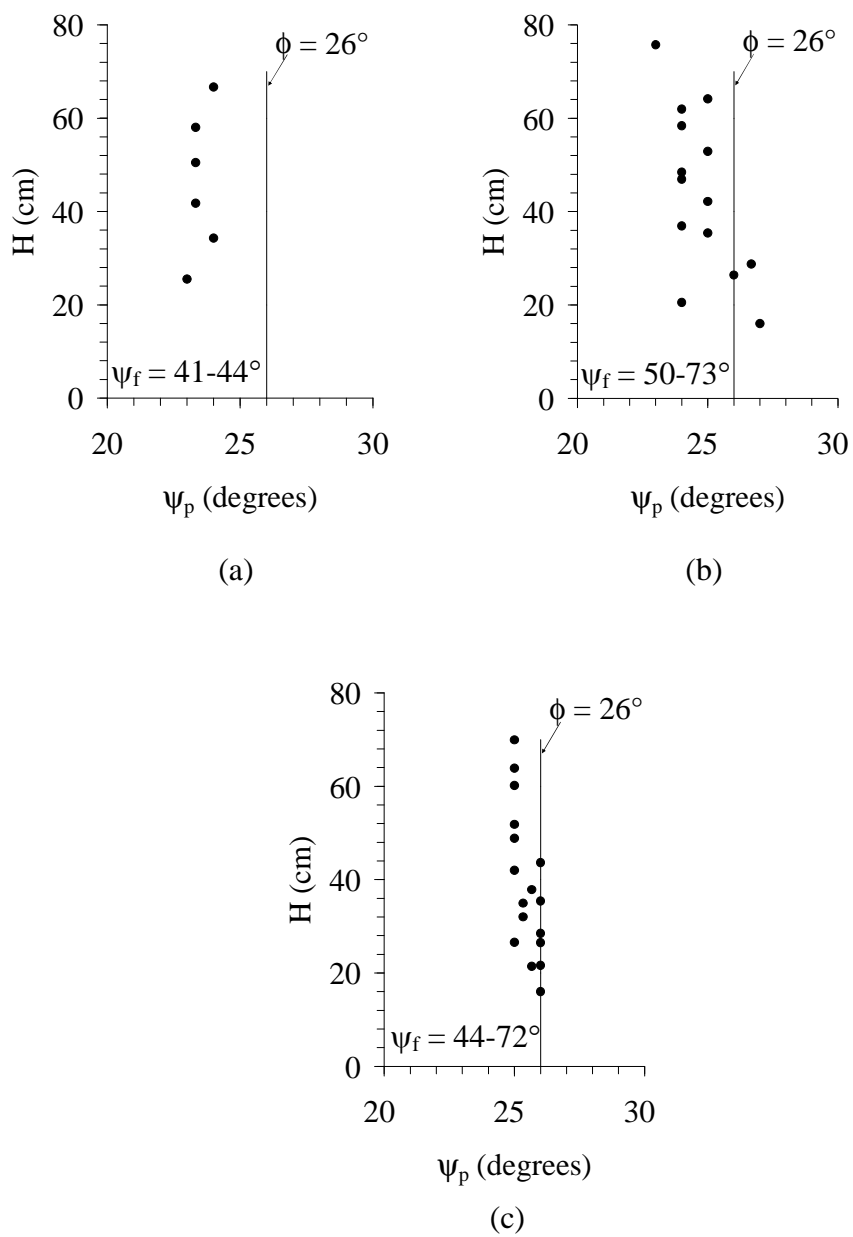
Figure 4.4 Sliding failure of dry slope on block size 4×4×4 cm (a), 4×4×8 cm (b), and 4×4×12 cm (c).

The sliding angle is also independent of the slope height. The observed sliding plane angles (ψ_p) tend to be lower than those determined by the deterministic method or the friction angle obtained from the tilt test. This is probably caused by the non-uniform distribution of the normal load and shear force on the sliding plane. From the tested geometry the highest shear force is probably near the slope toe while the normal load largely concentrates near the middle of the sliding plane. Such load distribution is probably similar to the actual in-situ slope conditions. The deterministic method however assumes a uniform load and shear force along the sliding plane.

Calculation of factor of safety for dry slope model

Based on Coulomb's failure criterion a factor of safety of the sliding failure of the slope models is determined here to show the discrepancies between the observations and the calculations by the deterministic method (Hoek and Bray, 1981):

$$FS = \frac{c \cdot A}{W \cdot \sin \psi_p} + \cot \psi_p \cdot \tan \phi \qquad (4.1)$$

where c is cohesion of rock surface, ϕ is friction angle, W is weight of the sliding block, A is sliding area, ψ_p is sliding plane angle.

The weight of rock wedges is calculated as (Figure 3.5):

$$W = W_1 + W_2 \qquad (4.2)$$

$$W_1 = \frac{1}{2} \cdot \gamma \cdot H^2 \cdot \left(\cot \psi_p - \cot \psi_f \right) \cdot t$$

$$W_2 = \frac{1}{2} \cdot \gamma \cdot H^2 \cdot \left(\frac{(\cot \psi_p - \cot \psi_f)^2}{\cot(\alpha - \psi_p) + \cot \psi_p} \right) \cdot t$$

where γ is unit weight of rock, ψ_f is slope face angle, H is the height of slope, α is angle of the back of slope model, and t is thickness of rock. The weight of the sliding block becomes:

$$W = \frac{1}{2} \cdot \gamma \cdot H^2 \cdot \left[(\cot \psi_p - \cot \psi_f) + \left(\frac{(\cot \psi_p - \cot \psi_f)^2}{\cot(\alpha - \psi_p) + \cot \psi_p} \right) \right] \cdot t \qquad (4.3)$$

Where : $A = H \cdot t \cdot \csc \psi_p$

By assuming that the plane sliding follows Coulomb criterion, the factor of safety of a dry slope model can be calculated by:

$$FS = 2 \cdot c / \left\{ \gamma \cdot H \cdot \sin^2 \cdot \psi_p \cdot \left[(\cot \psi_p - \cot \psi_f) + \left(\frac{(\cot \psi_p - \cot \psi_f)^2}{\cot(\alpha - \psi_p) + \cot \psi_p} \right) \right] \right\} + \frac{\tan \phi}{\tan \psi_p} \quad (4.4)$$

Figures 4.5 through 4.7 compare the factors of safety calculated from the model geometry at failure (Equation 4.4) with the actual factor of safety observed at failure from the simulation (FS = 1.0). It is clear that the deterministic method by Hoek & Bray (1981) over-estimate the factor of safety at failure by as high as 30% for the 4×4×4 blocks and about 10% for 4×4×12 blocks. This discrepancy is enhanced when the sliding plane angles become smaller. The calculated factor of safety seems to be insensitive to the slope face angle. The comparisons imply also that shorter blocks (4×4×4 cm) tend to slide easier than do longer ones (4×4×8 cm and 4×4×12 cm).
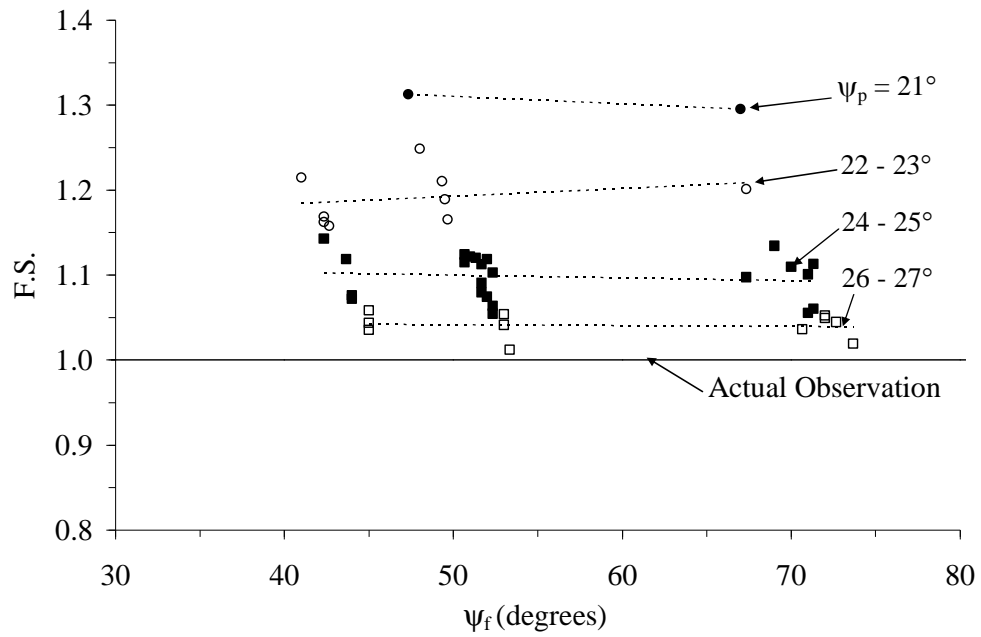
Figure 4.5 Factors of safety calculated from Eqn. (4.4) plotted as a function of ψ_f for block size 4×4×4 cm.
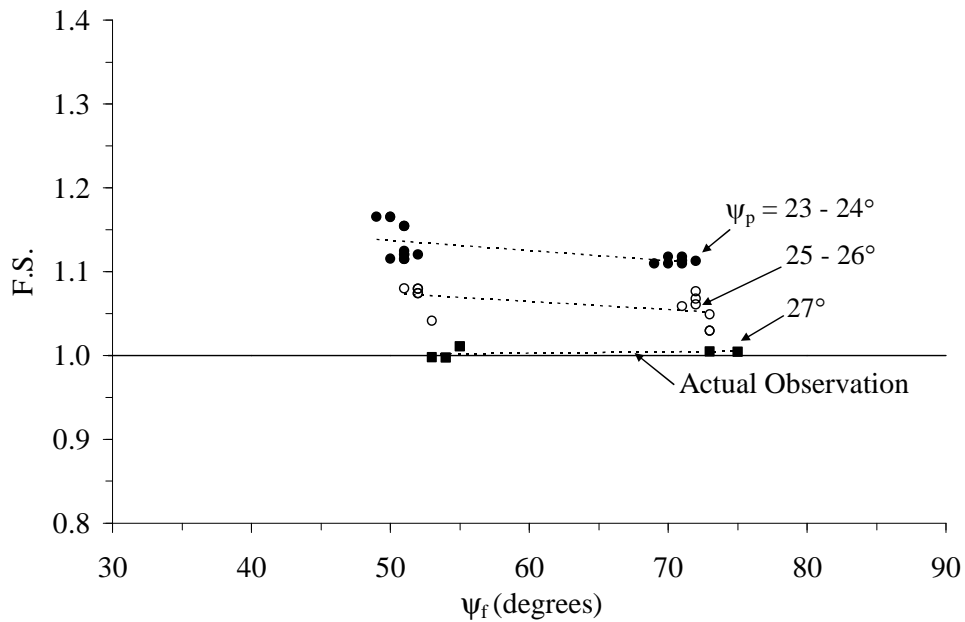
Figure 4.6 Factors of safety calculated from Eqn. (4.4) plotted as a function of ψ_f for block size 4×4×8 cm.
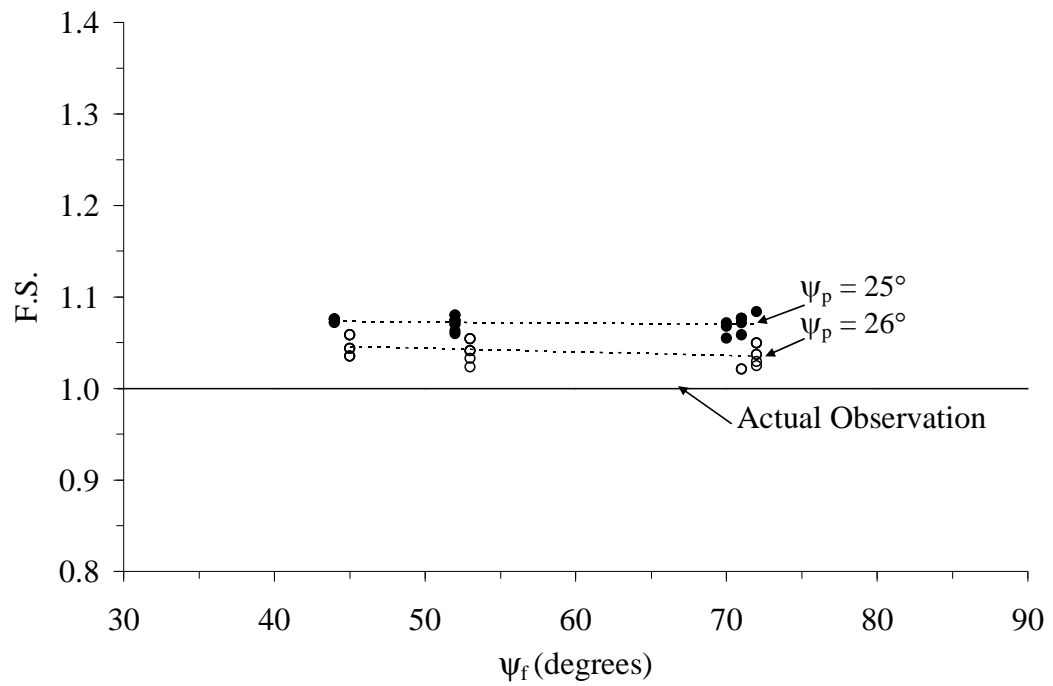
Figure 4.7 Factors of safety calculated from Eqn. (4.4) plotted as a function of ψ_f

for plane block size 4×4×12 cm.

Regardless the block dimensions, the difference between the calculated and observed

factors of safety becomes insignificant for higher sliding plane angles (Appendix B).

4.4   Simulation of plane sliding testing under submerged condition

Over thirty plane sliding failures have been simulated under submerged

condition with slope heights varying from 20 to 91 cm and slope face angles from 40

to 71. Each set of slope geometries is formed by sandstone blocks with the same

dimension, and is simulated at least 3 times to ensure the repeatability of the results.

Video records are taken during the test. Table 4.3 summarizes the test parameters and

results for modeling under submerged condition.   Figure 4.8 through 4.9 show

examples of the plane sliding failure for a slope model formed by 4×4×4 cm, 4×4×8

cm, and 4×4×12 cm blocks under submerged conditions. The video recorder allows

examining the failure process of the slope models after the test. The failure usually

initiates from the slope toe and progresses upward to the crest. A combination of

plane sliding near the slope toe and toppling failure near the slope crest is often found

for slope models formed by 4×4×4 cm blocks.

Figure 4.10 compares the simulation results by plotting the slope height at

failure as a function of sliding plane angle. Since the measured cohesion is very low

and negligible, the deterministic method simply yields the sliding plane angle equal to

the friction angle of the block surfaces. The observed sliding plane angles tend to be

lower than the rock friction angle. The discrepancy becomes larger for the slope

models formed by shorter sandstone blocks. The sliding plane angles (ψ_p) also seem

to be independent of the slope height. As expected, the observed sliding plane angles

under submerged condition are lower than those under dry condition.

Table 4.3 Test parameters and results of slope model simulations under submerged conditions.

Block Size	No. of Testing	H (cm)	ψ_f (degrees)	ψ_p (degrees)	H_w (cm)
4×4 cm	10	36-75	40-66	20-22	13-55
8×4 cm	10p	20-91	45-71	21-23	7-60
12×4 cm	11	22-70	49-69	22-24	8-54
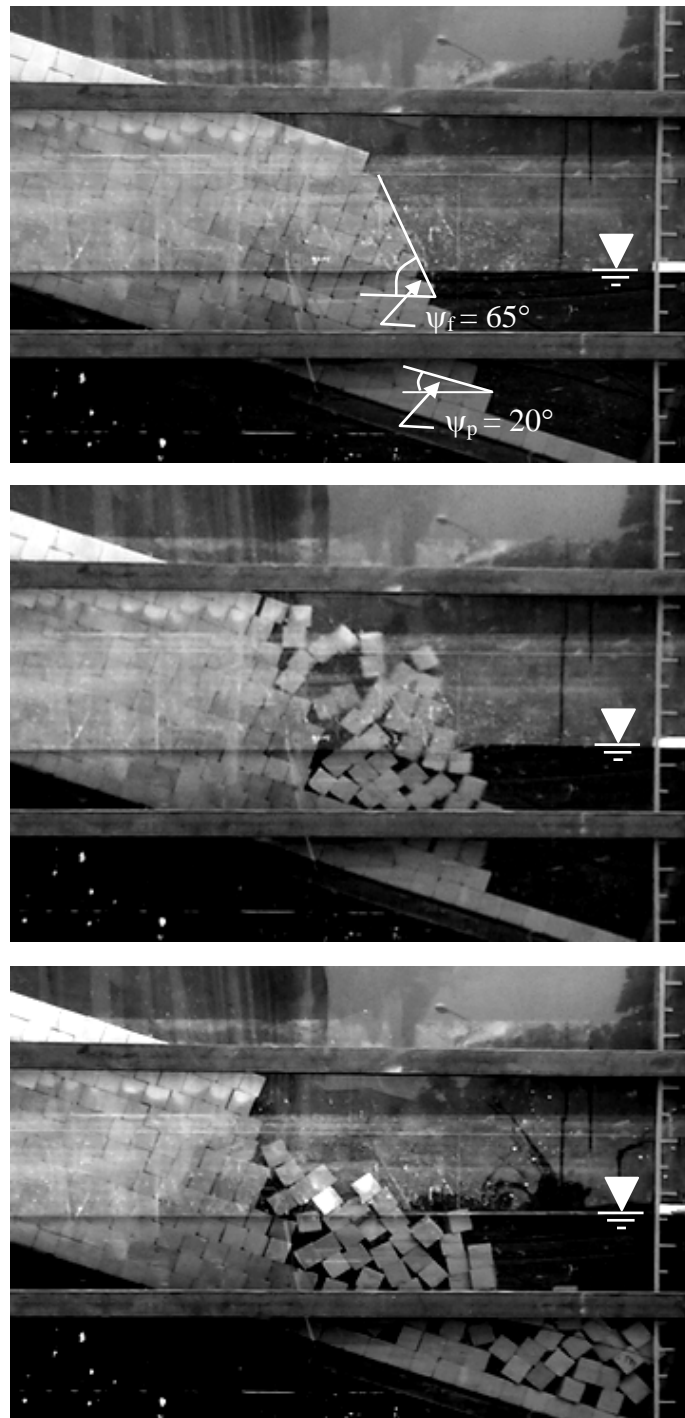
Figure 4.8 Example of failure of slope model formed by 4×4 cm blocks under submerged condition, showing combination of plane sliding at slope toe and toppling failure near slope crest. Failure occurred at $\psi_f=65°$, $\psi_p=20°$, H=57.3 cm, and $H_w=35$ cm.
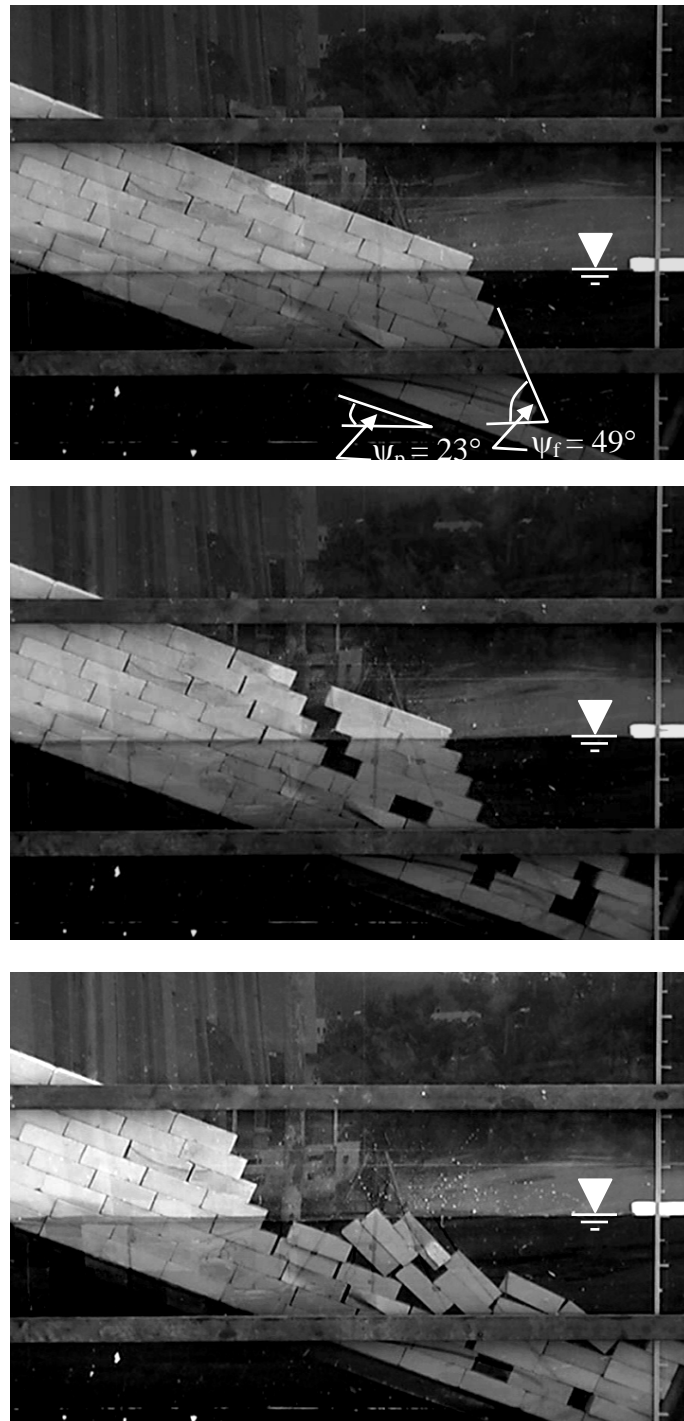
Figure 4.9 Example of failure of slope model formed by 4×4×12 cm blocks under submerged condition, showing combination of plane sliding at slope toe and toppling failure near slope crest. Failure occurred at ψ_f=49°, ψ_p=23°, H=55.6 cm, and H_w=42 cm.
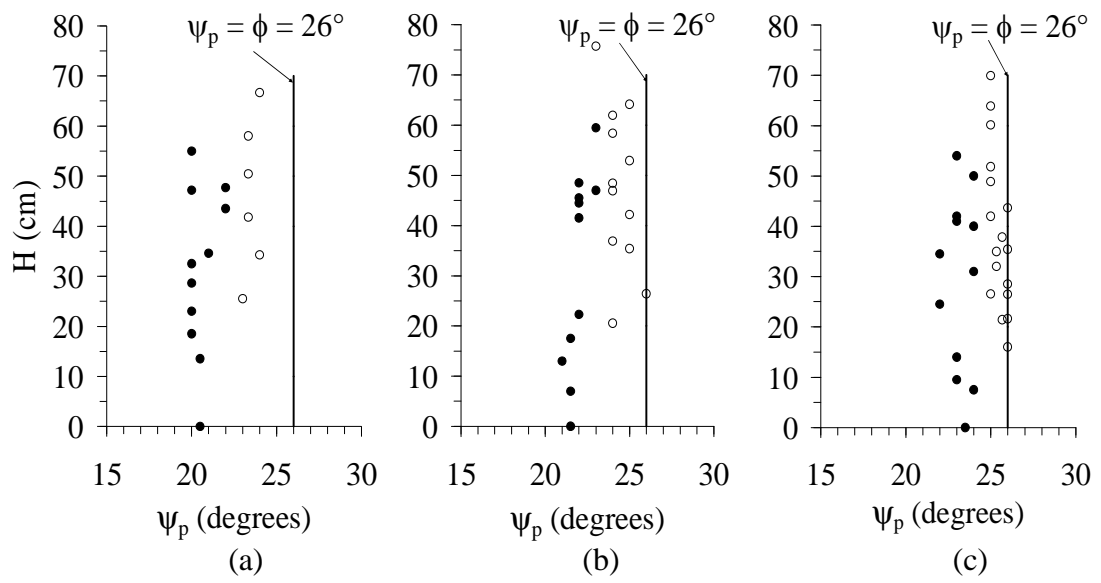
Figure 4.10 Slope height (H) as a function of sliding plane angle (ψ_p) for block

sizes of 4×4 cm (a), 8×4 cm (b) and 12×4 cm (c). Solid points

represent submerged condition.

However under the same slope conditions (e.g., slope height, face angle) the difference is less than 2-3 degrees.

4.5 Toppling failure simulation

Thirty seven toppling failures have been simulated for all block shapes under dry condition. The slope height varies from 27-85 cm, and slope face from 43-82 degrees (Appendix C). Each set of slope geometry is simulated 3 times or until the results are repeatable. Table 4.4 summarizes the test parameters and results for modeling. Figures 4.11 through 4.13 show examples of test arrangements to simulate toppling failures with 4×4×4 cm blocks, 4×4×8 cm blocks, and 4×4×12 cm blocks. Figure 4.14 shows the results from toppling failure simulations in terms of slope height (H) as a function of the angle of the base plane on which the toppling blocks situate (ψ_p). As expected the models with a gentle slope face (ψ_f) fail at a greater slope height. At the same slope height, models with a steep slope face fails at a lower ψ_p. The slope height at failure decreases with increasing ψ_p. The dependency of this base plane angle becomes smaller for the slopes comprising taller and narrower rock blocks.

Toppling failure determined by limit equilibrium analysis

Limit equibrium analysis of toppling on a stepped base proposed by Hoek & Bray (1981) can be written as:

$$P_{n-1} = \frac{P_n(M_n - \Delta x \tan \phi) + (W_n/2)(y_n \sin \alpha - \Delta x \cos \alpha)}{L_n} \qquad (4.5)$$

Table 4.4 Test parameters and results of toppling failure simulation.

Block Size	No. of Testing	H (cm)	ψ_f (degrees)	ψ_p (degrees)
4x4x4 cm	24	17-76	61-69	16-22
4x4x8 cm	53	27-75	43-82	5-19
4x4x12 cm	39	38-85	54-80	4-11
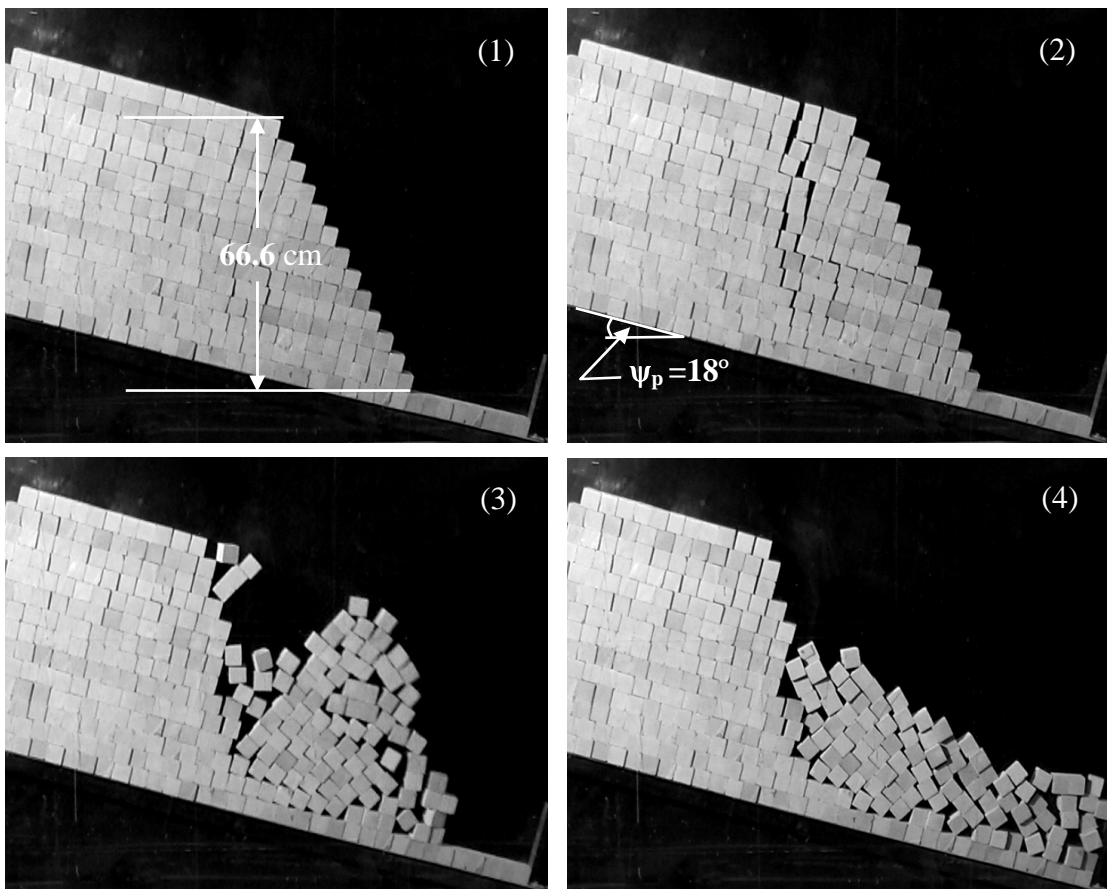
Figure 4.11 Simulation of toppling failure for block size 4×4×4 cm.
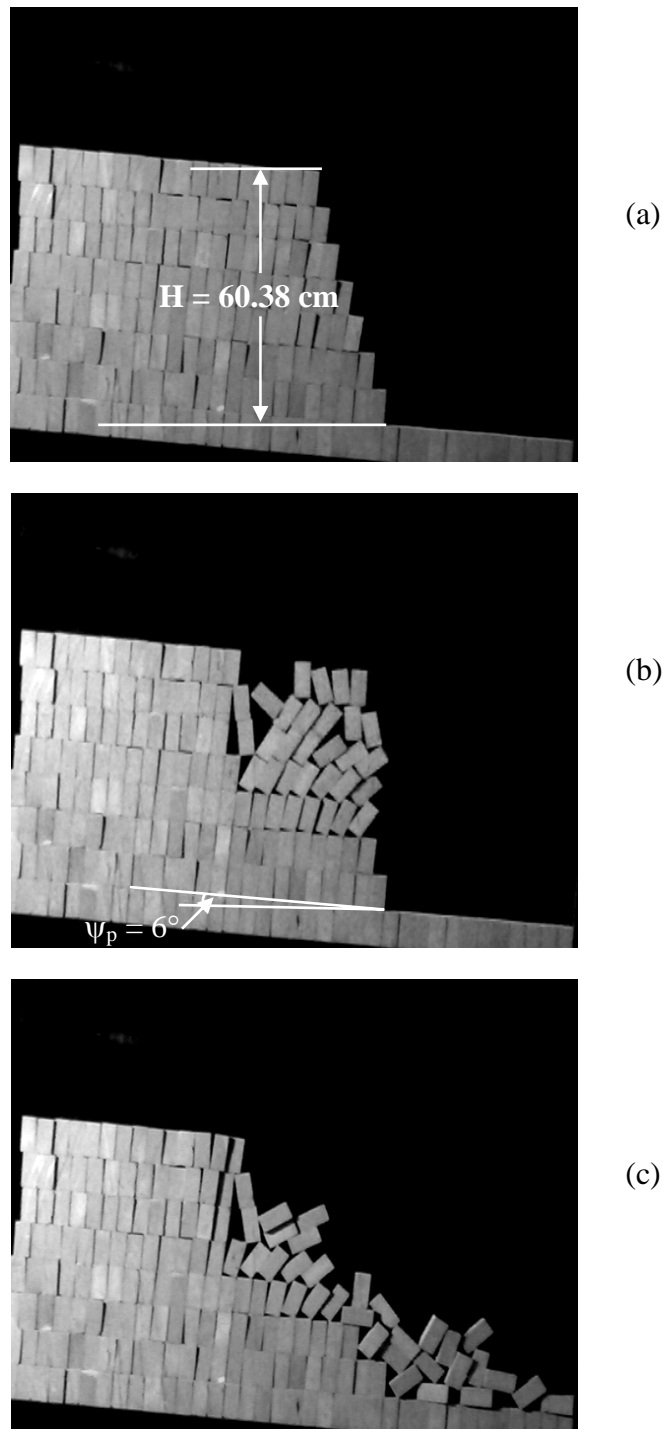
Figure 4.12 Simulation of toppling failure for block size 4×4×8 cm. (a) Immediately

before failure ($\psi_f = 72°$). (b) At failure. (c) After failure.
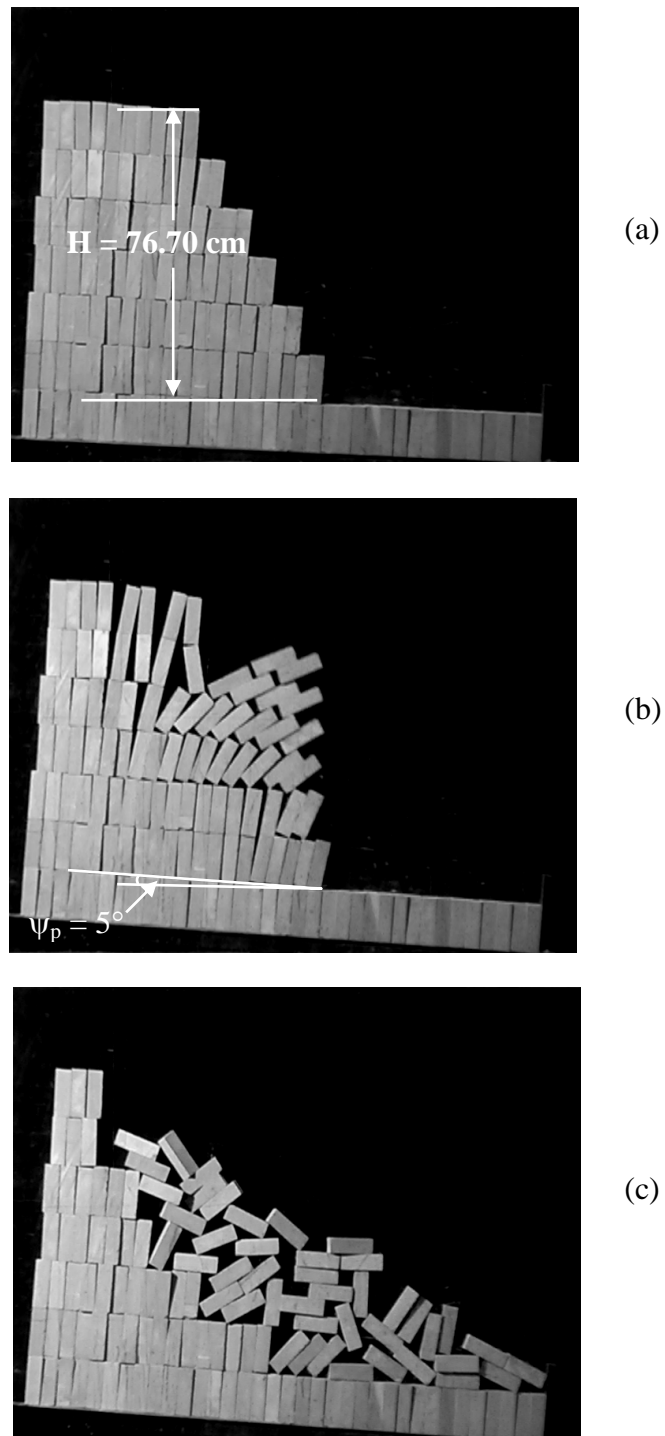
Figure 4.13 Simulation of toppling failure for block size 4×4×12 cm. (a) Immediately before failure ($\psi_f = 63°$). (b) At failure. (c) After failure.
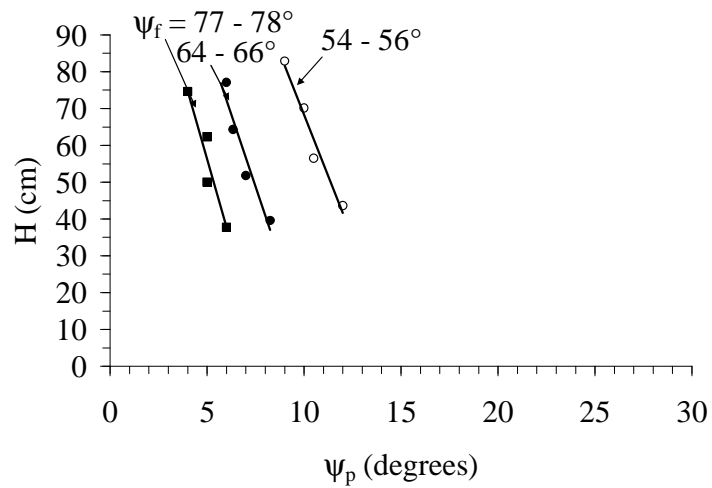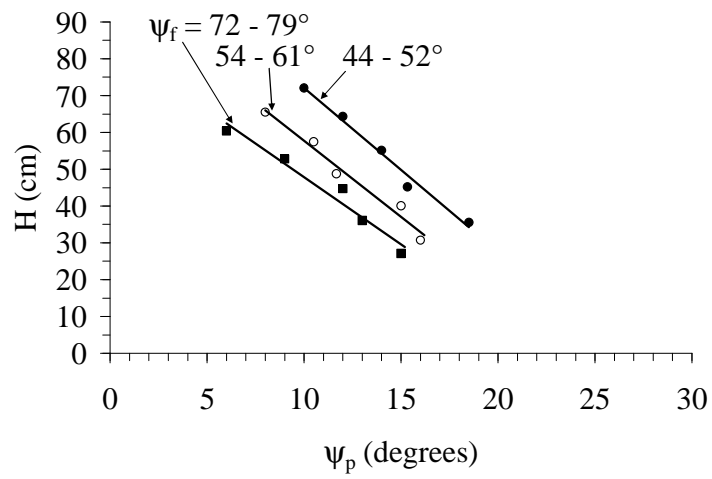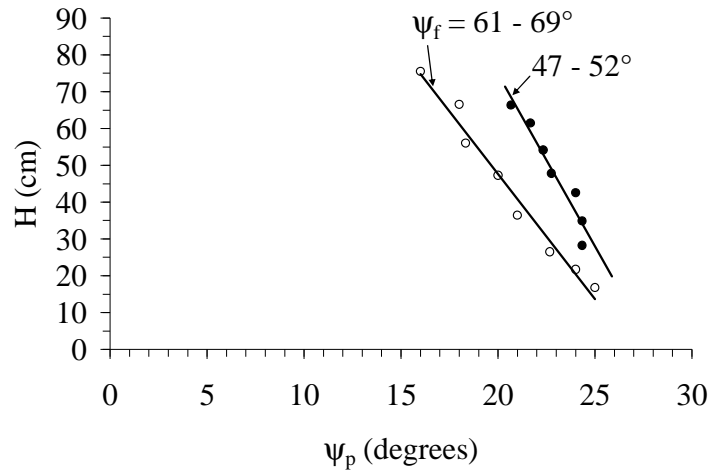
Figure 4.14 Results of toppling failures tested for block size 4×4×4 cm (top), 4×4×8 cm (middle), and 4×4×12 cm (bottom).

where: P_{n-1} = force preventing toppling of the nth block

               P_n = force inducing toppling of the nth block

               W_n = weight of nth block

               M_n = distance between block base and the point where P_n applies

               L_n = distance between block base and the point where P_{n-1} apples

               Δx = width of each block

               y_n = height of the nth block

               α = plane angle.

Since our slope model does not have stepped base. Equation (4.5) requires some modification as follows.

$$P_{n,t} = \frac{(P_n M_n - P_n \Delta x \tan\phi) - (P_R L_n + P_R \Delta x \tan\phi) + \frac{y_n}{2} W_n \sin\alpha - \frac{\Delta x}{2} W_n \cos\alpha}{L_n} \quad (4.6)$$

where: $P_{n,t}$ = force resisting toppling of nth block

         P_R = accumulate resisting force

Equation (4.6) is used to evaluate stability of slope and to estimate the extent of failure zone from slope toe. If $P_{n,t}$ of any block is positive or greater than zero, toppling of that block may occur.

Figure 4.15 gives the parameters used in the calculation of the probability of failure for each block. Figures 4.16 and 4.17 compare the calculated results with the actual observations (Appendix C). The observations on 4×4×8 cm blocks and 4×4×12 cm blocks agree well with those calculated by the equation modified from Hoek & Bray (1981).

4.6 Slope models tested under dynamic loading

The dynamic loading is studied by considering the effects of the horizontal pseudo-static acceleration induced by cyclic motions of the test platform in the direction parallel to the dip direction of the slope face. These cyclic motions are used to simulate the earthquake shaking. The vertical acceleration is assumed to be zero.

Over one hundred plane sliding failures have been simulated with the horizontal pseudo-static accelerations between 0.013 g and 0.225 g. These accelerations are within the range tested and observed elsewhere (Kramer, 1996; Maugeri et al., 2000; Hatzor et al., 2004). The amplitude is maintained constant at 23.5 mm. The slope models have the sliding plane angles varied from 1 to 22 degrees, heights from 44 to 83 cm, and slope face angles from 28 to 68 degrees (Appendix D). Table 4.5 summarizes the test parameters and the results. For all slope geometries the duration for cyclic motion is maintained at one minute. If failure does not occur within one minute of shaking, the sliding plane angle is progressively increased by one degree interval and the test is repeated. Figure 4.18 shows an example of the plane sliding failure for 4×4×8 cm blocks. It is generally observed that under similar slope geometry and block arrangement the failure zone induced under dynamic load is more extensive than those under static loading.
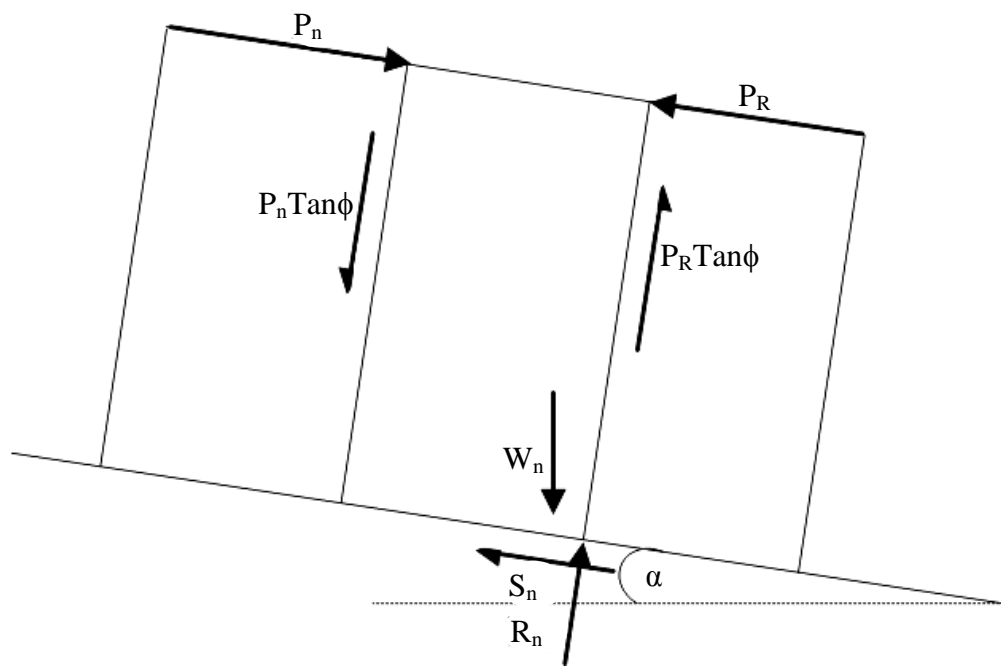
Figure 4.15 Parameters used in block toppling analysis.
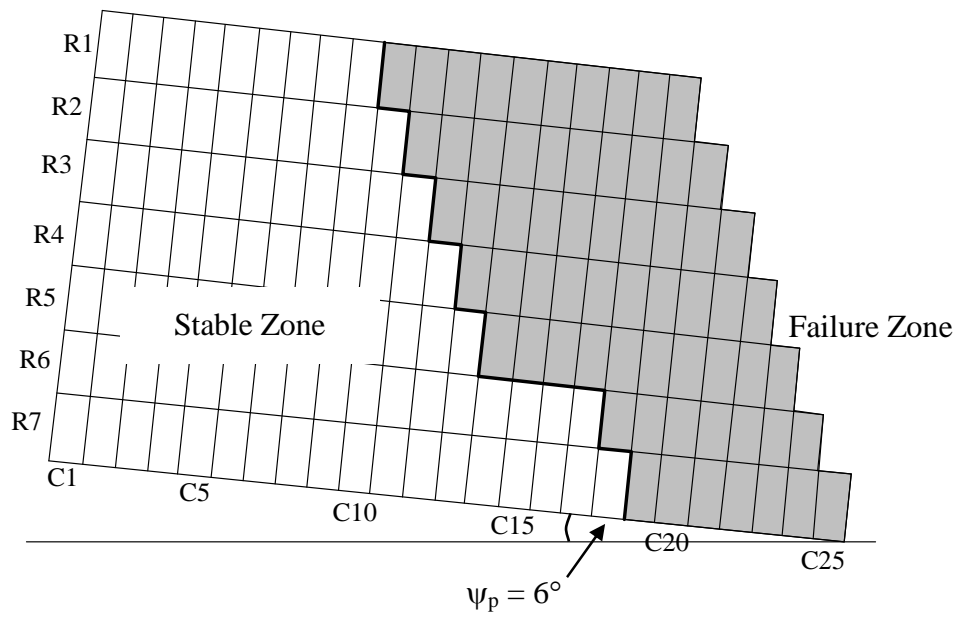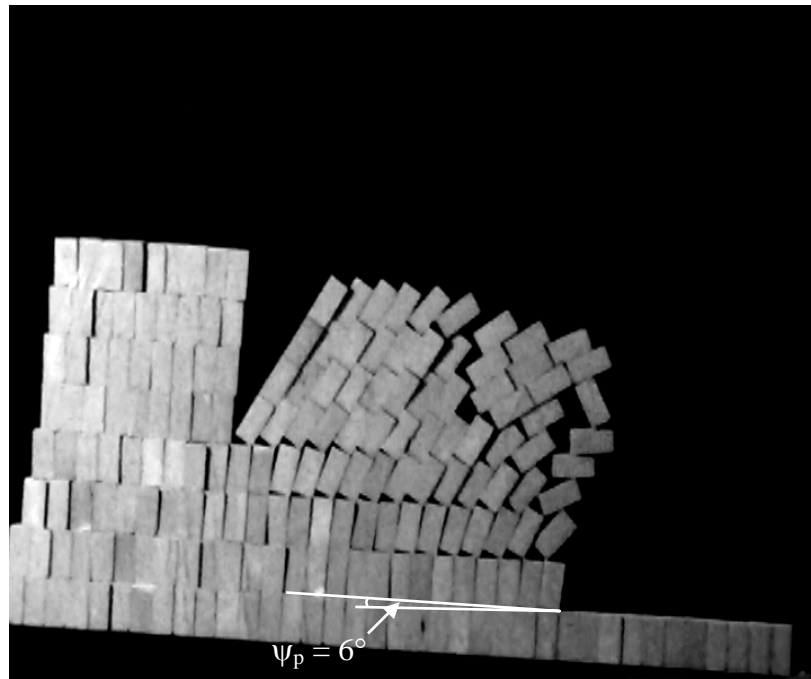
Figure 4.16 Results of observation (top) and calculation (bottom) of toppling failure for block size 4×4×8 cm. Failure occurred at $\psi_f = 72°$.
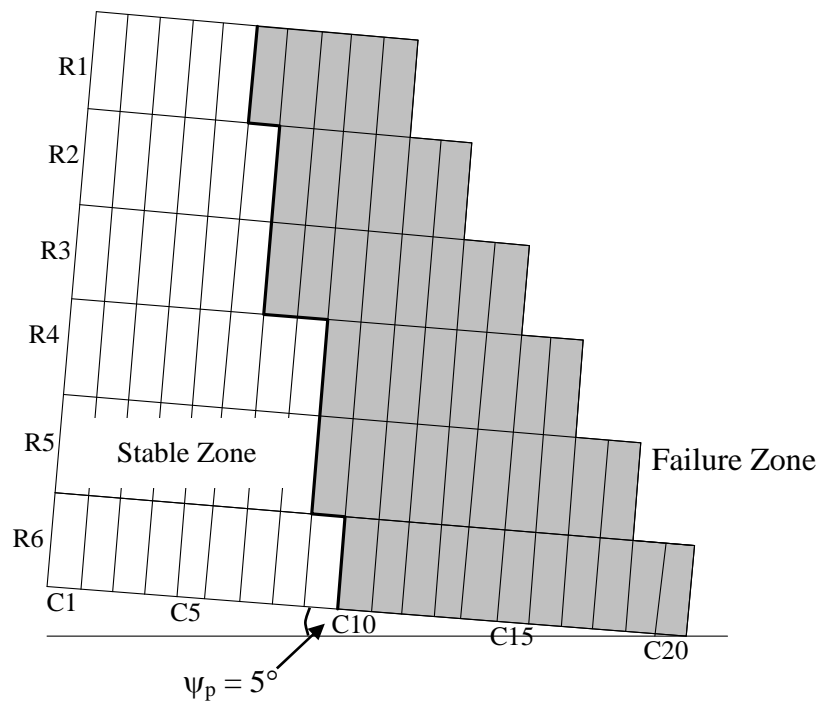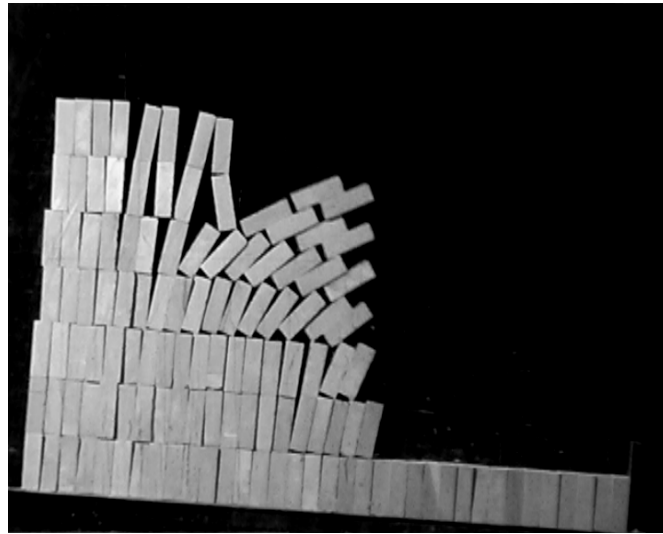
Figure 4.17 Results of observation (top) and data calculation (bottom) of toppling

failure for block size 4×4×12 cm. Failure occurred at $\psi_f = 63°$.

Table 4.5 Results of rock slope stability analysis under dynamic loading with amplitude = 23.5 mm.

Block Size	No.of Tests	Frequency (Hz)	a (g)	Modified Mercalli Intensity*	H (cm)	ψ_f (degrees)	ψ_p (degrees)
4×4 cm ▦	7	0.403	0.013	IV	69-83	40-44	15-18
	3	0.504	0.017	IV	80-82	40-43	15-17
	3	0.629	0.027	IV	76-78	41-44	14-16
	4	0.700	0.033	V	44-53	33-44	12-17
	7	0.833	0.046	V	50-77	31-41	4-15
	8	1.000	0.067	VI	46-75	28-38	1-12
	4	1.233	0.102	VI	49-54	28-32	3-6
	4	1.346	0.119	VI	46-62	28-32	1-4
	1	1.833	0.225	VII	46	46	1
8×4 cm ▭▭	7	0.403	0.013	IV	55-58	61-67	16-21
	7	0.504	0.017	IV	55-56	64-68	18-20
	3	0.629	0.027	IV	54-56	63-68	18-19
	3	0.700	0.033	V	55-57	60-64	15-18
	11	0.833	0.046	V	51-55	57-63	10-16
	8	1.000	0.067	VI	48-52	52-59	10-12
	6	1.346	0.119	VI	45-48	48-54	1-5
	1	1.700	0.193	VII	45	51	1
	1	1.833	0.225	VII	45	46	1
12×4 cm ▭▭	2	0.403	0.013	IV	58-59	66-67	21-22
	4	0.833	0.046	V	55-57	60-63	15-18
	2	1.117	0.083	VI	52-53	58-59	12-13
	2	1.429	0.136	VII	49-50	52-53	6-7
	1	1.700	0.193	VII	45	46	1
	1	1.833	0.225	VII	45	46	1

* Modified Mercalli Intensity from Richter (1958) and Wald et al. (1999) as:

IV = Felt indoors by many, outdoors by few during the day. At night, some awakened. Dishes, windows, doors disturbed; walls make cracking sound.

V   = Felt by nearly everyone; many awakened. Some dishes, windows broken. Unstable objects overturned.

VI = Felt by all; many frightened. Some heavy furniture moved; a few instances of fallen plaster. Damage slight.

VII = Damage negligible in building of good design and construction; slight to moderate in well-built ordinary structures; considerable damage in poorly built or badly designed structures; some chimneys broken.

4.6.1 Deterministic method calculation

To compare the test results with those calculated by the deterministic method, a closed-form solution given by Kramer (1996) is adopted here. The solution offers a simple approach to calculate the factor of safety of plane failure per unit thickness of slope mass under vertical and horizontal pseudo-static accelerations.

$$FS = \frac{\text{Resisting force}}{\text{Driving force}} = \frac{c \cdot l + [(W - F_v)\cos\psi_p - F_h \sin\psi_p]\tan\phi}{(W - F_v)\sin\psi_p + F_h \cos\psi_p} \qquad (4.7)$$

$$F_h = a\,W/g = k_h W \qquad (4.8)$$

$$F_v = a_v\,W/g = k_v W \qquad (4.9)$$

where F_h and F_v = horizontal and vertical inertial forces, a = horizontal pseudo-static acceleration, a_v = vertical pseudo-static acceleration (assumed here = 0), W = weight of the failure mass, ψ_p = angle of planar failure surface, g = gravitational acceleration, l = the length of the failure plane, and k_h and k_v = dimensionless horizontal and vertical pseudo-static accelerations.

In relation to the earthquake phenomena Kramer (1996) postulate that the horizontal pseudo-static force decreases the factor of safety by reducing the resisting force and increasing the driving force. The vertical pseudo-static force typically has less influence on the factor of safety since it reduces (or increases, depending on its direction) both the driving force and the resisting force. As a result, the effects of vertical accelerations are frequently neglected in pseudo-static analyses resolving the forces on the potential failure mass in a direction parallel to the failure surface.
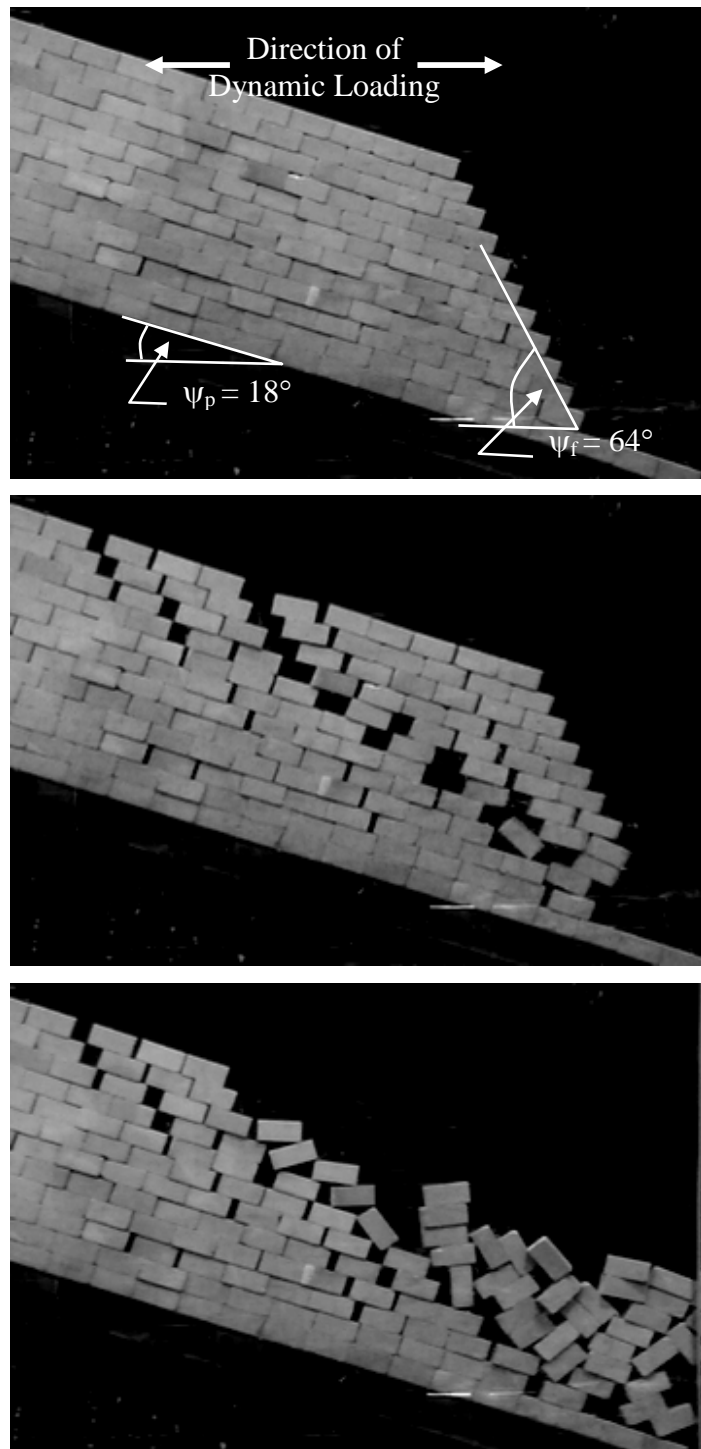
Figure 4.18. Simulation of sliding failure for 8×4 cm blocks at a = 0.046 g and

amplitude = 23.5 mm.

In this study the vertical pseudo-static acceleration (a_v) is assumed to be zero, subsequently the vertical inertial force (F_v) becomes zero. This assumption conforms to Kramer's conclusion above. The above equation is therefore reduced to:

$$FS = \frac{c \cdot l + [W \cos \psi_p - F_h \sin \psi_p] \tan \phi}{(W \sin \psi_p + F_h \cos \psi_p)} \qquad (4.10)$$

4.6.2 Calculation results

By setting FS=1, the relationship between the acceleration, a, and the angle of the failure plane, ψ_p, can be developed. Under this condition the acceleration required to induce plane failure for a rock slope decreases with increasing failure plane angle (Figures 4.19 and 4.20). Figure 4.19 shows how the acceleration decreases with increasing the failure plane angle under various joint cohesions with a constant friction angle of 26 degrees. The joint cohesion is equal to zero in Figure 4.20 while the friction angles vary from 15 to 35 degrees. Results of the test models under dynamic loading are plotted in terms of the acceleration as a function of the sliding plane angle in Figure 4.21. A failure envelope (line separating the stable and failure conditions) can be drawn from the test results for each block size, and is compared with the results from the deterministic method using FS=1. It is clearly shown that the deterministic method significantly over-estimates the actual observations. Under the same sliding plane angle the deterministic solution gives the acceleration at failure at more than twice of those observed from the test models. This is probably because the deterministic method assumes a rigid and continuous mass of rock above the incipient sliding plane while the slope models are formed by
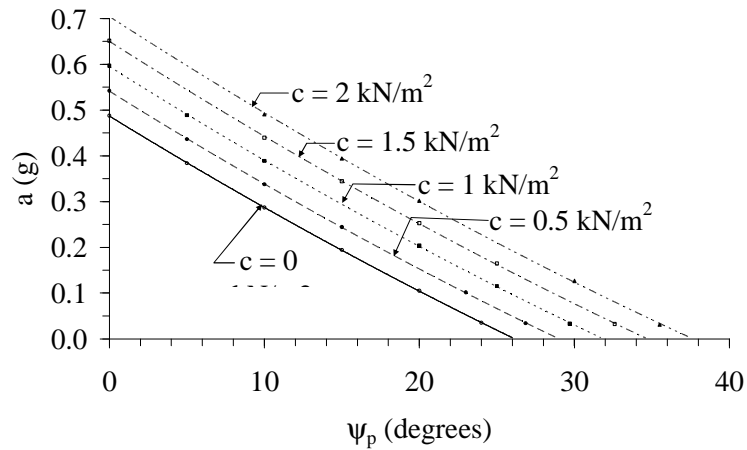
Figure 4.19 Pseudo-static acceleration (a) that induces plane failure as a function of sliding plane angle (ψ_p) for various joint cohesions, for $\phi = 26°$.
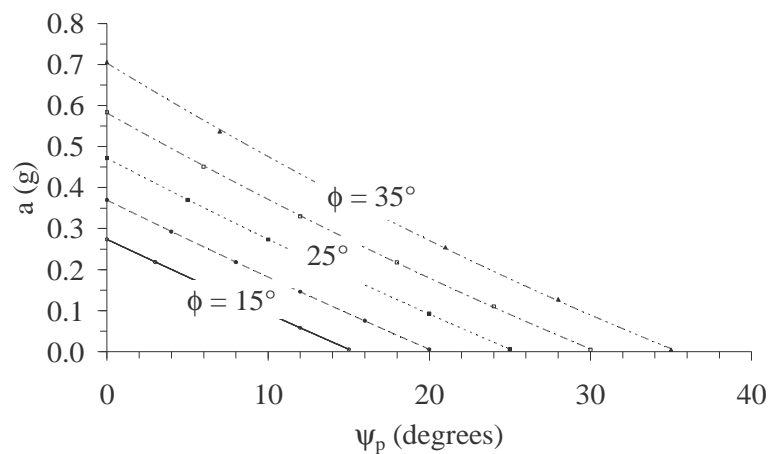
Figure 4.20 Pseudo-static acceleration (a) that induces plane failure as a function of sliding plane angle (ψ_p) for various joint friction angles, for cohesion = 0.053 kPa.
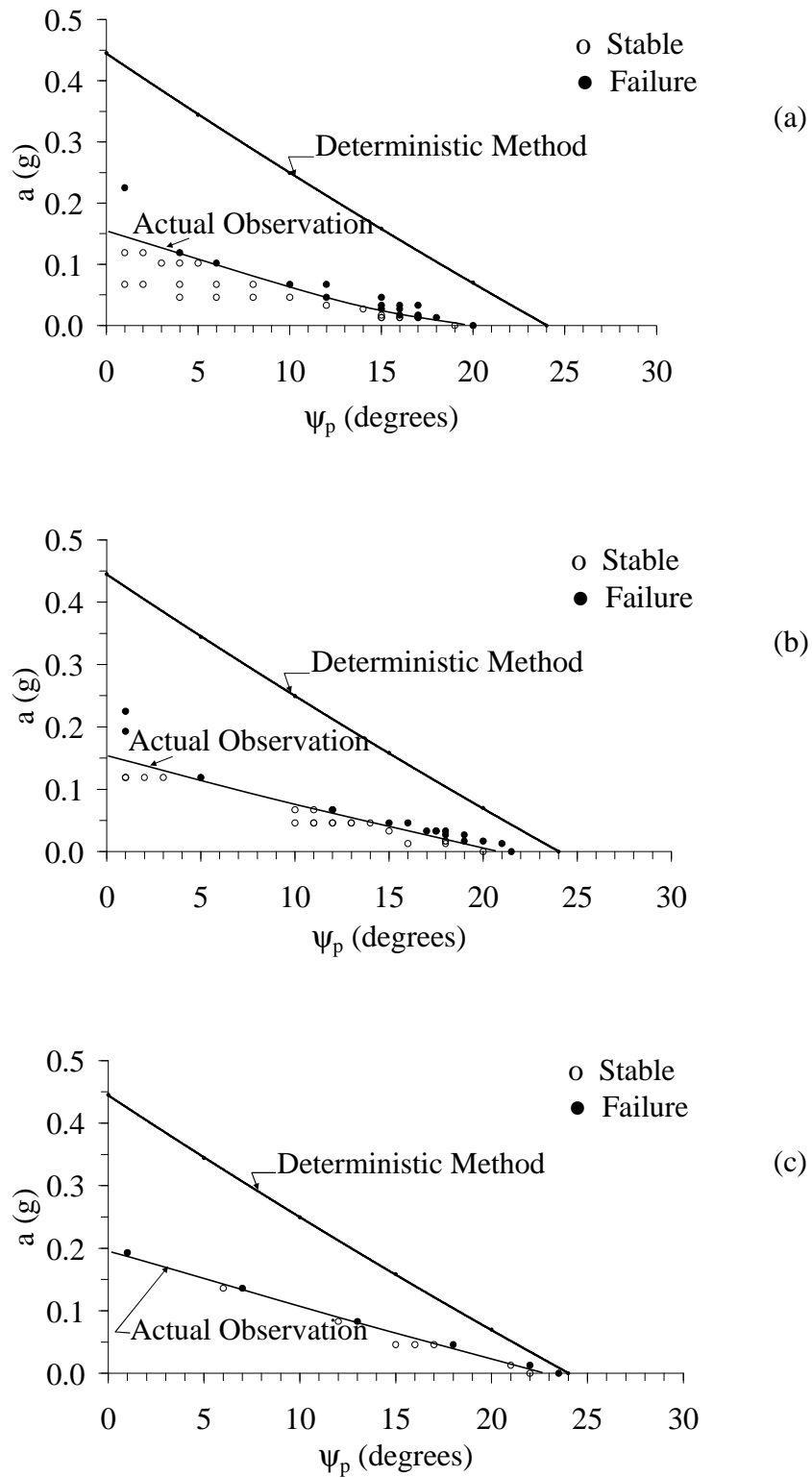
Figure 4.21 Pseudo-static acceleration (a) as a function of sliding plane angle (ψ_p) at failure for 4×4 cm (a), 8×4 cm (b), and 12×4 cm (c) blocks.

discrete rock blocks. The deterministic method also assumes that all relevant forces pass through the centroid of the sliding mass. The presence of interaction forces between the blocks in the slope model could enhance the shape effect of the individual blocks above the sliding plane. This behavior may be better demonstrated by a discrete element analysis that can incorporate the effect of dynamic loading. The discrepancy between deterministic method and test models becomes greater for a lower sliding plane angle, and particularly for the slope models formed by short blocks (4×4×4 cm). In addition the acceleration required to fail slope models with the shorter blocks tends to be lower than those with longer ones (4×4×8 cm and 4×4×12 cm).

CHAPTER V

FINITE DIFFERENCE ANALYSIS

5.1   Introduction

This chapter describes the method and results of finite difference simulation for the slope models under dry and submerged conditions. The results are compared with those of the model test observations to reveal the predictability of the numerical simulation and the performance of the physical modeling.

5.2   Finite difference simulation of plane sliding failure under dry and submerged condition

Finite difference analyses using FLAC_Slope code (Itasca, 1992) have been performed to calculate the factor of safety of some slope models. Twelve finite difference models have been constructed to represent the physical model geometry. For the dry condition, the simulations use the sliding plane angle of 25 degrees with slope heights varying from 21 to 70 cm, and slope face angles from 51 to 72 degrees. Under submerged condition the sliding angles are taken as 20 to 23 degrees, with slope heights varying from 52 to 58 cm, slope face angles from 48 to 68 degrees, and water level heights (H_w) from 30 to 69 cm. For all simulations the friction angle is maintained constant at 26 degrees with cohesion equal to 0.053 kPa. The results are compared with those observed from the physical model tests. Figures 5.1 and 5.2 show examples of the shape the failure zone from the numerical simulation results
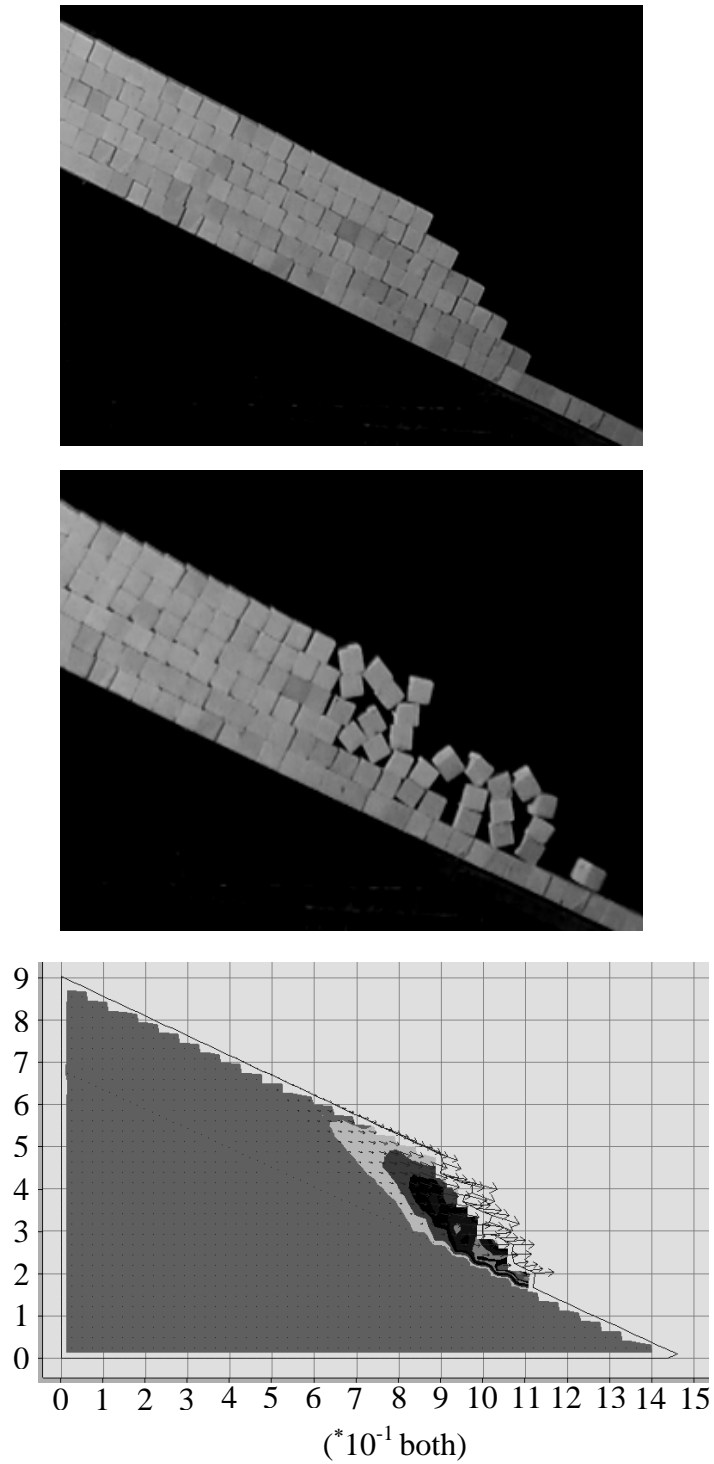
Figure 5.1 Comparison of FLAC simulation with physical model testing for

$4 \times 4 \times 4$ cm block for $\psi_p = 25°$, $\psi_f = 51°$, slope height = 36.2 cm,

and factor of safety = 1.07.
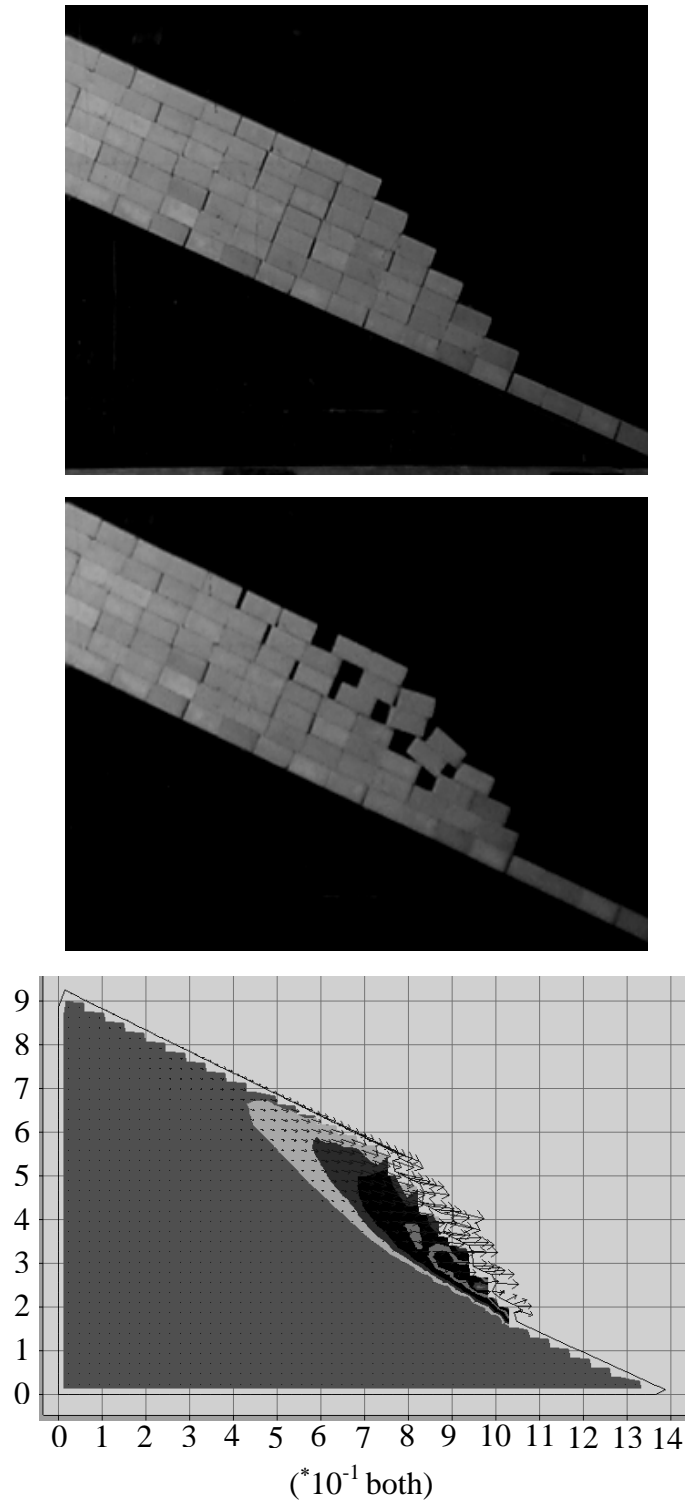
Figure 5.2 Comparison of FLAC simulation with physical model testing for

$4\times4\times8$ cm block for $\psi_p = 25°$, $\psi_f = 52°$, slope height = 41.6 cm,

and factor of safety = 1.05.

with the slope model observations for 4×4×4 cm 4×4×8 cm block size under dry condition. Figure 5.3 compares the shape of failure zone from the numerical simulation results with the slope model observations under dry and submerged conditions. The FLAC_Slope can well predict the shape and extent of the failure zone with the factor of safety close to those observed from the tested models.

Figure 5.4 compares the factors of safety calculated by FLAC code and by deterministic method with those of the physical model tests for the same slope geometry under dry condition. The factor of safety of 1.0 is taken to represent the condition at which failure occurs in the slope models. Assuming that the plane sliding mechanism follows the Coulomb criterion, the deterministic method uses an equation modified from Hoek & Bray (1981) to calculate the factor of safety (equation 4.4).

The results from the three methods agree reasonably well. Very small discrepancies remain. Under dry condition, the deterministic method yields the highest factor of safety, which is about 10% greater than those observed from the test models. The factors of safety from FLAC simulations are less than 5% greater than the observations. This may be because the deterministic method assumes that the sliding block is a single and rigid mass lying on an incipient failure plane while the actual test models are a discontinuous mass formed by rock blocks. The discrepancies become even smaller for a greater slope face angle.
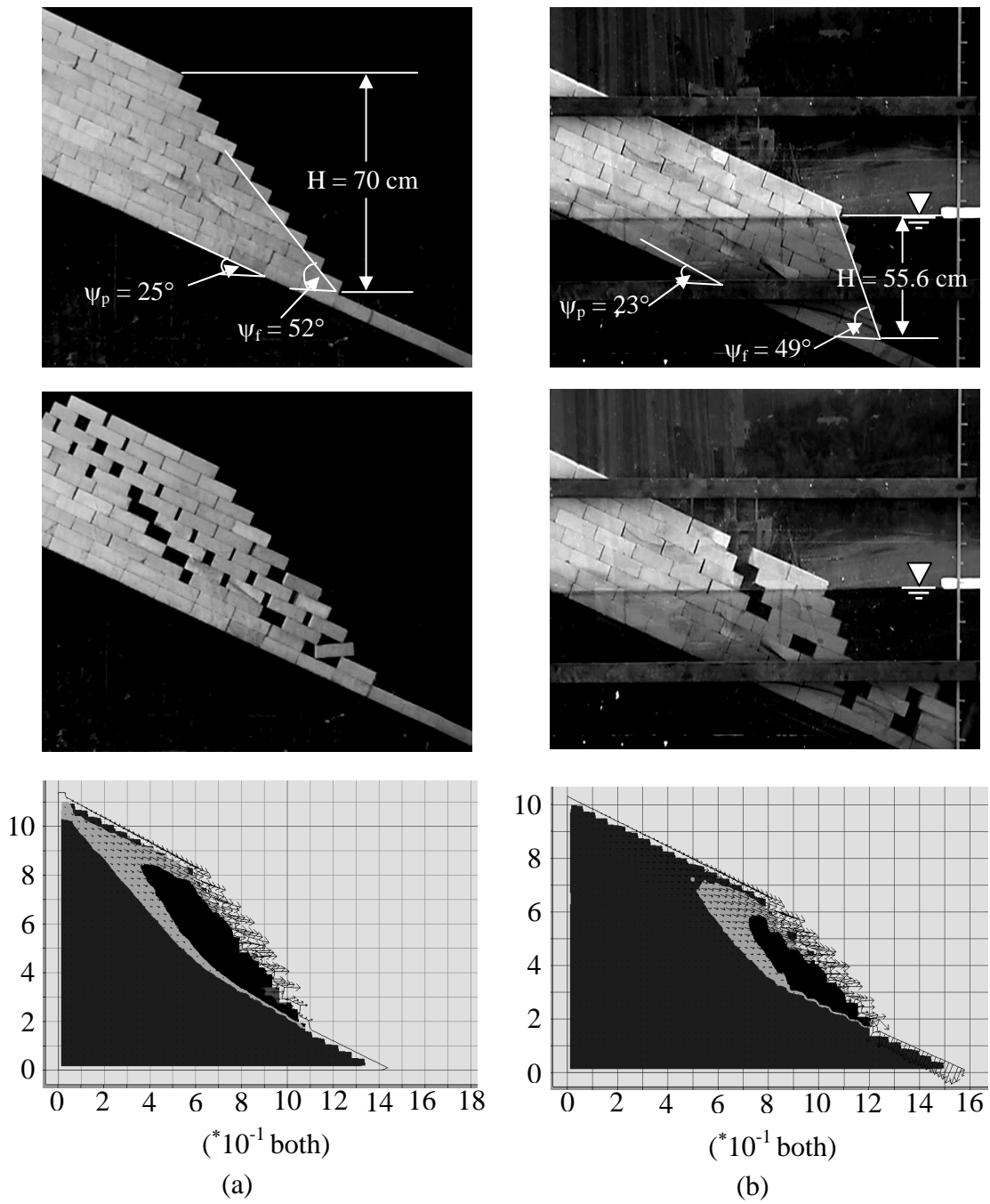
Figure 5.3 Comparison of FLAC simulations with physical model tests for 4×4×12 cm blocks under dry condition (a) and submerged condition (b).
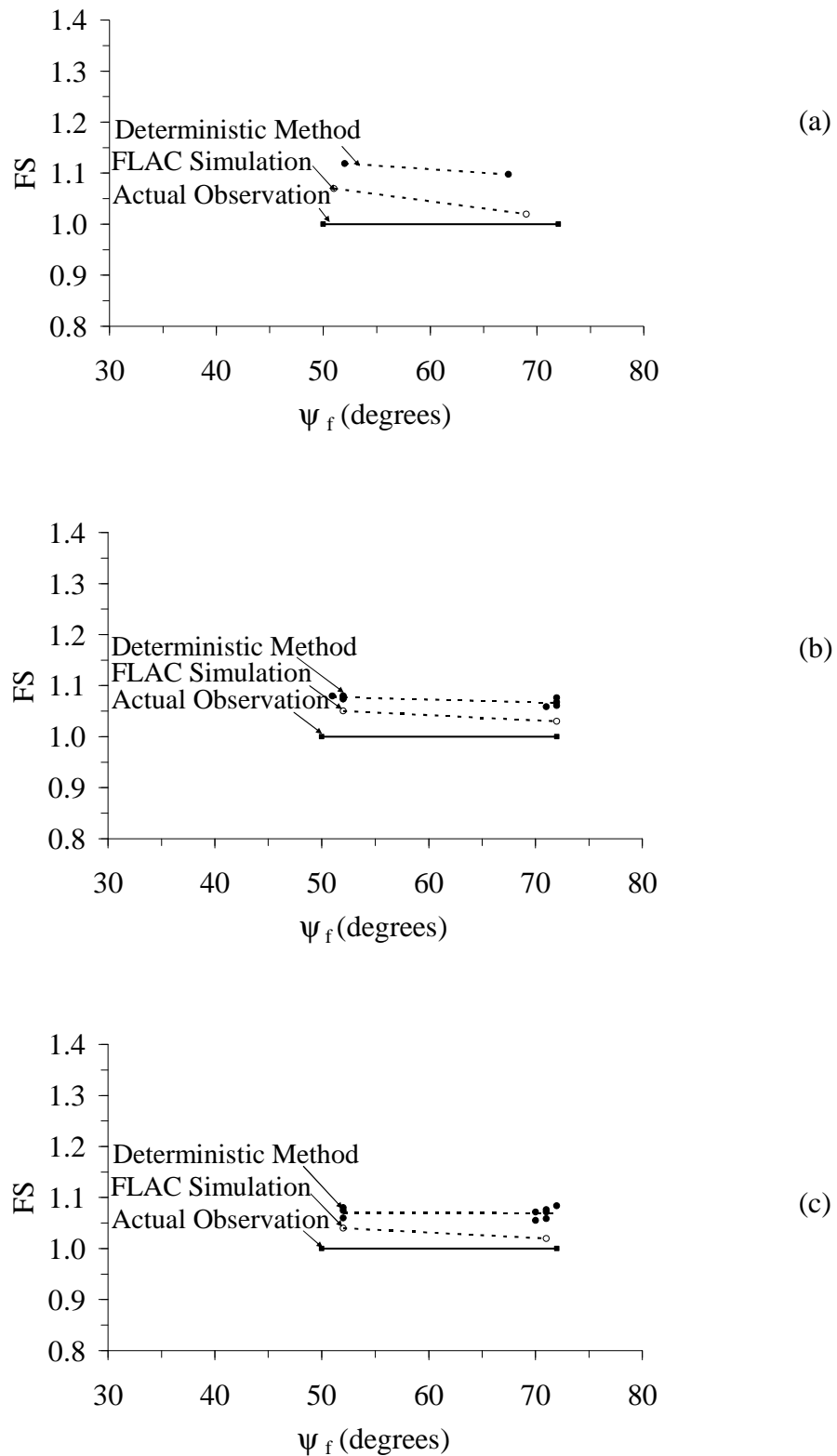
Figure 5.4 Factors of safety determinated for 4×4×4 cm blocks (a), 4×4×8 cm

blocks (b), and 4×4×12 cm blocks (c) at ψ_p equal 25 degrees.

CHAPTER VI

DISCUSSIONS, CONCLUSIONS, AND

RECOMMENDATIONS FOR FUTURE STUDIES

6.1   Discussions

The simulation results indicate that the deterministic method of Hoek and Bray over-estimates the stability conditions of actual slope models under the test parameters used here. This is probably due to the assumption of the uniform load and shear on the incipient sliding plane used in the calculation. It does not imply here that the deterministic method is entirely not conservative for plane sliding analysis. One should realize that the simulated plane sliding here is under overly-simplified conditions, e.g. smooth joint with effectively no cohesion, continuous and easily detached joint planes, and truly friction free on the released surfaces. This means that under more realistic or different test parameters and conditions the deterministic method may perform better in describing the factor of safety of the plane sliding models.

The comparisons of the test results with the deterministic solutions (by Hoek and Bray, 1981) and computer simulations (FLAC_Slope code) under the same test parameters (e.g., joint properties and slope characteristics) have revealed significant implications.   Under static condition the deterministic method and computer simulation over-estimate the factor of safety for the plane sliding failure by about 5 to

10%, particularly for the slope models with shorter blocks. This is probably due to the impacts of the block spacing, block shape and interaction forces between the discrete blocks in the sliding mass. This implies that stability analysis by assuming that the sliding mass is continuous as used by the deterministic method may not be conservative, particularly for slope masses with short-spaced joints compared to the slope height.

6.2   Conclusions

A test platform has been constructed for use in the simulation of scaled-down rock slope models comprising sets of cubical or rectangular sandstone blocks. True gravitational force is used to initiate the failure. Observations of the failure behavior during video playback reveal that for plane sliding the failure is initiated near the slope toe. The failure occurs at sliding plane angles (ψ_p) considerably lower than those determined from the tilt test and deterministic method, particularly for the slope models comprising shorter blocks. This is probably because the deterministic method assumes uniform normal load and shear force along the sliding plane while these loads in the slope models largely concentrate near the slope toe and virtually zero near the upper slope face. This also implies that shorter blocks (cubical shaped) slide easier than do longer ones (rectangular shaped) even though they have the same spacing (block height). For block toppling, the slope height at failure increases with decreasing the base plane angle (ψ_p) and slope face angle (ψ_f). The observed zone of instability agrees well with that determined by Hoek and Bray's method. Based on the failure behavior observed during video playback, the physical model performs

well in simulating the plane sliding and toppling under the simplified joint characteristics and spacing.

The discrepancy between the deterministic method and the test results under dynamic loading is highly significant. The deterministic solution proposed by Kramer (1996) over-estimates the acceleration at failure by more than twice those observed from the test models. The discrepancy however reduces for slope models formed by larger sandstone blocks and under a greater sliding plane angle. This is again probably due to the assumption of the continuous mass imposed by the deterministic method. These findings indicate that under dynamic loading plane sliding analysis using the simple deterministic method for rock slopes with small joint spacing compared to the slope height will give a non-conservative result. In addition, the deterministic approach for stability analysis of low-angled sliding planes under dynamic loading may be inappropriate. In this case an additional physical model testing or discrete element analysis that is capable of dynamic simulation should be performed.

6.3   Recommendations for future studies

The physical models tested here have a narrow range of the size and shape of the rock blocks used to simulate the joint spacing in the test frame. Additional test results obtained from slope models with larger blocks, probably up to 20×20 cm, and with smaller blocks, 2×2 cm, would provide a clearer indication of the effect of joint spacing on slope stability. More testing is required to assess the effects of surface roughness, submerging condition and static acceleration. Studying the impact of joint roughness determined from the physical test models is also desirable. It would reveal

the adequacy or inadequacy of the deterministic methods and the sensitivity of the induced acceleration to the joint roughness. This may be experimentally assessed by using cast cement blocks with various degrees of pre-defined roughness on the surfaces.

REFERENCES

Barton, N. R. (1973). Review of a new shear strength criterion for rock joints. **Engineering Geology**. 7: 287-332.

Bhasin, R. and Kaynia, A. M. (2004). Static and dynamic simulation of a 700-m high rock slope in western Norway. **Engineering Geology**. 71: 213-226.

Bray, J. W. and Goodman, R. E. (1981). The theory of base friction models. **International Journal of Rock Mechanics and Mining Science and Geomechanics**. 8(6): 453-468.

Crawford, A. M. and Curran, J. H. (1982). The influence of rate- and displacement-dependent shear resistance on the response of rock slopes to seismic loads. **International Journal of Rock Mechanics and Mining Science & Geomechanics**. 19(1): 1-8.

Fuenkajorn, K. and Kamutchat, S. (2001). Rock slope design using expert system: ROSES program. **6th Mining, Metallurgical, and Petroleum Engineering Conference**. Chulalongkorn University, Bangkok.

Fuenkajorn, K. and Kamutchat, S. (2003). Neural Network for Rock Slope Stability Evaluation. In **Proceedings of the 4th Regional Symposium on Infrastructure Development in Civil Engineering** (pp. 655-664). Bangkok.

Gendzwill, D. (2008). **Glossary of Seismic Techniques and Terminology**. [On-line]. Available: http://www.usask.ca/geology/labs/seismo/glossary.html

Giani, G. P. (1992). **Rock Slope Stability Analysis**. Rotterdam: A. A. Balkema.

Gondzwill, d. (2008). Glossary of seismic techniques and terminology. **University of Saskatchewan**. Canada.

Goodman, R. E. (1976). **Models of Geological Engineering in Discontinuous Rock**. St Paul, Minnesota: West Publishing Company.

Goodman, R. E. (1989). **Introduction to Rock Mechanics**. New York: John Wiley and Son. 562 pp.

Goodman, R. E. and Shi, G. H. (1985). **Block Theory and Its Application to Rock Engineering**. New Jersey: Prentice-Hall, Inc. 338 pp.

Gutenberg, B. and Richter, C. F. (1956). Earthquake magnitude: intensity, energy, and accleration. **Bulletin of The Seismological Society of America**. 46: 104-145.

Hittinger, M. (1978). **Numerical Analysis of Toppling Failures in Jointed Rock**. Ph.D. Thesis, University of California, Berkeley, USA.

Hoek, E. (1968). Brittle failure of rock. Rock Mechanics in Engineering Practice. **Edited by K.G. Stagg and O.C. Zienkiewicz, Published by J. Willey**, London. pp 99-124.

Hoek, E. (2000). **Factor of Safety and Probability of Failure**. [On-line]. Available: http: www.rocscience.com/roc/ Hoek/Hoeknotes2000.htm

Hoek, E. and Bray, J. W. (1981). **Rock Slope Engineering**, **3rd edition**. London: Institute of Mining and Metallurgy.

Hu, Y-X., Liu, S-C. and Dong, W. (1996). **Earthquake Engineering**. London: E & FN SPON, An Imprint of Chapman & Hall.

Kamutchat, S. (2004). **Rock Slope Design Using Expert System**. M. Eng. Thesis, Suranaree University of Technology, Nakhon Ratchasima.

Kemthong, R. (2006). **Determination of Rock Joint Shear Strength Based on Rock Physical Properties**. M. Eng. Thesis, Suranaree University of Technology, Nakhon Ratchasima.

Kim, Y. G. and Lee, H. K. (1992). Slope stability analysis in discontinuous rocks by base friction model test and its numerical analysis. **Regional Symposium on Rock Slopes**. India.

Kokusho, T. and Ishizawa, T. (2005). Energy approach for earthquake induced slope failure evaluation. **Soil Dynamics and Earthquake Engineering**. Article in press: 1-10.

Kramer, S. L. (1996). **Geotechnical Earthquake Engineering**. New Jersey: Prentice Hall.

Kumsar, H., Akgun, M. and Aydan, O. (1998). A Back Analysis of Circular Slope Failure at Pamukkale-Golemezli Irrigation Canal in Turkey. **Regional Symposium on Sedimentary Rock Engineering** 1998 (pp 197-203). Taipei, Taiwan: Pssre.

Kumsar, H., Aydan, O. and Ulusay, R. (2000). Dynamics and static stability assessment of rock slopes against wedge failures. **Rock Mechanics and Rock Eng**ineering. 33(1): 31-51.

Lanaro, F., Jing, L., Stephansson, O. and Barla, G. (1997). D.E.M. Modeling of laboratory tests of block toppling. **International Journal of Rock Mechanics and Mining Sciences**. 34(3-4): 173.

Landanyi, B. and Archambault, G. (1970). Simulation of shear behaviour of a jointed rock mass. In **Proceeding of 11ᵗʰ Symposium on Rock Mechanics, Published by AIME** (pp 105-125). New York.

Ladanyi, B. and Archambault, G. (1972). Evaluation de la resistance au cisaillement d'un massif rocheux fragmente. In **Proceeding of 24ᵗʰ International Geological Congress, (Montreal, 1972), Section 13D** (pp 249-260). Sweden: Division of Rock Mechanics Lulea University of technology.

Maugeri, M., Musumeci, G., Novita, D. and Taylor, C. A. (2000). Shaking table test of failure of a shallow foundation subjected to an eccentric load. **Soil dynamics and Earthquake Engineering**. 20: 435-444.

Patton, F. D. (1966). Multiple modes of shear failure in rock. In **Proceeding of 1 Congress International Society for Rock Mechanics** (vol. 1, pp. 509-513). Lisabon.

Richter, C. (1958). Elementary Seismology. **W. H. Freeman and Co.**, San Francisco.

Sard, D., Pasamehmetoglu, A. G. and Bozdag, T. (1997). Modelling of Earthquake Fault by A New Computer Controlled Direct-Shear apparatus. **International Journal of Rock Mechanics and Mining Sciences**. 34: 3-4, pp. 269.

Sarkar, I. and Chander, R. (2003). A simulation of earthquake induced undrained pore pressure changes with bearing on some soil liquefaction observations following the 2001 Bhuj earthquake. **Indian Academy of Sciences (Earth and Planetary Sciences)**. 112(3): 471-477.

Sepulveda, S. A., Murphy, W., Jibson, R. W. and Petley, D. N. (2005). Seismically induced rock slope failures resulting from topographic amplification of strong ground motions: The case of Pacoima Canyon, California. **Engineering Geology**. 80: 336-348.

Shamir, G., Baer, G. and Hofstetter, A. (2003). Three-dimensional elastic earthquake modelling based on integrated seismological and InSAR data: the Mw = 7.2 Nuweiba earthquake, gulf of Elat/Aquba 1995 November. **Geophysical Journal International**. 154: 731-744.

Siad, L. (2003). Seismic stability analysis of fracture rock slopes by yield design theory. **Soil and Earthquake Engineering**. 23: 203-212.

Simons, N., Menzies, B. and Matthews, M. (2000). **A Short Course in Soil and Rock Slope Engineering**. London: Thomas Telford.

Teme, S. C. (1987). Short contribution: A kinematic modeling machine for rock slope studies. **International Journal of Mining and Geological Engineering**. 5: 75-81.

Terzaghi, K. (1950). Mechanisms of landslides. In **Application of Geology to Engineering Practice**. **Geology Society of America**. Berkely, pp 83-123.

USGS. (2008). **Magnitudes Commonly used by Seismic Networks**. [On-line]. Available: http://earthquake.usgs.gov/eqcenter/glossary.php

Utkucu, M., Pinar, A. and Alptekin, O. (2002). A detailed slip model for the 1995, October 1, Dinar, Turkey, earthquake (Ms = 6.1) determined from inversion of teleseismic P and SH waveforms. **Geophysical Journal International**. 151: 184-194.

Wald, D. A., Quitoriano, V., Heaton, T. H. and Kanamori, H. (1999). Relationships between peak ground acceleration, peak ground velocity, and modified Mercalli intensity in California. **Earthquake Spectra**. 15: 557-564.

APPENDIX A

SIMULATION RESULTS OF ROCK SLOPE UNDER

STATIC LOAD
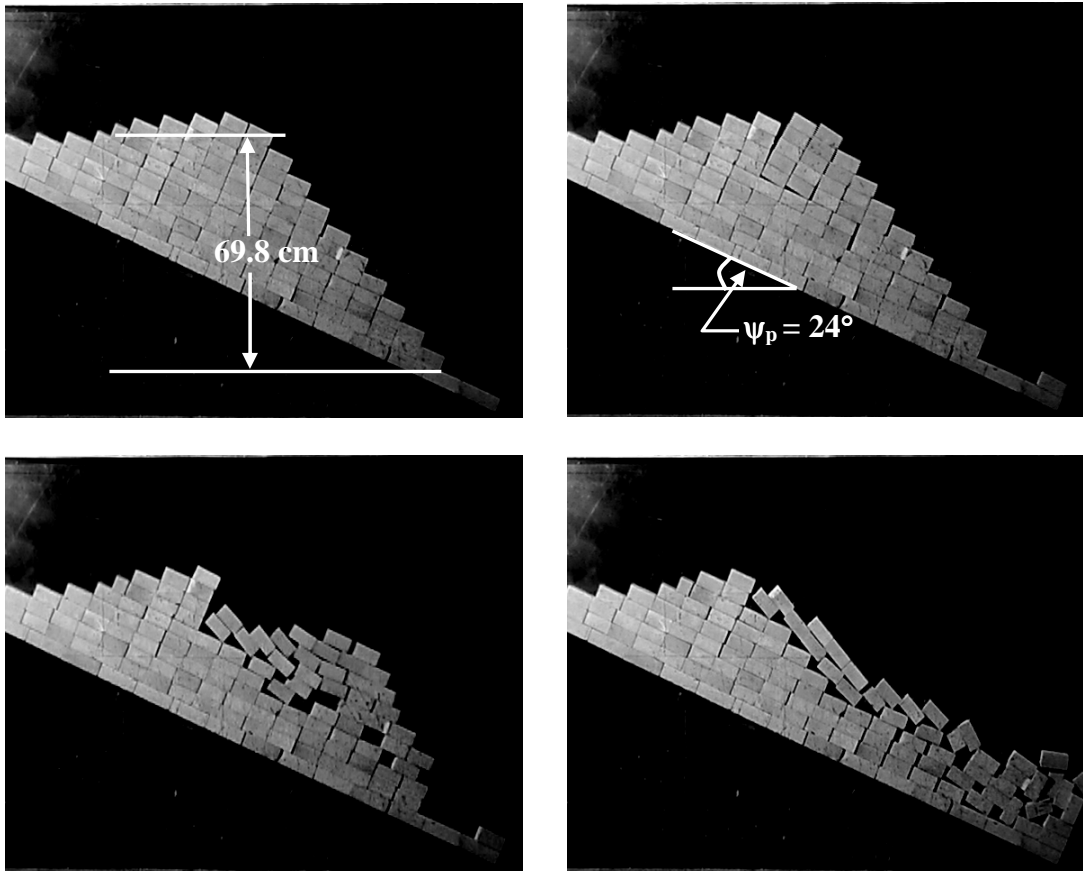
Figure A-1 Results of plane sliding failure simulation for 4×4×8 cm blocks

size at $\psi_f = 51°$.
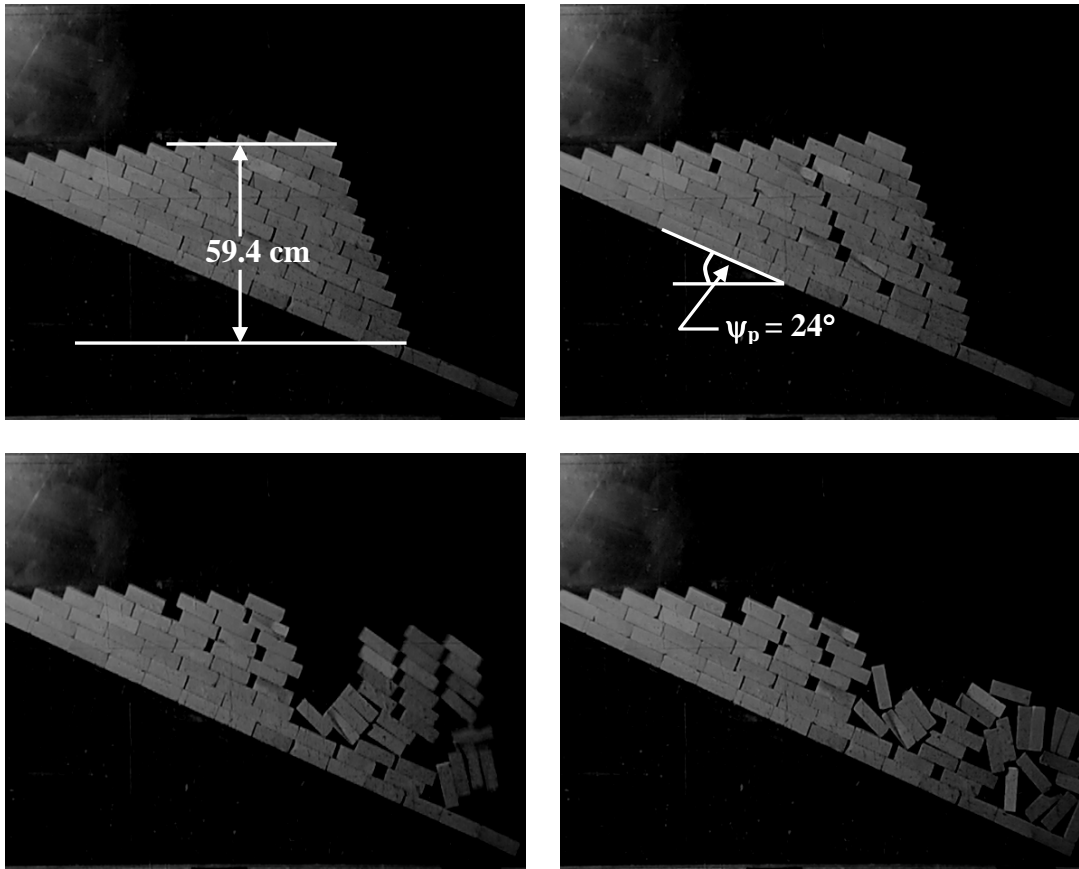
Figure A-2 Results of plane sliding failure simulation for 4×4×12 cm blocks

size at $\psi_f = 68°$.
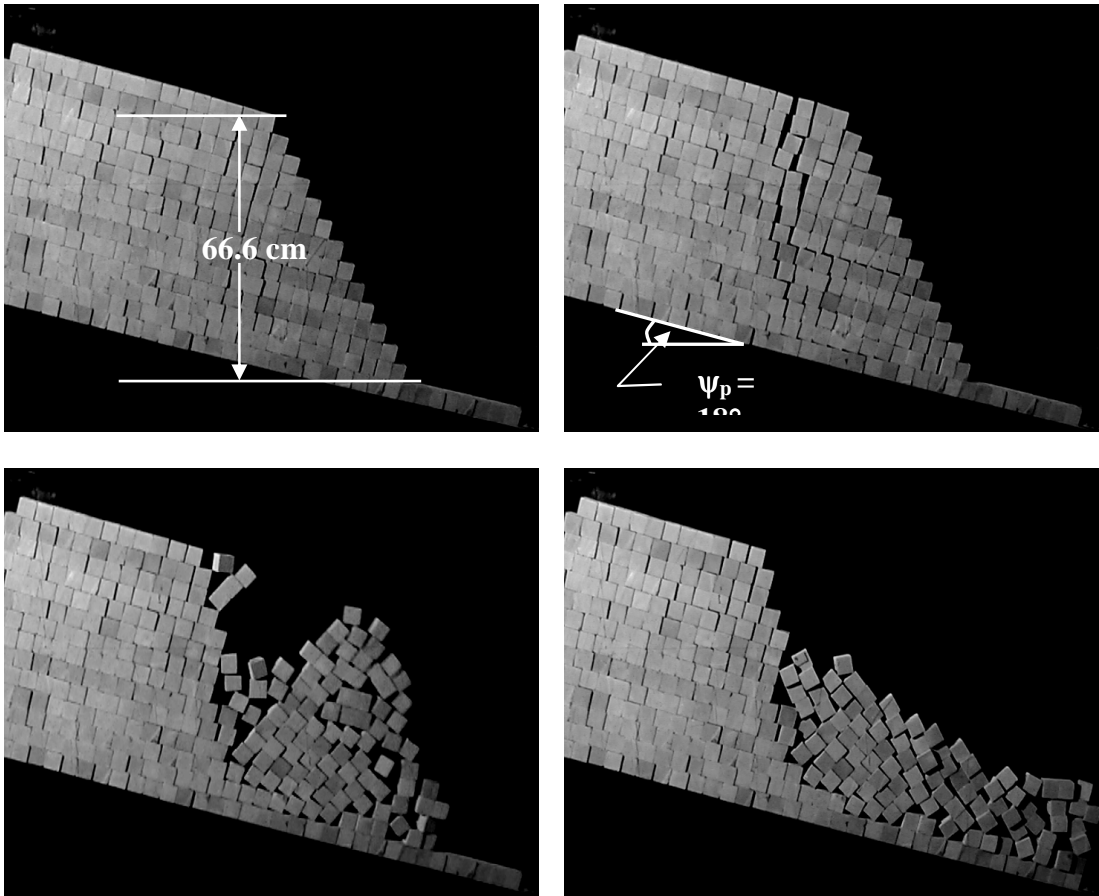
Figure A-3 Results of plane sliding failure simulation for 4×4×4 cm blocks size

at $\psi_f = 63°$.
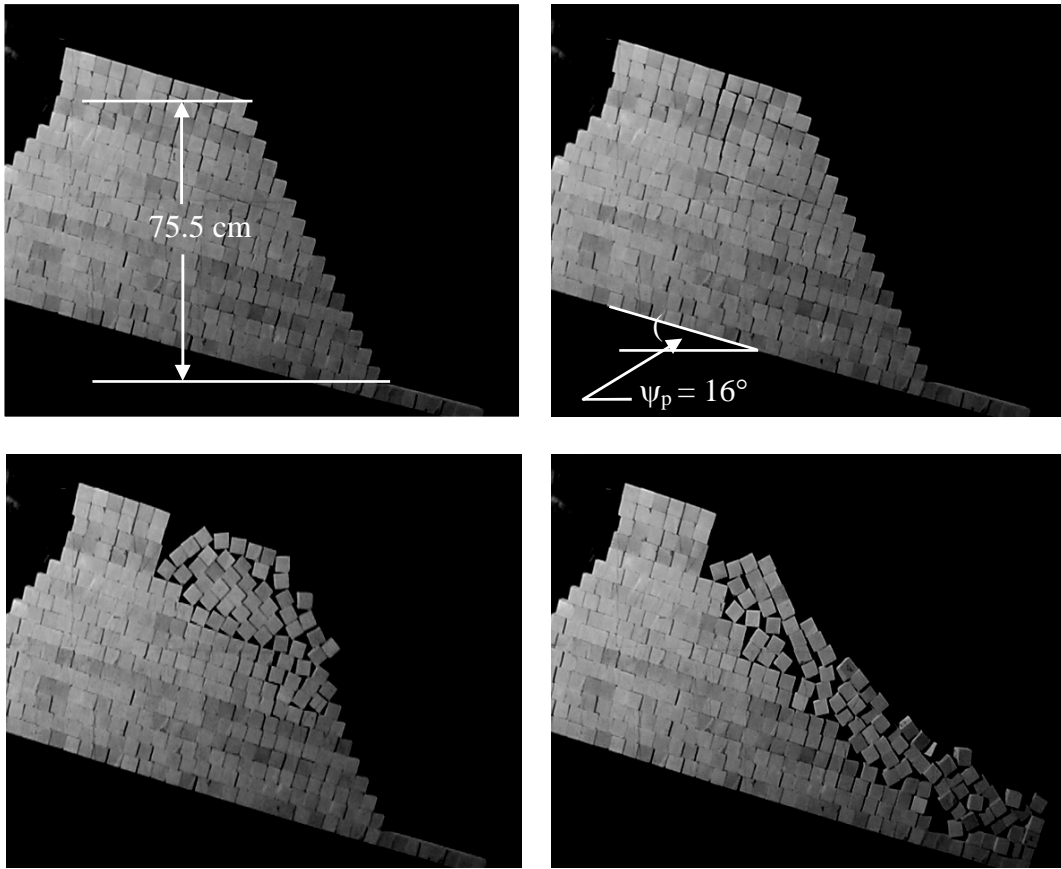
Figure A-4 Results of plane sliding failure simulation for 4×4×4 cm blocks size

at $\psi_f = 61°$.
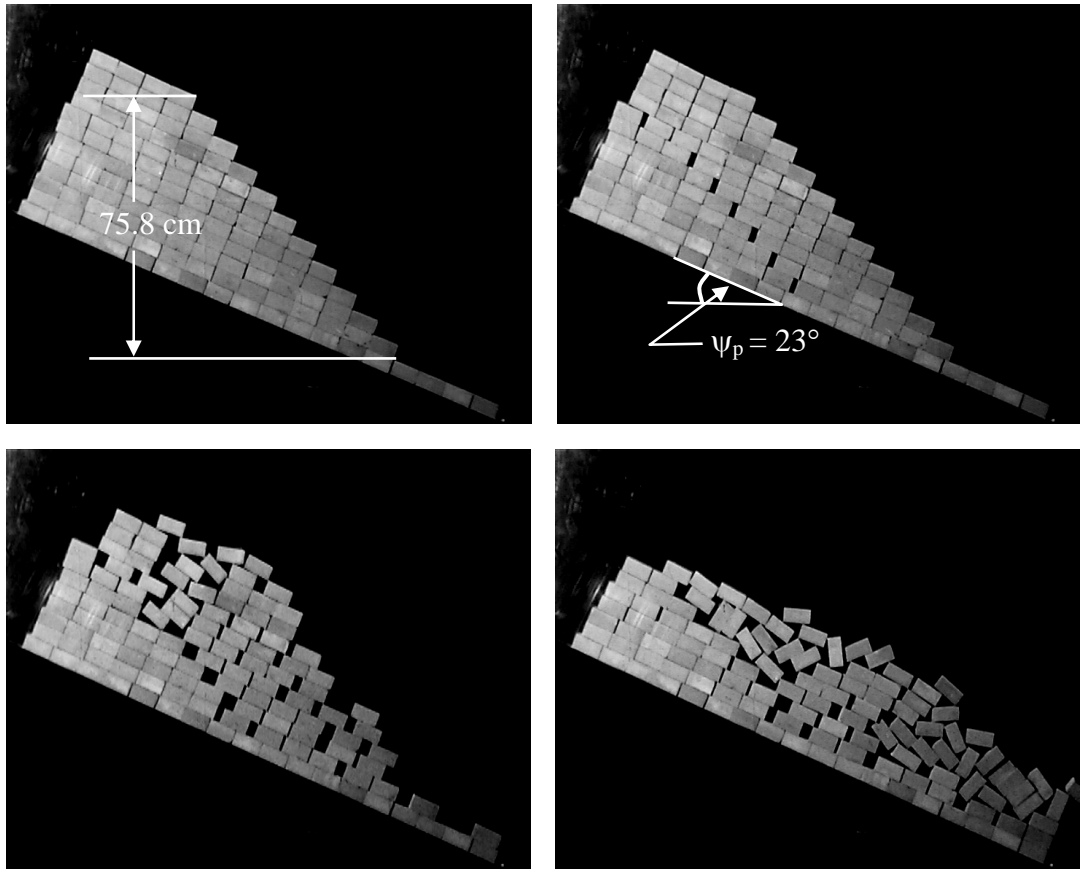
Figure A-5 Results of plane sliding failure simulation for 4×4×8 cm blocks size

at $\psi_f = 50°$.
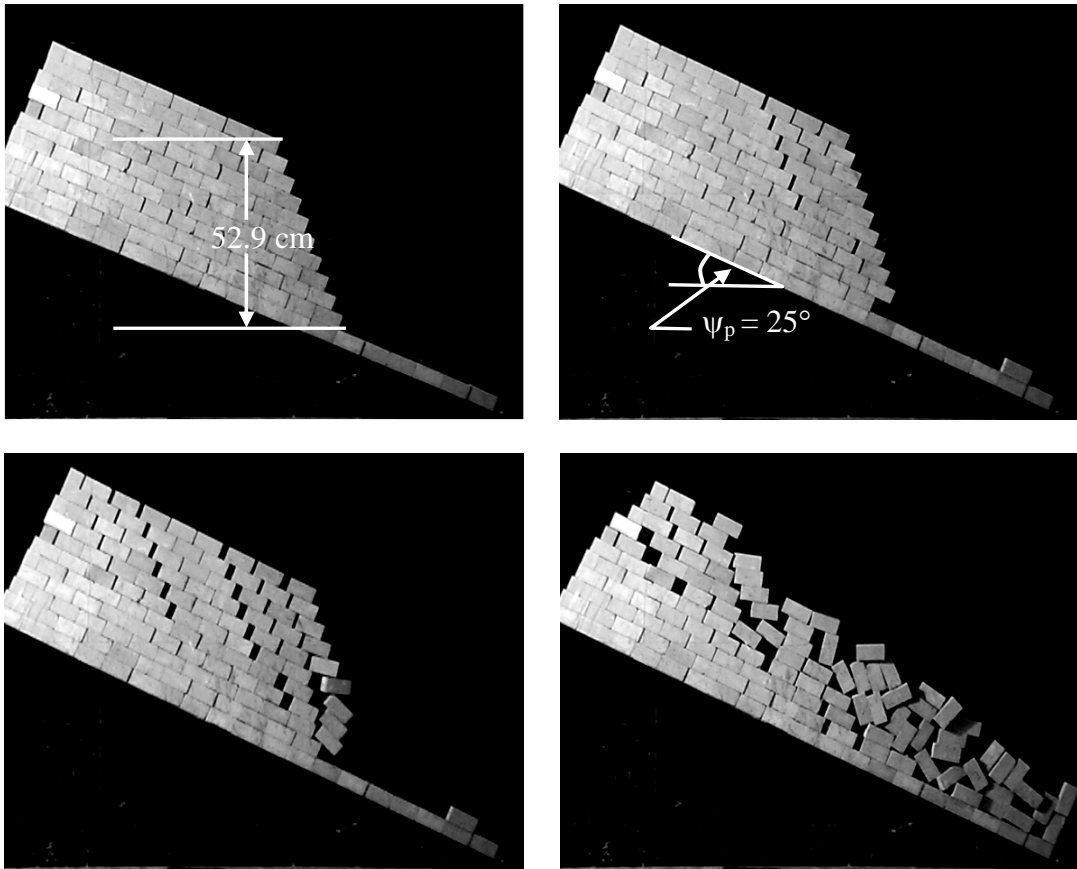
Figure A-6 Results of plane sliding failure simulation for 4×4×8 cm blocks size

at $\psi_f = 72°$.
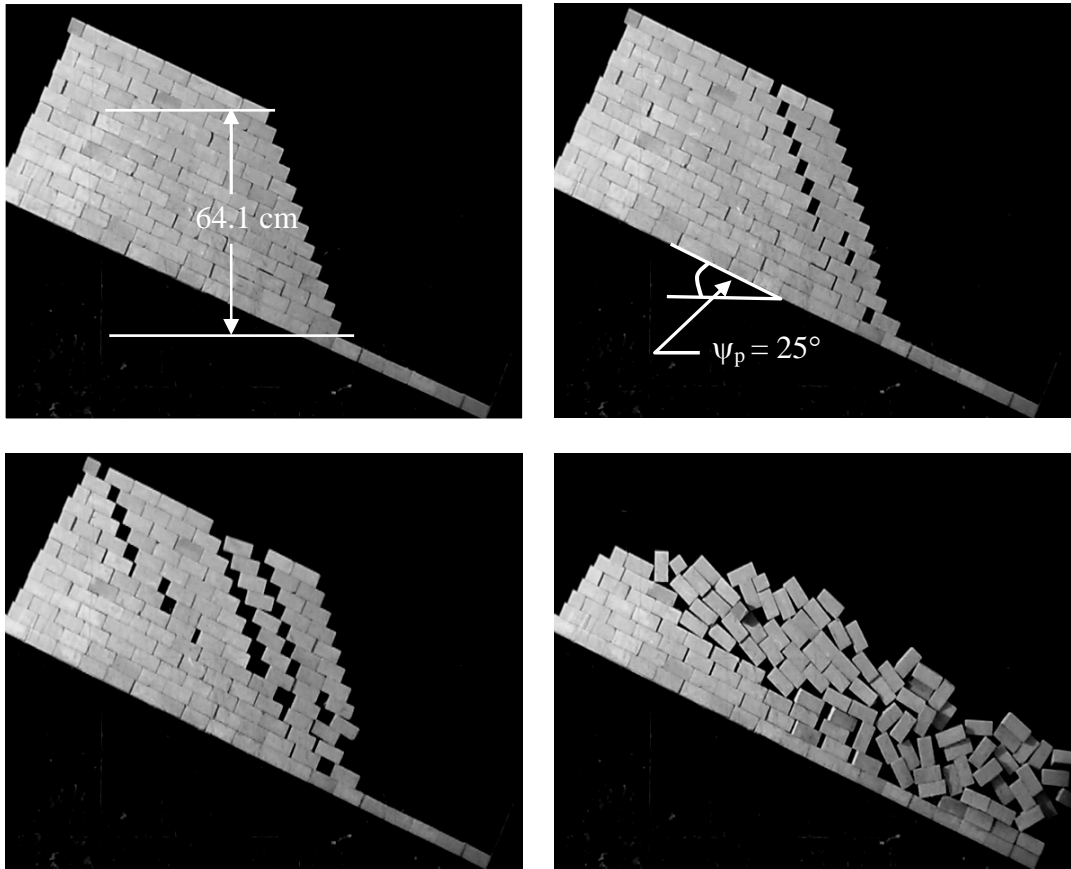
Figure A-7 Results of plane sliding failure simulation for 4×4×8 cm blocks size at

$\psi_f = 71°$.
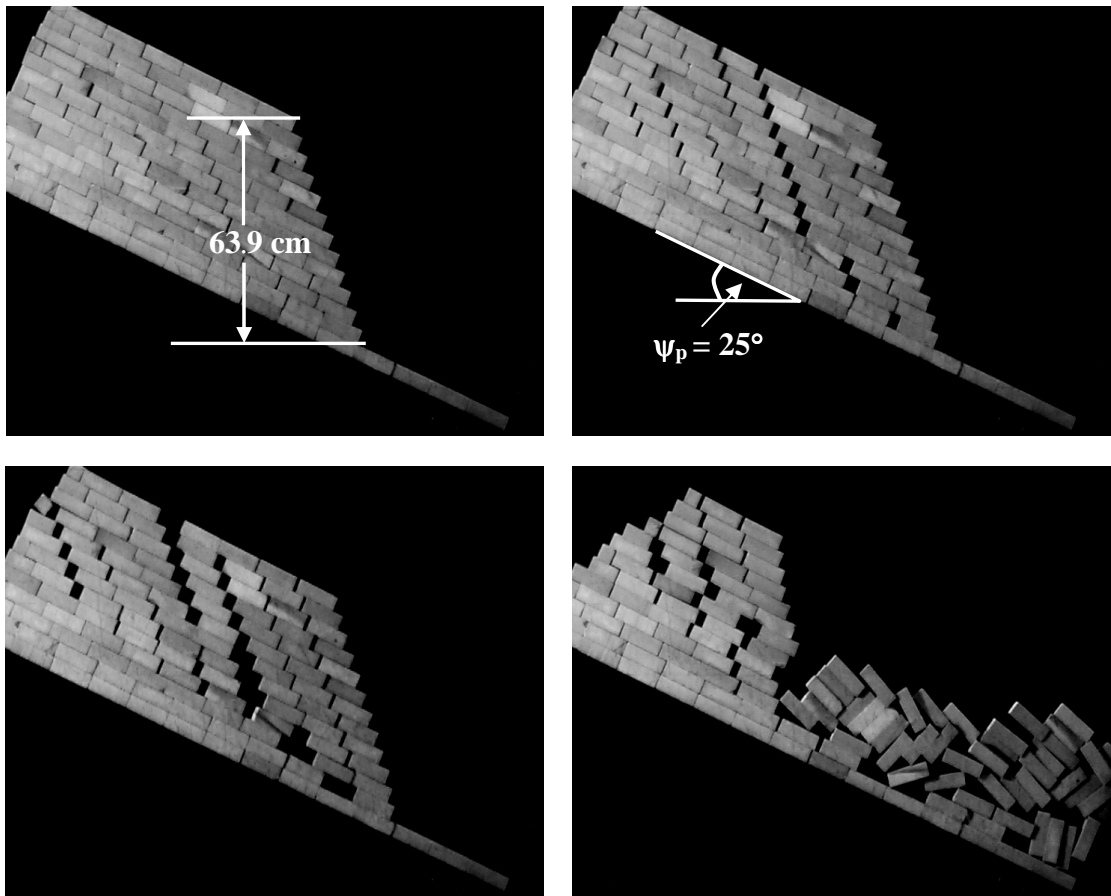
Figure A-8 Results of plane sliding failure simulation for 4×4×12 cm blocks
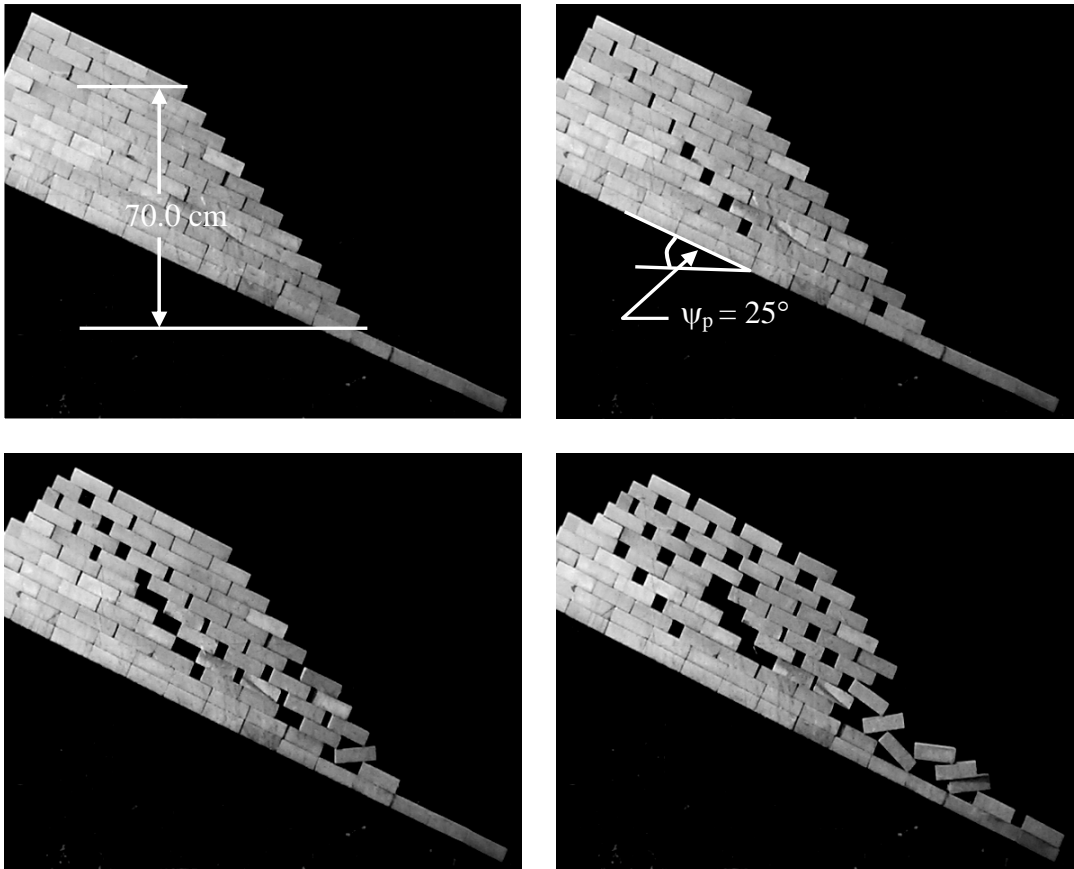
size at $\psi_f = 71°$.

Figure A-9 Results of plane sliding failure simulation for 4×4×12 cm blocks size
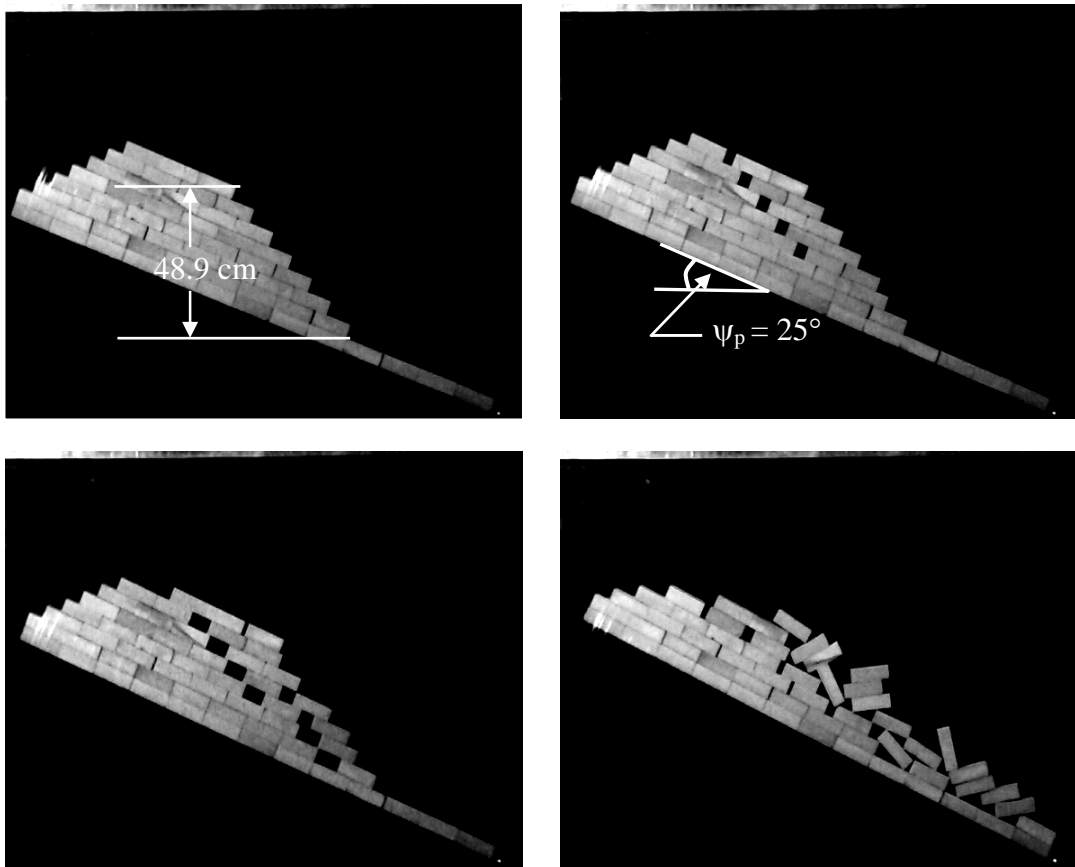
at $\psi_f = 52°$.

Figure A-10 Results of plane sliding failure simulation for 4×4×12 cm blocks size

at $\psi_f = 52°$.
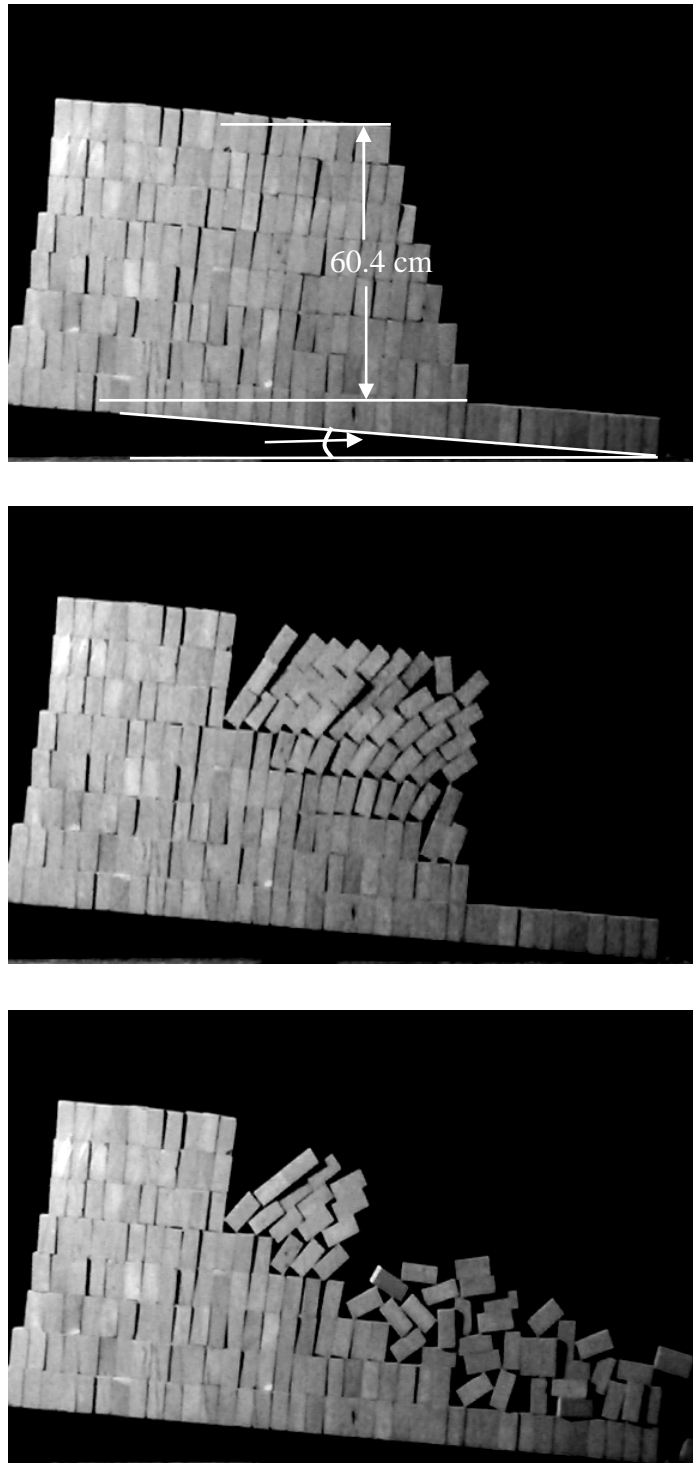
Figure A-11 Results of toppling failure simulation for 4×4×8 cm blocks size at ψ_f

$= 72°$.
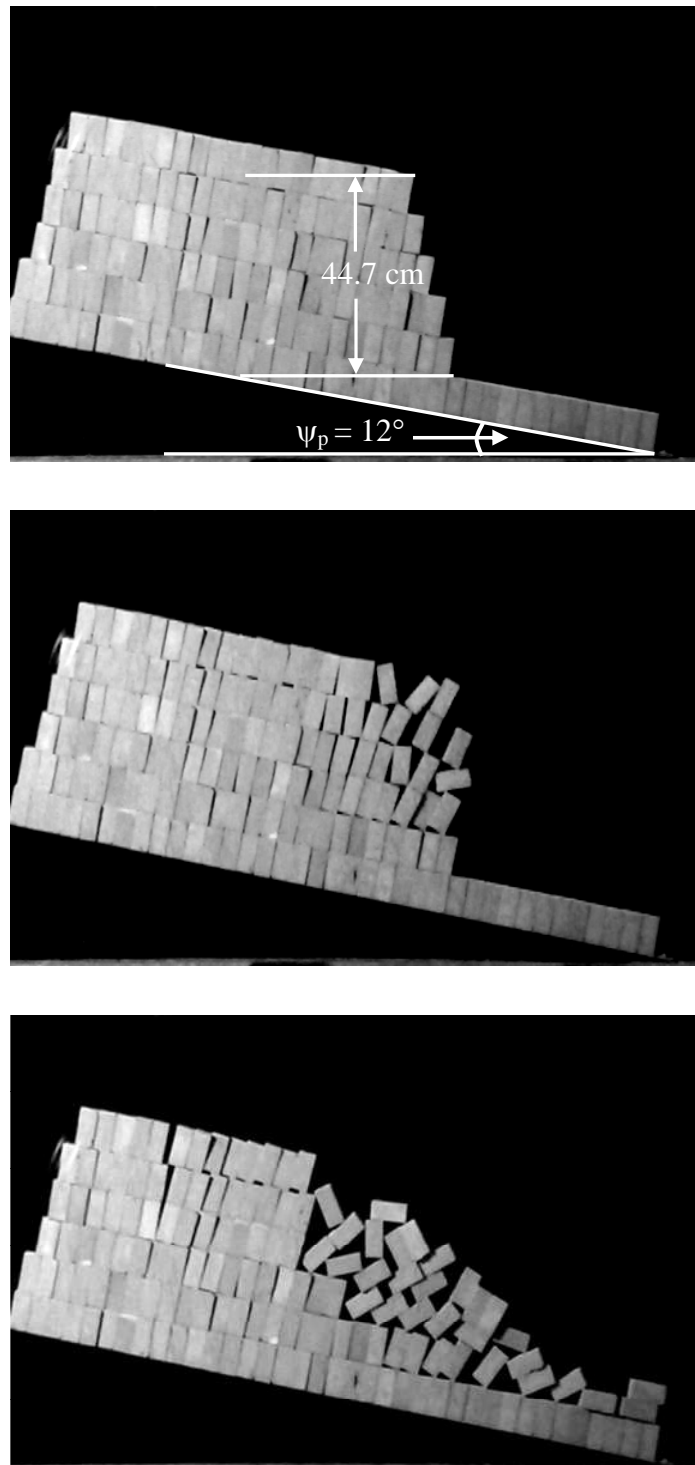
Figure A-12 Results of toppling failure simulation for 4×4×8 cm blocks size at ψ_f

$= 76°$.
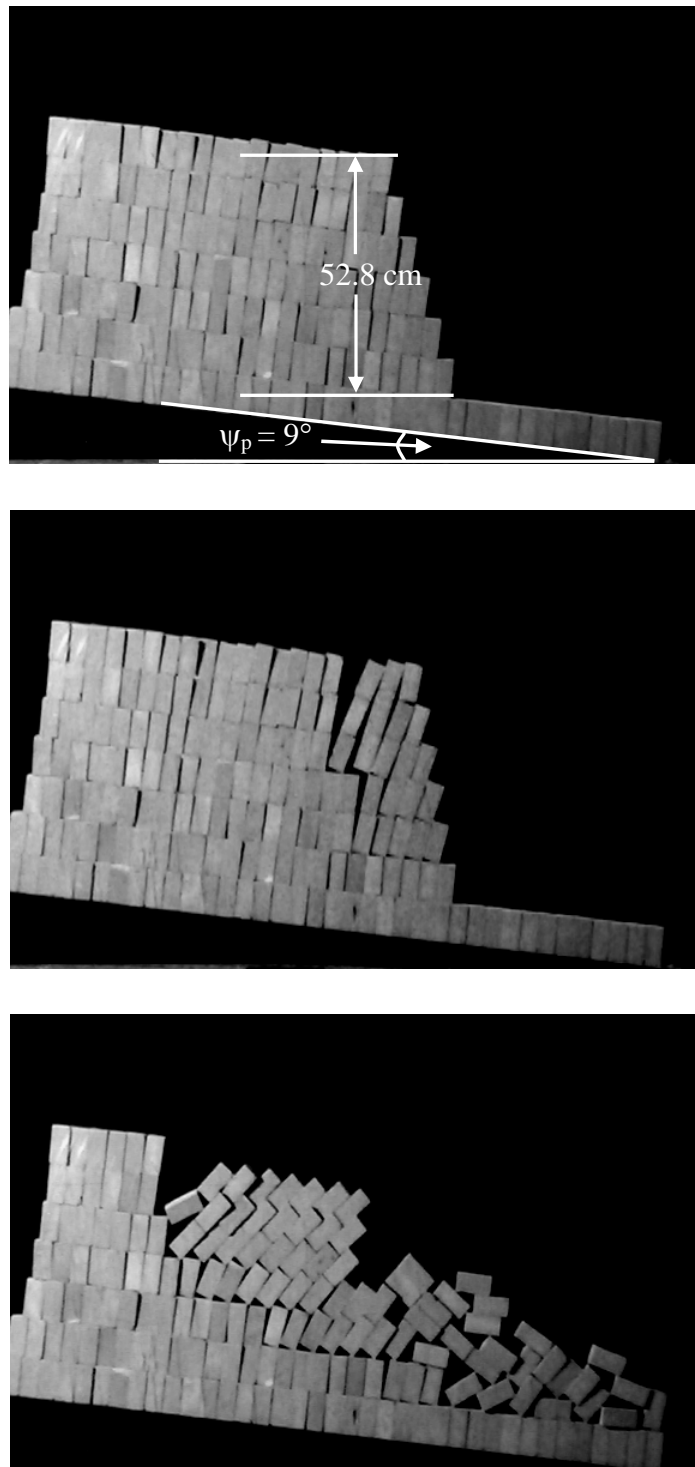
Figure A-13 Results of toppling failure simulation for 4×4×8 cm blocks size at ψ_f

= 73°.
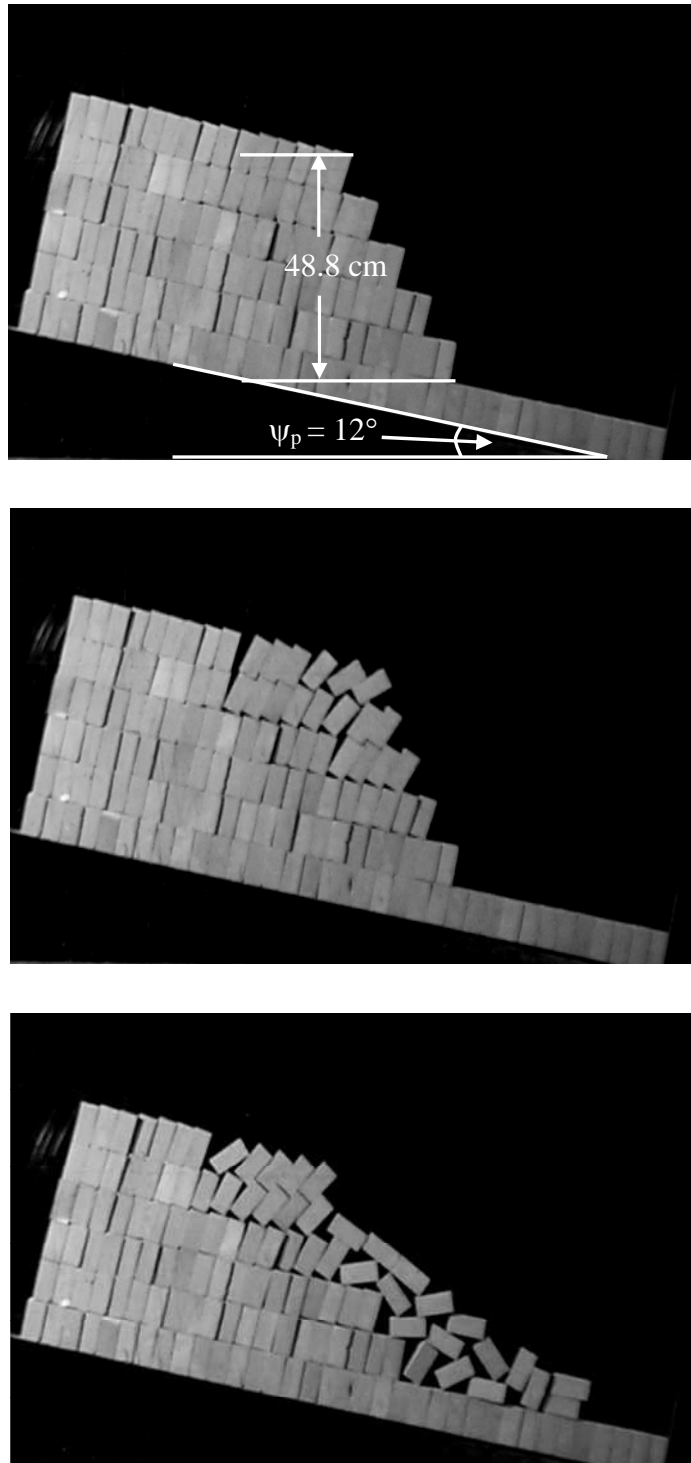
Figure A-14 Results of toppling failure simulation for 4×4×8 cm blocks size at ψ_f

= 57°.
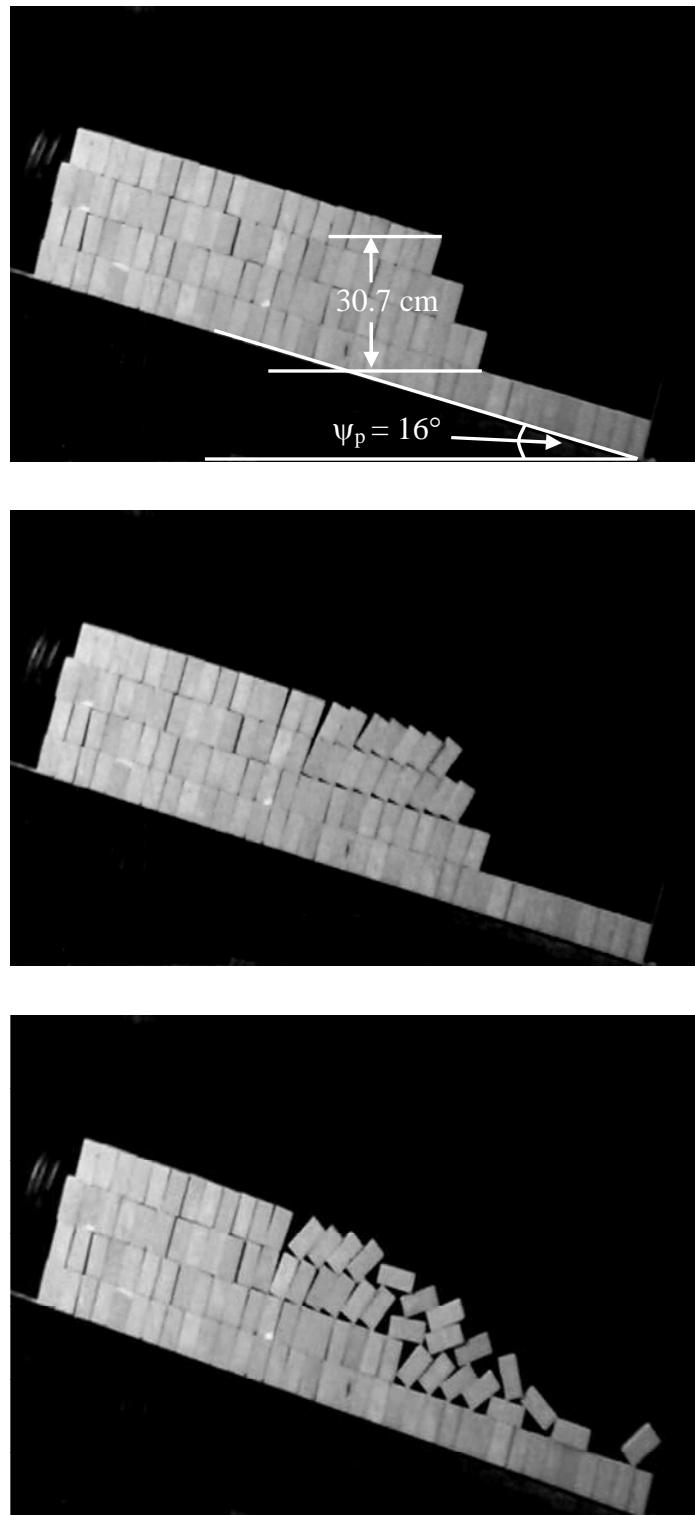
Figure A-15 Results of toppling failure simulation for 4×4×8 cm blocks size at ψ_f

$= 61°$.
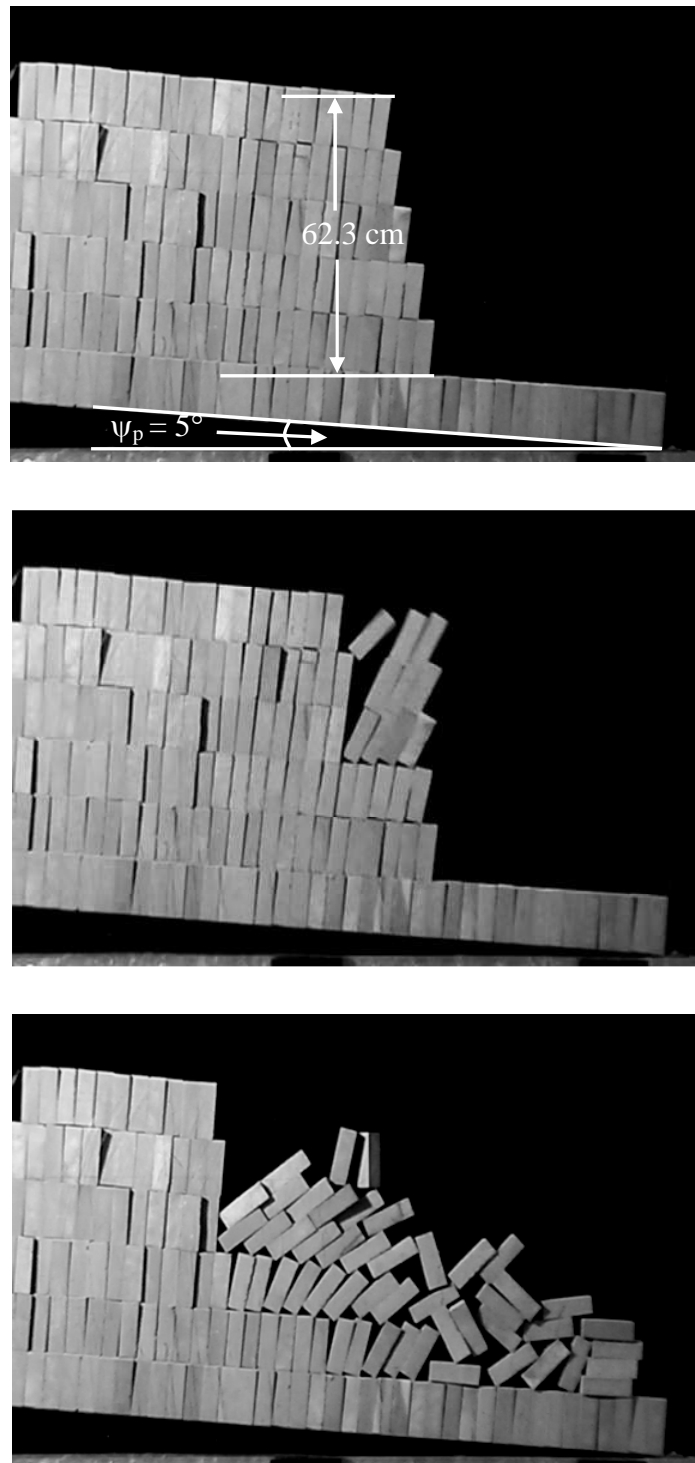
Figure A-16 Results of toppling failure simulation for 4×4×12 cm blocks size at ψ_f

$= 77°$.
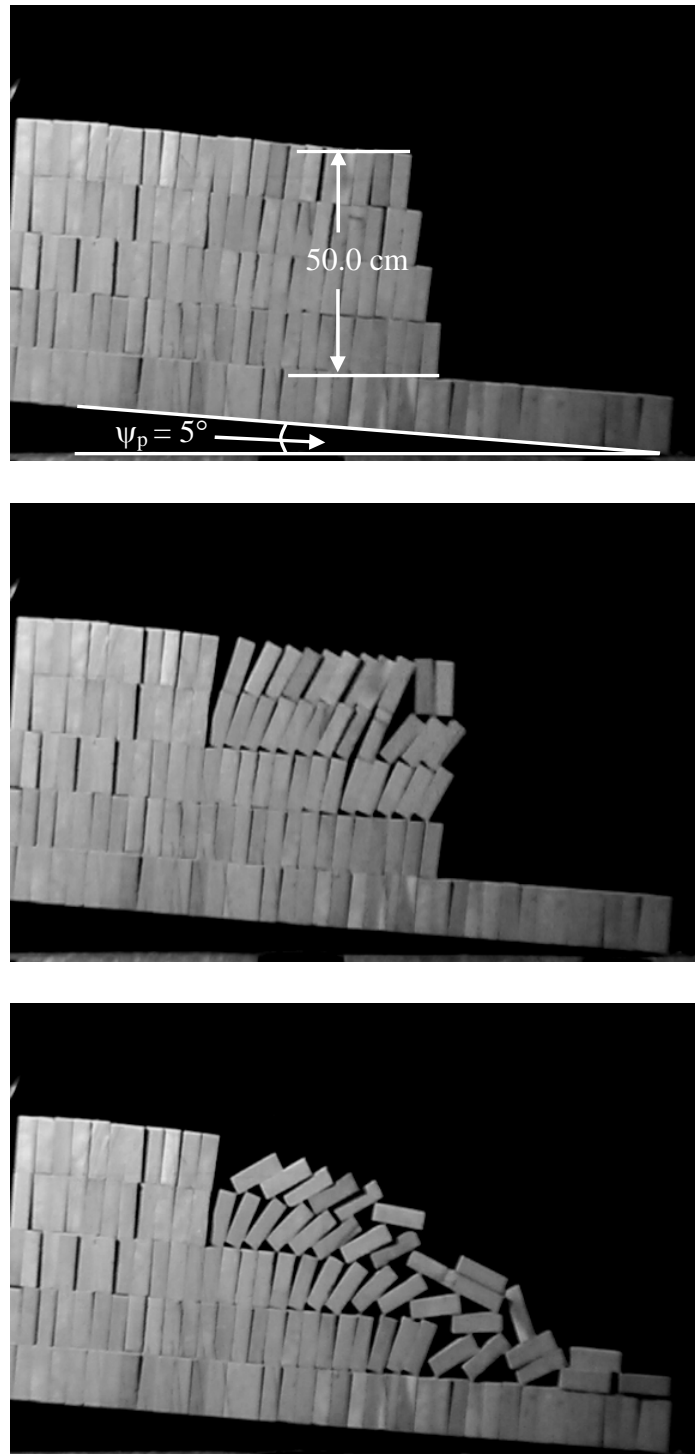
Figure A-17 Results of toppling failure simulation for 4×4×12 cm blocks size   at

$\psi_f = 77°$.
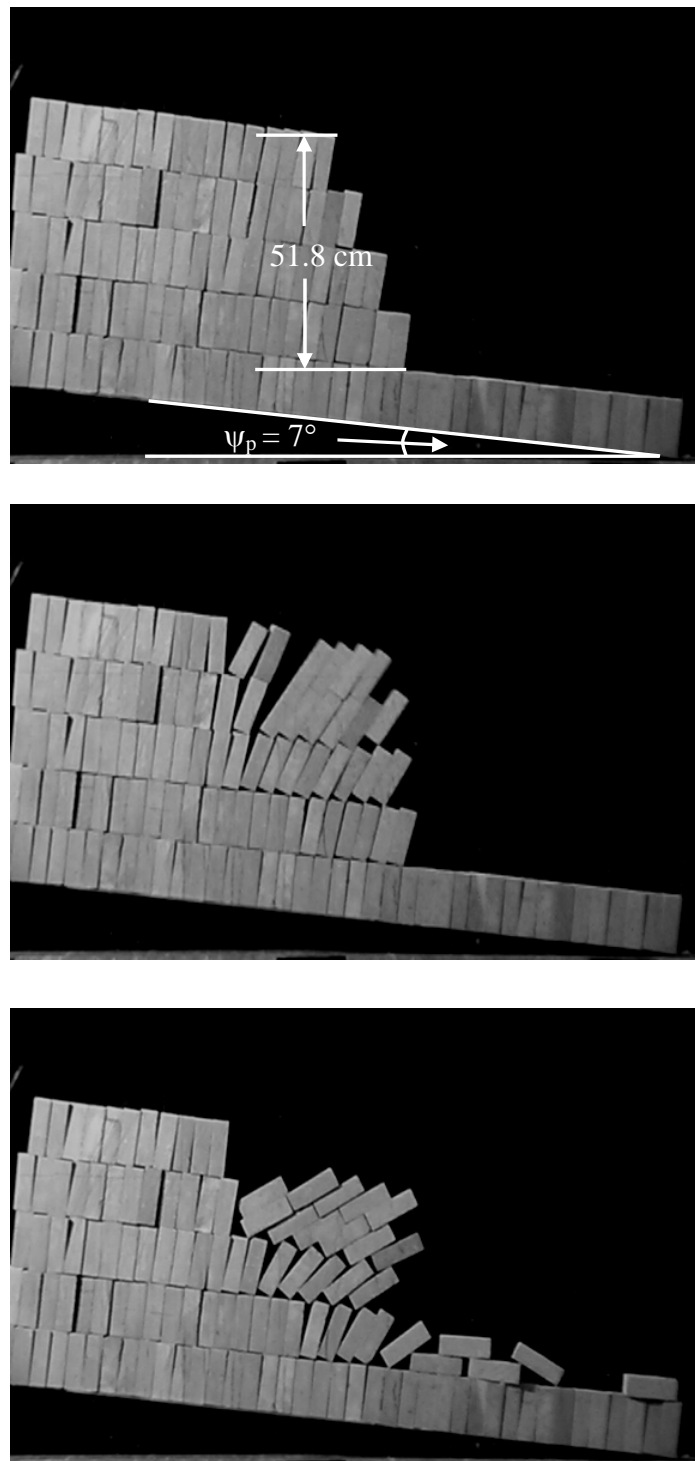
Figure A-18 Results of toppling failure simulation for 4×4×12 cm blocks size

at $\psi_f = 65°$.
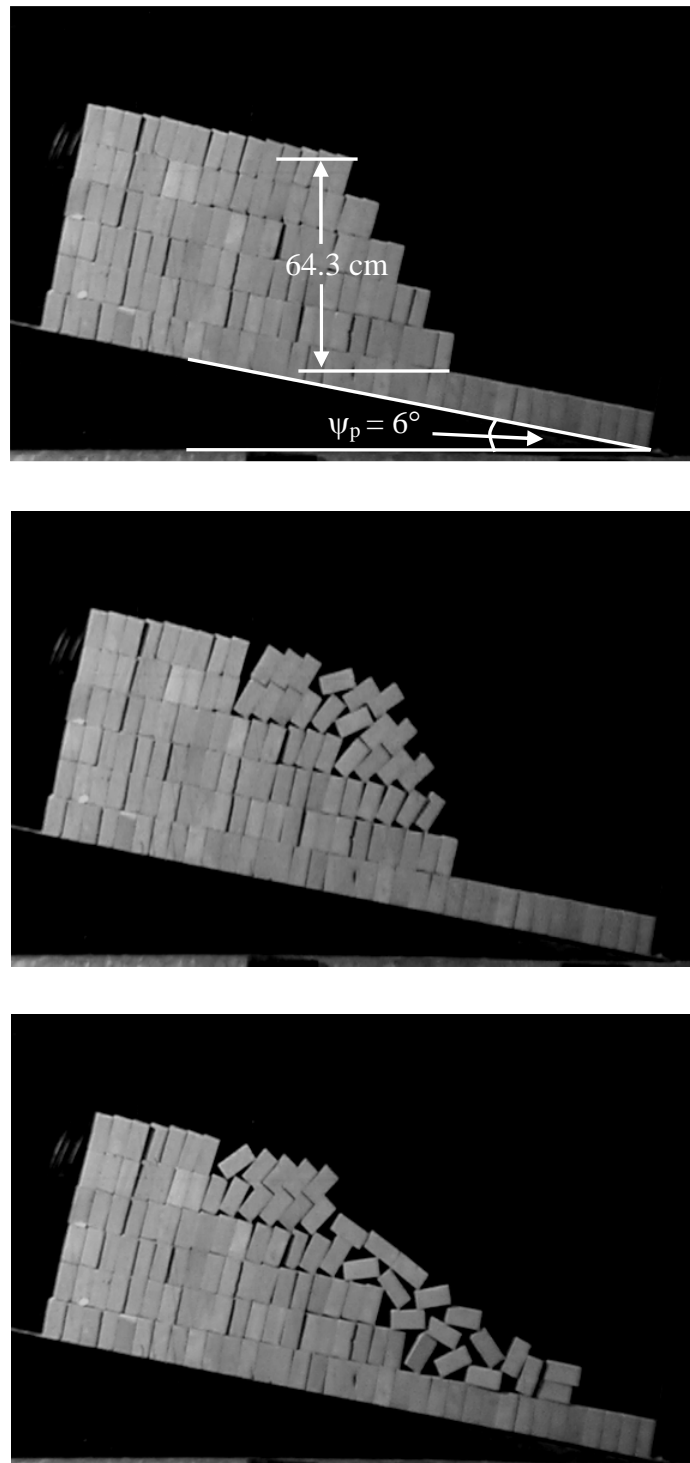
Figure A-19 Results of toppling failure simulation for 4×4×12 cm blocks size

at $\psi_f = 64°$.
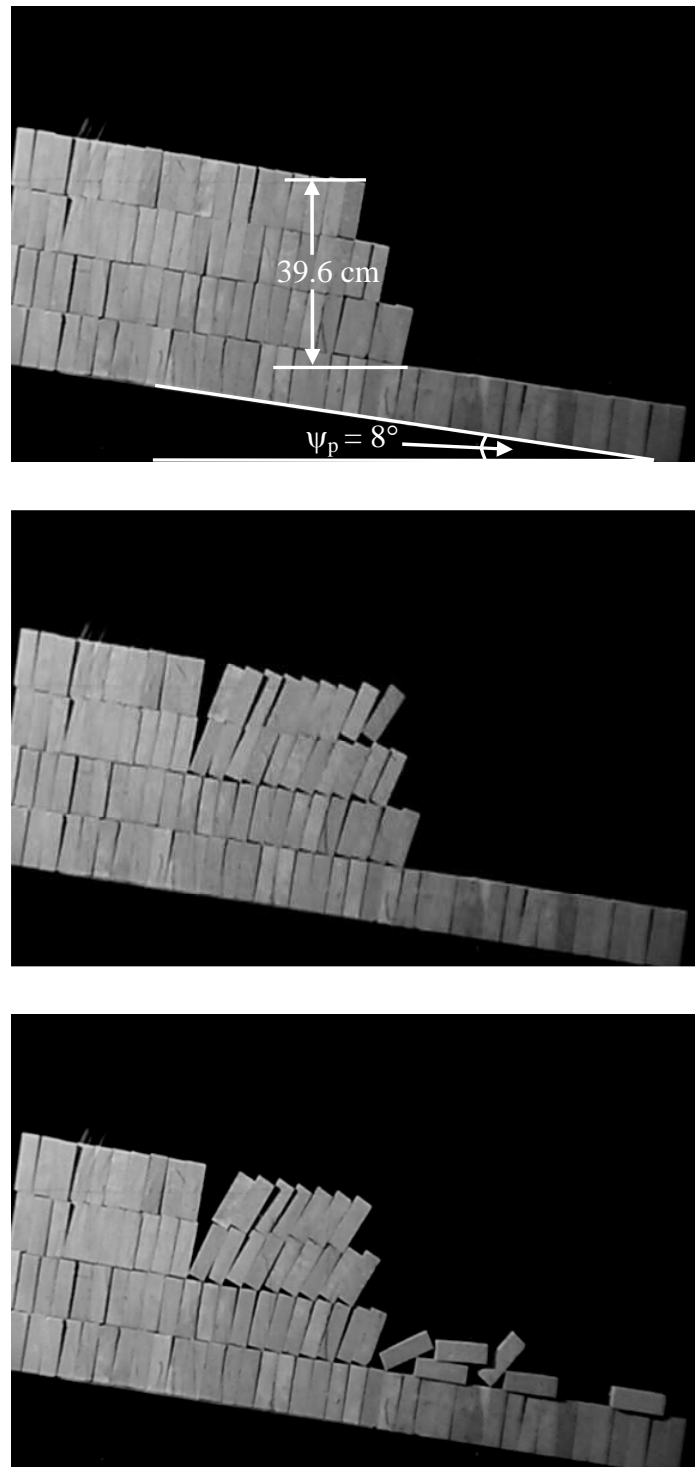
Figure A-20 Results of toppling failure simulation for 4×4×12 cm blocks size

at $\psi_f = 66°$.
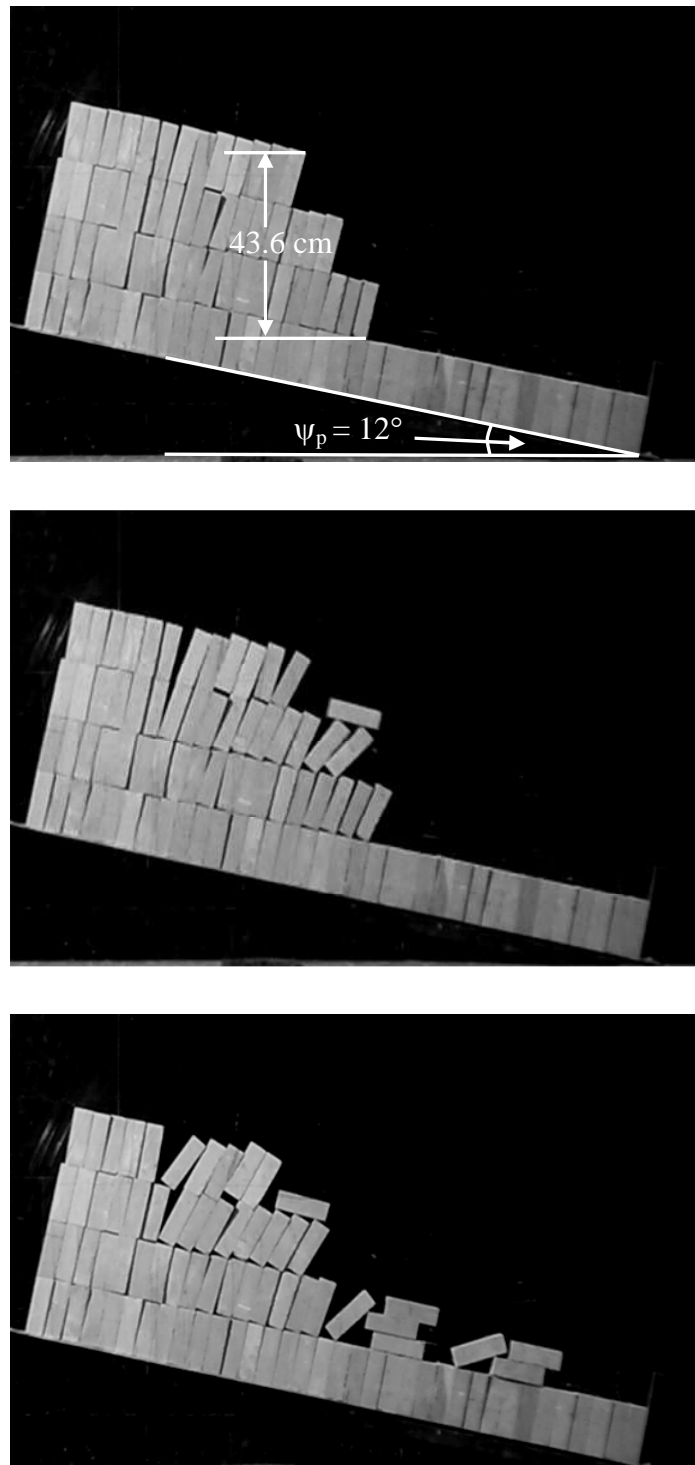
Figure A-21 Results of toppling failure simulation for 4×4×12 cm blocks size at ψ_f = 56°.
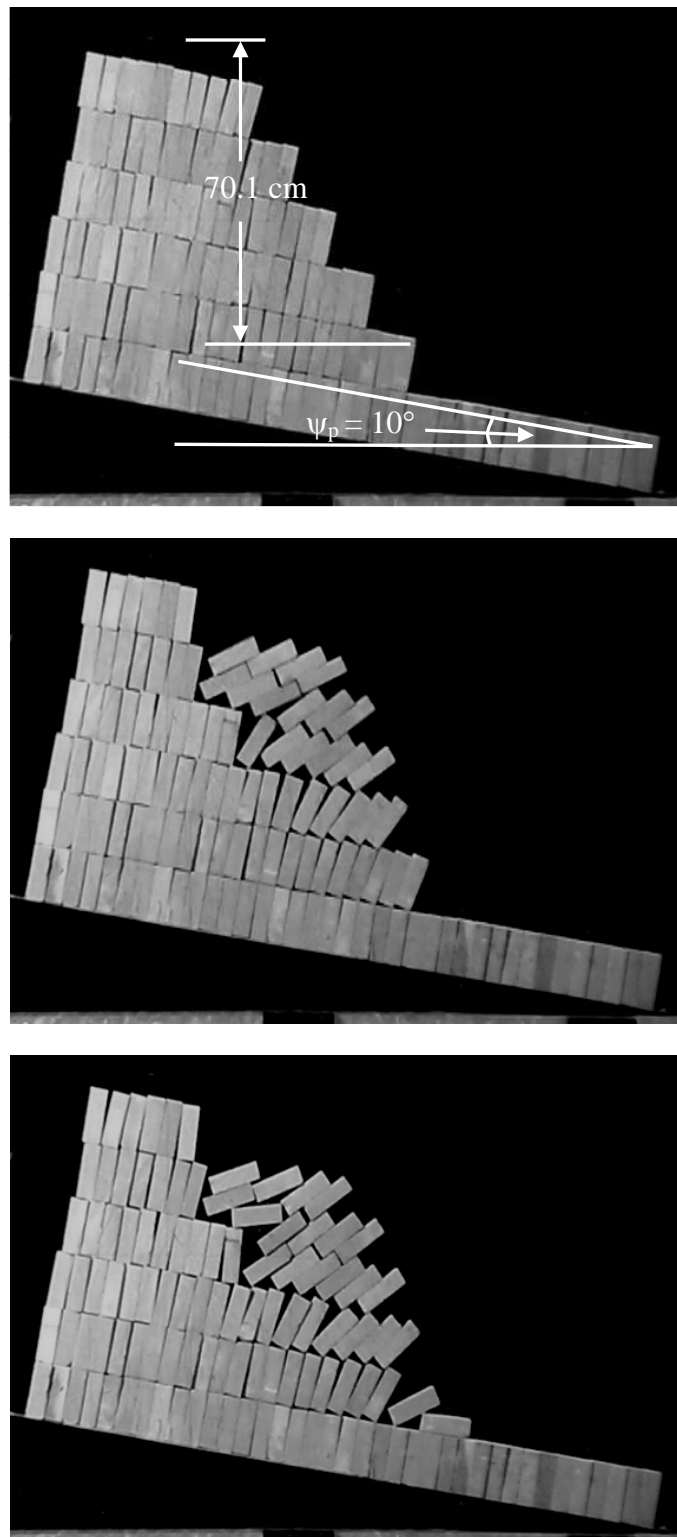
Figure A-22 Results of toppling failure simulation for 4×4×12 cm blocks size at ψ_f = 55°.

Table A-1 Simulation results of rock slope failure of 4×4×4 cm blocks size under static condition.

Series	θ_0 (degrees)	ψ_{f0} (degrees)	h (cm)	a (cm)	α (degrees)	ψ_p (degrees)	ψ_f (degrees)	H (cm)	Mode of Failure
C-S1-H1-1	4	47	12.1	130.6	86	25	68	16.5	Sliding Failure
C-S1-H1-2	5	45	12.1	127.7	51	25	65	17.1	Sliding Failure
C-S1-H1-3	5	47	12.1	119.0	85	27	69	16.9	(1) Sliding at the bottom (2) Toppling at the top
C-S1-H2-1	3	48	16.3	118.8	85	24	69	21.5	Sliding Failure
C-S1-H2-2	3	47	16.3	119.1	85	24	68	21.8	Sliding Failure
C-S1-H2-3	3	47	16.3	113.5	69	25	69	21.9	Sliding Failure
C-S1-H3-1	3	46	20.2	113.5	87	22	65	26.8	(1) Sliding at the bottom (2) Toppling at the middle
C-S1-H3-2	3	48	20.2	118.2	55	23	68	26.5	(1) Toppling at the middle (2) Sliding near bottom
C-S1-H3-3	3	49	20.2	130.0	79	23	69	26.2	Sliding and Toppling Failure
C-S1-H4-1	3	49	28.5	125.5	77	21	67	36.5	(1) Toppling at the middle (2) Sliding near bottom
C-S1-H4-2	3	49	28.5	125.5	67	22	68	36.7	Sliding and Toppling Failure
C-S1-H4-3	3	49	28.5	125.6	69	20	66	36.2	(1) Sliding at the bottom (2) Toppling at the top
C-S1-H5-1	3	48	37.0	125.5	70	20	65	47.4	Sliding and Toppling Failure

Table A-1 Simulation results of rock slope failure of 4×4×4 cm blocks size under static condition. (cont.)

Series	θ_0 (degrees)	Ψ_{f0} (degrees)	h (cm)	a (cm)	α (degrees)	Ψ_p (degrees)	Ψ_f (degrees)	H (cm)	Mode of Failure
C-S1-H5-2	3	48	37.0	125.8	87	19	64	47.0	(1) Sliding at the middle (2) Toppling at the top
C-S1-H5-3	3	49	37.0	125.8	58	21	67	47.3	(1) Sliding at the bottom (2) Toppling at the top
C-S1-H6-1	3	49	44.5	126.2	65	20	66	56.5	(1) Sliding at the bottom (2) Toppling at the top
C-S1-H6-2	3	48	44.5	125.2	60	19	64	56.6	(1) Sliding at the bottom (2) Toppling at the middle
C-S1-H6-3	3	48	44.5	125.3	71	16	61	55.0	(1) Toppling at the top (2) Sliding at the middle
C-S1-H7-1	3	48	53.0	125.4	72	19	64	67.4	(1) Toppling at the top (2) Toppling at the middle (3) Sliding near bottom
C-S1-H7-2	3	48	53.0	125.5	77	16	61	65.6	Toppling and Sliding Failure
C-S1-H7-3	3	49	53.0	125.5	65	19	65	66.8	(1) Sliding at the bottom (2) Toppling at the top
C-S1-H8-1	3	48	61.2	125.5	65	16	61	75.7	(1) Toppling at the Top (2) Sliding near bottom

Table A-1 Simulation results of rock slope failure of 4×4×4 cm blocks size under static condition. (cont.)

Series	θ_0 (degrees)	ψ_{f0} (degrees)	h (cm)	a (cm)	α (degrees)	ψ_p (degrees)	ψ_f (degrees)	H (cm)	Mode of Failure
C-S1-H8-2	3	49	61.2	125.5	79	16	62	75.1	(1) Sliding near bottom (2) Toppling at the middle to top
C-S1-H8-3	3	48	61.2	125.5	87	16	61	75.7	(1) Toppling at the top (2) Toppling at the middle
C-S2-H1-1	3	31	12.0	125.5	46	24	52	20.1	Sliding Failure
C-S2-H1-2	3	30	12.3	124.2	72	25	52	21.3	Sliding Failure
C-S2-H1-3	3	30	12.3	124.2	46	25	52	21.3	Sliding Failure
C-S2-H2-1	3	30	16.3	124.5	87	24	51	27.9	(1) Sliding at the top (2) Sliding at the bottom
C-S2-H2-2	3	29	16.3	121.7	76	24	50	28.5	(1) Sliding at the middle (2) Toppling at the top
C-S2-H2-3	3	30	16.3	123.0	63	25	52	28.3	(1) Sliding at the bottom (2) Toppling at the top
C-S2-H3-1	3	29	20.4	123.2	70	25	51	36.2	(1) Sliding at the middle
C-S2-H3-2	3	31	20.4	123.2	63	24	52	34.2	(1) Sliding at the bottom
C-S2-H3-3	3	31	20.4	123.0	59	24	52	34.2	(1) Sliding at the middle
C-S2-H4-1	3	29	24.7	123.0	68	24	50	43.2	(1) Sliding at the bottom

Table A-1. Simulation results of rock slope failure of 4×4×4 cm blocks size under static condition. (cont.)

Series	θ_0 (degrees)	ψ_{f0} (degrees)	h (cm)	a (cm)	α (degrees)	ψ_p (degrees)	ψ_f (degrees)	H (cm)	Mode of Failure
C-S2-H4-2	3	30	24.7	123.0	65	24	51	42.3	(1) Sliding at the bottom
C-S2-H4-3	3	30	24.7	123.0	66	24	51	42.3	(1) Sliding at bottom
C-S2-H5-1	3	30	28.3	123.0	66	23	50	47.8	(1) Sliding at bottom (2) Toppling at the top
C-S2-H5-2	3	30	28.3	123.0	70	23	50	47.8	(1) Toppling at the top (2) Sliding at bottom
C-S2-H5-3	3	30	28.3	121.7	62	23	50	47.8	(1) Sliding at the top (2) Sliding at the bottom
C-S2-H5-4	3	29	28.3	122.8	55	22	48	48.0	(1) Sliding at the bottom (2) Toppling at the middle
C-S2-H6-1	3	30	32.4	122.0	55	23	50	54.7	(1) Toppling at the top (2) Sliding near bottom
C-S2-H6-2	3	30	32.4	122.0	63	22	49	53.9	(1) Sliding at the bottom (2) Toppling at the top
C-S2-H6-3	3	30	32.4	121.8	64	22	49	53.9	(1) Sliding at the bottom (2) Sliding at the top
C-S2-H7-1	3	30	36.7	121.8	62	22	49	61.0	(1) Sliding at the middle (2) Sliding at the bottom

Table A-1 Simulation results of rock slope failure of 4×4×4 cm blocks size under static condition. (cont.)

Series	θ_0 (degrees)	ψ_{f0} (degrees)	h (cm)	a (cm)	α (degrees)	ψ_p (degrees)	ψ_f (degrees)	H (cm)	Mode of Failure
C-S2-H7-2	3	29	36.7	121.8	75	21	47	61.2	(1) Sliding at the middle (2) Toppling at the top
C-S2-H7-3	3	29	36.7	121.8	60	22	48	62.2	(1) Sliding at the middle (2) Toppling at top
C-S2-H8-1	3	30	40.5	121.8	87	21	48	66.3	(1) Toppling at the middle (2) Sliding at the bottom
C-S2-H8-2	3	30	40.5	121.8	68	21	48	66.3	(1) Sliding at the middle (2) Toppling at the top
C-S2-H8-3	3	29	40.5	121.8	68	20	46	66.5	(1) Sliding at the bottom (2) Toppling at the top
C-S3-H1-1	3	20	12.0	121.8	87	23	40	26.4	Sliding Failure
C-S3-H1-2	3	22	12.0	121.8	54	23	42	24.7	Sliding Failure
C-S3-H1-3	3	21	12.0	124.8	87	23	41	25.5	Sliding Failure
C-S3-H2-1	3	22	16.0	125.0	87	24	43	33.5	Sliding Failure
C-S3-H2-2	3	21	16.0	123.0	46	24	42	34.6	Sliding Failure
C-S3-H2-3	3	21	16.0	124.9	53	24	42	34.6	Sliding Failure
C-S3-H3-1	3	22	20.2	125.0	53	24	43	42.3	Sliding Failure

Table A-1 Simulation results of rock slope failure of 4×4×4 cm blocks size under static condition. (cont.)

Series	θ_0 (degrees)	ψ_{f0} (degrees)	h (cm)	a (cm)	α (degrees)	ψ_p (degrees)	ψ_f (degrees)	H (cm)	Mode of Failure
C-S3-H3-2	3	22	20.2	123.0	87	23	42	41.5	Sliding Failure
C-S3-H3-3	3	22	20.2	123.2	87	23	42	41.5	Sliding Failure
C-S3-H4-1	3	22	24.4	123.1	87	23	42	50.1	Sliding Failure
C-S3-H4-2	3	22	24.4	123.0	63	23	42	50.1	Sliding Failure
C-S3-H4-3	3	22	24.4	123.0	65	24	43	51.1	Sliding Failure
C-S3-H5-1	3	22	28.4	123.0	63	24	43	59.5	Sliding Failure
C-S3-H5-2	3	22	28.2	123.0	71	23	42	58.0	Sliding Failure
C-S3-H5-3	3	23	28.4	123.2	73	23	43	56.6	Sliding Failure
C-S3-H6-1	3	22	32.5	127.5	71	24	43	68.1	Sliding Failure
C-S3-H6-2	3	23	32.5	127.0	87	24	44	66.0	Sliding Failure
C-S3-H6-3	3	23	32.5	127.0	70	24	44	66.0	Sliding Failure

Table A-2 Simulation results of rock slope failure of 4×4×8 cm blocks size under static condition.

Series	θ_0 (degrees)	Ψ_{f0} (degrees)	h (cm)	a (cm)	α (degrees)	Ψ_p (degrees)	Ψ_f (degrees)	H (cm)	Mode of Failure
R8H-S1-H1-1	3	50	12.2	132.0	39	26	73	16.0	Sliding Failure
R8H-S1-H1-2	3	49	12.2	132.0	39	27	73	16.2	Sliding Failure
R8H-S1-H1-3	3	51	12.2	131.0	39	27	75	15.9	Sliding Failure
R8H-S1-H2-1	3	50	20.2	132.0	36	26	73	26.4	Sliding Failure
R8H-S1-H2-2	3	50	20.2	131.9	39	25	72	26.3	Sliding Failure
R8H-S1-H2-3	3	50	20.2	132.0	37	26	73	26.4	Sliding Failure
R8H-S1-H3-1	3	50	28.4	132.0	39	24	71	36.7	Sliding Failure
R8H-S1-H3-2	3	50	28.4	132.0	38	25	72	36.9	Sliding Failure
R8H-S1-H3-3	3	49	28.4	132.0	38	24	70	37.1	Sliding Failure
R8H-S1-H4-1	3	50	36.3	131.9	37	24	71	46.9	Sliding Failure
R8H-S1-H4-2	3	50	36.3	132.0	37	24	71	46.9	Sliding Failure
R8H-S1-H4-3	3	51	36.3	132.0	38	24	72	46.5	Sliding Failure
R8H-S1-H5-1	3	49	44.7	132.0	38	24	70	58.4	Sliding Failure
R8H-S1-H5-2	3	48	44.7	132.0	42	24	69	59.0	Sliding Failure
R8H-S1-H5-3	3	50	44.7	132.0	42	24	71	57.8	Sliding Failure
R8H-S1-H6-1	3	50	40.7	107.4	87	25	72	52.9	Sliding Failure
R8H-S1-H7-1	3	49	48.8	107.4	87	25	71	64.1	Sliding Failure

Table A-2 Simulation results of rock slope failure of 4×4×8 cm blocks size under static condition. (cont.)

Series	θ_0 (degrees)	ψ_{f0} (degrees)	h (cm)	a (cm)	α (degrees)	ψ_p (degrees)	ψ_f (degrees)	H (cm)	Mode of Failure
R8H-S2-H1-1	3	30	12.0	132.1	87	24	51	20.5	Sliding Failure
R8H-S2-H1-2	3	30	12.0	124.0	87	24	51	20.5	Sliding Failure
R8H-S2-H1-3	3	31	12.0	115.3	87	27	55	20.9	Sliding Failure
R8H-S2-H2-1	3	29	16.1	115.2	87	27	53	29.3	Sliding Failure
R8H-S2-H2-2	3	30	16.1	115.0	87	26	53	28.3	Sliding Failure
R8H-S2-H2-3	3	30	16.1	115.2	87	27	54	28.7	Sliding Failure
R8H-S2-H3-1	3	30	20.4	115.2	87	25	52	35.4	Sliding Failure
R8H-S2-H3-2	3	30	20.4	115.3	87	25	52	35.4	Sliding Failure
R8H-S2-H3-3	3	29	20.4	115.3	87	25	51	36.2	Sliding Failure
R8H-S2-H4-1	3	30	24.3	115.5	87	24	51	41.6	Sliding Failure
R8H-S2-H4-2	3	30	24.3	115.3	87	25	52	42.2	Sliding Failure
R8H-S2-H4-3	3	30	24.3	115.5	87	25	52	42.2	Sliding Failure
R8H-S2-H5-1	3	30	28.3	115.2	87	24	51	48.4	Sliding Failure
R8H-S2-H5-2	3	31	28.3	115.3	87	24	52	47.5	Sliding Failure
R8H-S2-H5-3	3	30	28.3	115.5	87	24	51	48.4	Sliding Failure
R8H-S2-H6-1	3	30	36.2	115.5	87	24	51	62.0	Sliding Failure
R8H-S2-H6-2	3	29	36.2	115.2	87	24	50	63.3	Sliding Failure

Table A-2 Simulation results of rock slope failure of 4×4×8 cm blocks size under static condition. (cont.)

Series	θ_0 (degrees)	Ψ_{f0} (degrees)	h (cm)	a (cm)	α (degrees)	Ψ_p (degrees)	Ψ_f (degrees)	H (cm)	Mode of Failure
R8H-S2-H6-3	3	30	36.2	115.3	87	24	51	62.0	Sliding Failure
R8H-S2-H7-1	3	29	44.6	115.4	87	23	49	76.8	Sliding Failure
R8H-S2-H7-2	3	30	45.2	115.5	87	23	50	76.3	Sliding Failure
R8H-S2-H7-3	3	30	44.6	115.3	87	23	50	75.3	Sliding Failure
R8H-S3-H1-1	3	49	12.1	121.0	23	26	72	16.0	Sliding Failure
R8H-S3-H1-2	3	49	12.1	120.8	22	26	72	16.0	Sliding Failure
R8H-S3-H1-3	3	49	12.1	108.6	23	26	72	16.0	Sliding Failure
R8H-S3-H2-1	3	49	16.2	121.0	22	26	72	21.4	Sliding Failure
R8H-S3-H2-2	3	49	16.2	120.8	22	26	72	21.4	Sliding Failure
R8H-S3-H2-3	3	50	16.2	121.0	22	25	72	21.1	Sliding Failure
R8H-S3-H3-1	3	49	20.2	121.0	22	26	72	26.7	Sliding Failure
R8H-S3-H3-2	3	49	20.2	108.7	22	25	71	26.6	Sliding Failure
R8H-S3-H3-3	3	49	20.2	108.6	23	25	71	26.6	Sliding Failure
R8H-S3-H4-1	3	48	24.2	108.7	23	25	70	32.2	Sliding Failure
R8H-S3-H4-2	3	49	24.3	108.6	23	26	72	32.1	Sliding Failure
R8H-S3-H4-3	3	49	24.2	108.6	23	25	71	31.8	Sliding Failure
R8H-S3-H5-1	3	48	28.4	108.7	23	26	71	38.0	Sliding Failure
R8H-S3-H5-2	3	48	28.5	108.6	22	25	70	37.9	Sliding Failure

Table A-2 Simulation results of rock slope failure of 4×4×8 cm blocks size under static condition. (cont.)

Series	θ_0 (degrees)	ψ_{f0} (degrees)	h (cm)	a (cm)	α (degrees)	ψ_p (degrees)	ψ_f (degrees)	H (cm)	Mode of Failure
R8H-S3-H5-3	3	48	28.2	108.6	22	26	71	37.7	Sliding Failure
R8V-S1-H1-1	3	68	24.7	127.7	87	16	81	26.9	Toppling Failure
R8V-S1-H1-2	3	66	24.8	102.6	87	15	78	27.2	Toppling Failure
R8V-S1-H1-3	3	65	24.6	102.5	87	15	77	27.2	Toppling Failure
R8V-S1-H2-1	3	66	33.0	102.5	87	19	82	36.7	Toppling Failure
R8V-S1-H2-2	3	66	33.0	102.8	87	14	77	36.1	Toppling Failure
R8V-S1-H2-3	3	67	33.1	103.0	87	18	82	36.5	Toppling Failure
R8V-S1-H2-4	3	67	33.5	107.7	87	13	77	36.3	Toppling Failure
R8V-S1-H2-5	3	67	33.0	99.1	87	13	77	35.8	Toppling Failure
R8V-S1-H3-1	3	67	41.5	102.8	87	13	77	45.0	Toppling Failure
R8V-S1-H3-2	3	67	41.4	102.9	87	11	75	44.5	Toppling Failure
R8V-S1-H3-3	3	67	41.4	102.7	87	12	76	44.7	Toppling Failure
R8V-S1-H4-1	3	68	49.8	103.2	87	9	74	52.8	Toppling Failure
R8V-S1-H4-2	3	68	50.0	103.2	87	7	72	52.5	Toppling Failure
R8V-S1-H4-3	3	67	49.9	102.7	87	9	73	53.1	Toppling Failure
R8V-S1-H5-1	3	69	58.0	103.0	87	6	72	60.4	Toppling Failure
R8V-S1-H5-2	3	69	58.0	106.9	87	6	72	60.4	Toppling Failure
R8V-S1-H5-3	3	69	58.0	106.9	87	5	71	60.0	Toppling Failure

Table A-2 Simulation results of rock slope failure of 4×4×8 cm blocks size under static condition. (cont.)

Series	θ_0 (degrees)	ψ_{f0} (degrees)	h (cm)	a (cm)	α (degrees)	ψ_p (degrees)	ψ_f (degrees)	H (cm)	Mode of Failure
R8V-S2-H1-1	3	49	25	103.1	87	16	62	30.7	Toppling Failure
R8V-S2-H1-2	3	49	25	103.2	87	14	60	30.1	Toppling Failure
R8V-S2-H1-3	3	49	25	94.6	87	16	62	30.7	Toppling Failure
R8V-S2-H1-4	3	46	24.8	129.0	87	17	60	31.5	Toppling Failure
R8V-S2-H2-1	3	49	33.2	94.9	87	15	61	40.4	Toppling Failure
R8V-S2-H2-2	3	49	33.2	94.2	87	12	58	39.1	Toppling Failure
R8V-S2-H2-3	3	49	33.2	94.8	87	18	64	41.5	Toppling Failure
R8V-S2-H2-4	3	47	33	128.7	87	15	59	40.7	Toppling Failure
R8V-S2-H3-1	3	49	41.5	94.9	87	15	61	50.5	Toppling Failure
R8V-S2-H3-2	3	49	41.5	94.6	87	10	56	47.8	Toppling Failure
R8V-S2-H3-3	3	49	41.5	94.9	87	12	58	48.9	Toppling Failure
R8V-S2-H3-4	1	46	41.3	128.7	87	13	58	49.5	Toppling Failure
R8V-S2-H4-1	3	49	49.6	95	87	15	61	60.3	Toppling Failure
R8V-S2-H4-2	3	49	49.6	94.6	87	11	57	57.8	Toppling Failure
R8V-S2-H4-3	3	49	49.6	93.9	87	10	56	57.2	Toppling Failure
R8V-S2-H5-1	3	49	58	94.2	87	9	55	66.1	Toppling Failure
R8V-S2-H5-2	3	49	58	94.1	87	8	54	65.2	Toppling Failure
R8V-S2-H5-3	3	49	58.5	94	87	8	54	65.8	Toppling Failure

Table A-2 Simulation results of rock slope failure of 4×4×8 cm blocks size under static condition. (cont.)

Series	θ_0 (degrees)	ψ_{f0} (degrees)	h (cm)	a (cm)	α (degrees)	ψ_p (degrees)	ψ_f (degrees)	H (cm)	Mode of Failure
R8V-S3-H1-1	3	37	25.0	94.2	87	14	48	33.2	Toppling Failure
R8V-S3-H1-2	3	36	25.0	94.2	87	16	49	34.6	Toppling Failure
R8V-S3-H1-3	3	36	25.0	93.9	87	18	51	35.7	Toppling Failure
R8V-S3-H1-4	3	36	24.5	128.7	87	19	52	35.5	Toppling Failure
R8V-S3-H2-1	3	37	33.4	94.1	87	19	53	47.7	Toppling Failure
R8V-S3-H2-2	3	37	33.4	90.2	87	15	49	45.1	Toppling Failure
R8V-S3-H2-3	3	37	33.5	90.2	87	15	49	45.2	Toppling Failure
R8V-S3-H2-4	3	37	33	133.1	87	16	50	45.2	Toppling Failure
R8V-S3-H3-1	3	37	41.5	90.1	87	14	48	55.2	Toppling Failure
R8V-S3-H3-2	3	37	41.5	90.3	87	15	49	56.0	Toppling Failure
R8V-S3-H3-3	3	37	41.5	90.2	87	14	48	55.2	Toppling Failure
R8V-S3-H4-1	3	37	50.0	98.8	87	11	45	63.2	Toppling Failure
R8V-S3-H4-2	3	37	50.0	98.6	87	12	46	64.3	Toppling Failure
R8V-S3-H4-3	3	37	50.0	94.3	87	12	46	64.3	Toppling Failure
R8V-S3-H5-1	3	37	58.0	107.0	87	9	43	70.7	Toppling Failure
R8V-S3-H5-2	3	37	58.0	107.0	87	10	44	72.1	Toppling Failure
R8V-S3-H5-3	3	37	58.0	103.0	87	12	46	74.6	Toppling Failure
R8V-S3-H5-4	3	37	58	140.5	87	9	43	70.7	Toppling Failure

Table A-3 Simulation results of rock slope failure of 4×4×12 cm blocks size under static condition.

Series	θ_0 (degrees)	ψ_{f0} (degrees)	h (cm)	a (cm)	α (degrees)	ψ_p (degrees)	ψ_f (degrees)	H (cm)	Mode of Failure
R12H-S1-H1-1	3	49	12.1	121.0	23	26	72	16.0	Sliding Failure
R12H-S1-H1-2	3	49	12.1	120.8	22	26	72	16.0	Sliding Failure
R12H-S1-H1-3	3	49	12.1	108.6	23	26	72	16.0	Sliding Failure
R12H-S1-H2-1	3	49	16.2	121.0	22	26	72	21.4	Sliding Failure
R12H-S1-H2-2	3	49	16.2	120.8	22	26	72	21.4	Sliding Failure
R12H-S1-H2-3	3	50	16.2	121.0	22	25	72	21.1	Sliding Failure
R12H-S1-H3-1	3	49	20.2	121.0	22	26	72	26.7	Sliding Failure
R12H-S1-H3-2	3	49	20.2	108.7	22	25	71	26.6	Sliding Failure
R12H-S1-H3-3	3	49	20.2	108.6	23	25	71	26.6	Sliding Failure
R12H-S1-H4-1	3	48	24.2	108.7	23	25	70	32.2	Sliding Failure
R12H-S1-H4-2	3	49	24.3	108.6	23	26	72	32.1	Sliding Failure
R12H-S1-H4-3	3	49	24.2	108.6	23	25	71	31.8	Sliding Failure
R12H-S1-H5-1	3	48	28.4	108.7	23	26	71	38.0	Sliding Failure
R12H-S1-H5-2	3	48	28.5	108.6	22	25	70	37.9	Sliding Failure
R12H-S1-H5-3	3	48	28.2	108.6	22	26	71	37.7	Sliding Failure
R12H-S1-H6-1	3	48	70.2	120.7	87	25	70	93.3	Sliding Failure
R12H-S1-H7-1	3	49	48.6	120.7	87	25	71	63.9	Sliding Failure
R12H-S2-H1-1	3	30	12.3	108.5	39	26	53	21.6	Sliding Failure

Table A-3 Simulation results of rock slope failure of 4×4×12 cm blocks size under static condition. (cont.)

Series	θ_0 (degrees)	ψ_{f0} (degrees)	h (cm)	a (cm)	α (degrees)	ψ_p (degrees)	ψ_f (degrees)	H (cm)	Mode of Failure
R12H-S2-H1-2	3	30	12.3	108.6	40	26	53	21.6	Sliding Failure
R12H-S2-H1-3	3	30	12.3	108.6	40	26	53	21.6	Sliding Failure
R12H-S2-H2-1	3	30	16.2	108.6	40	26	53	28.5	Sliding Failure
R12H-S2-H2-2	3	30	16.2	108.7	40	26	53	28.5	Sliding Failure
R12H-S2-H2-3	3	30	16.2	109.0	39	26	53	28.5	Sliding Failure
R12H-S2-H3-1	3	30	20.1	108.7	40	25	52	34.9	Sliding Failure
R12H-S2-H3-2	3	30	20.2	108.9	40	25	52	35.1	Sliding Failure
R12H-S2-H3-3	3	30	20.2	108.9	40	26	53	35.5	Sliding Failure
R12H-S2-H4-1	3	30	24.2	109.2	40	25	52	42.0	Sliding Failure
R12H-S2-H4-2	3	30	24.2	108.8	40	25	52	42.0	Sliding Failure
R12H-S2-H4-3	3	30	24.2	108.7	40	25	52	42.0	Sliding Failure
R12H-S2-H5-1	3	30	28.1	109.2	40	25	52	48.8	Sliding Failure
R12H-S2-H5-2	3	30	28.2	109.0	40	26	53	49.6	Sliding Failure
R12H-S2-H5-3	3	30	28.2	108.8	41	25	52	48.9	Sliding Failure
R12H-S2-H6-1	3	30	40.3	120.7	87	25	52	70.0	Sliding Failure
R12H-S2-H7-1	3	30	48.5	120.7	87	25	52	84.2	Sliding Failure
R12H-S3-H1-1	3	22	12.2	108.5	87	26	45	26.5	Sliding Failure
R12H-S3-H1-2	3	22	12.2	108.4	87	26	45	26.5	Sliding Failure

Table A-3 Simulation results of rock slope failure of 4×4×12 cm blocks size under static condition. (cont.)

Series	θ_0 (degrees)	ψ_{f0} (degrees)	h (cm)	a (cm)	α (degrees)	ψ_p (degrees)	ψ_f (degrees)	H (cm)	Mode of Failure
R12H-S3-H1-3	3	22	12.2	108.5	87	26	45	26.5	Sliding Failure
R12H-S3-H2-1	3	22	16.3	108.6	87	26	45	35.4	Sliding Failure
R12H-S3-H2-2	3	22	16.3	108.4	87	26	45	35.4	Sliding Failure
R12H-S3-H2-3	3	22	16.3	108.7	87	26	45	35.4	Sliding Failure
R12H-S3-H3-1	3	22	20.1	108.6	87	26	45	43.7	Sliding Failure
R12H-S3-H3-2	3	22	20.1	108.6	87	26	45	43.7	Sliding Failure
R12H-S3-H3-3	3	22	20.1	108.6	87	26	45	43.7	Sliding Failure
R12H-S3-H4-1	3	22	24.3	108.5	87	25	44	51.8	Sliding Failure
R12H-S3-H4-2	3	22	24.3	108.9	87	25	44	51.8	Sliding Failure
R12H-S3-H4-3	3	22	24.3	108.8	87	25	44	51.8	Sliding Failure
R12H-S3-H5-1	3	22	28.2	108.9	87	25	44	60.2	Sliding Failure
R12H-S3-H5-2	3	22	28.2	109.1	87	25	44	60.2	Sliding Failure
R12H-S3-H5-3	3	22	28.2	108.9	87	25	44	60.2	Sliding Failure
R12V-S1-H1-1	3	74	36.7	106.2	87	6	77	37.8	Toppling Failure
R12V-S1-H1-2	3	74	36.7	106.5	87	8	79	38.1	Toppling Failure
R12V-S1-H1-3	3	75	36.7	106.5	87	6	78	37.7	Toppling Failure
R12V-S1-H2-1	3	75	48.8	106.7	87	5	77	50.0	Toppling Failure
R12V-S1-H2-2	3	75	48.8	106.7	87	5	77	50.0	Toppling Failure

Table A-3 Simulation results of rock slope failure of 4×4×12 cm blocks size under static condition. (cont.)

Series	θ_0 (degrees)	ψ_{f0} (degrees)	h (cm)	a (cm)	α (degrees)	ψ_p (degrees)	ψ_f (degrees)	H (cm)	Mode of Failure
R12V-S1-H2-3	3	75	48.8	106.8	87	4	76	49.8	Toppling Failure
R12V-S1-H3-1	3	75	60.8	107.0	87	5	77	62.3	Toppling Failure
R12V-S1-H3-2	3	75	60.8	107.0	87	6	78	62.5	Toppling Failure
R12V-S1-H3-3	3	75	60.8	106.6	87	7	79	62.8	Toppling Failure
R12V-S1-H4-1	3	76	73.0	111.0	87	7	80	75.2	Toppling Failure
R12V-S1-H4-2	3	76	73.2	77.8	87	7	80	75.4	Toppling Failure
R12V-S1-H4-3	3	76	73.2	78.3	87	7	80	75.4	Toppling Failure
R12V-S1-H4-4	3	76	73.2	130.1	87	4	77	74.6	Toppling Failure
R12V-S2-H1-1	3	61	36.5	94.0	87	6	64	38.7	Toppling Failure
R12V-S2-H1-2	3	61	36.5	94.2	87	9	67	39.6	Toppling Failure
R12V-S2-H1-3	3	60	36.5	93.9	87	8	65	39.4	Toppling Failure
R12V-S2-H1-4	3	61	37.2	117.0	87	10	68	40.7	Toppling Failure
R12V-S2-H2-1	3	61	48.5	94.2	87	7	65	51.8	Toppling Failure
R12V-S2-H2-2	3	61	48.5	94.1	87	7	65	51.8	Toppling Failure
R12V-S2-H2-3	3	61	48.5	94.3	87	7	65	51.8	Toppling Failure
R12V-S2-H3-1	3	61	60.5	94.6	87	6	64	64.1	Toppling Failure
R12V-S2-H3-2	3	61	60.5	94.3	87	5	63	63.6	Toppling Failure
R12V-S2-H3-3	3	61	60.6	94.5	87	8	66	65.3	Toppling Failure

Table A-3 Simulation results of rock slope failure of 4×4×12 cm blocks size under static condition. (cont.)

Series	θ_0 (degrees)	ψ_{f0} (degrees)	h (cm)	a (cm)	α (degrees)	ψ_p (degrees)	ψ_f (degrees)	H (cm)	Mode of Failure
R12V-S2-H4-1	3	61	72.6	94.0	87	9	67	78.8	Toppling Failure
R12V-S2-H4-2	3	61	73.0	81.9	87	5	63	76.7	Toppling Failure
R12V-S2-H4-3	3	61	72.6	82.1	87	6	64	76.9	Toppling Failure
R12V-S2-H4-4	3	61	72.7	117.7	87	7	65	77.7	Toppling Failure
R12V-S3-H1-1	3	47	36.5	77.6	87	12	56	43.6	Toppling Failure
R12V-S3-H1-2	3	47	36.5	77.7	87	10	54	42.5	Toppling Failure
R12V-S3-H1-3	3	48	36.5	77.7	87	10	55	42.3	Toppling Failure
R12V-S3-H1-4	3	48	36.8	114.3	87	11	56	43.1	Toppling Failure
R12V-S3-H2-2	3	48	48.5	77.5	87	11	56	56.9	Toppling Failure
R12V-S3-H2-3	3	48	48.5	81.8	87	10	55	56.2	Toppling Failure
R12V-S3-H3-1	3	48	60.9	94.5	87	10	55	70.5	Toppling Failure
R12V-S3-H3-2	3	48	60.2	90.8	87	10	55	69.7	Toppling Failure
R12V-S3-H3-3	3	48	60.5	90.5	87	10	55	70.1	Toppling Failure
R12V-S3-H4-1	3	48	72.5	94.5	87	9	54	82.9	Toppling Failure
R12V-S3-H4-2	3	48	73.0	98.4	87	10	55	84.6	Toppling Failure
R12V-S3-H4-3	3	48	72.5	98.3	87	9	54	82.9	Toppling Failure

APPENDIX B

RESULTS OF FACTOR SAFETY CALCULATION

Table B-1 Results of factor safety calculation of 4×4×4 cm blocks size.

Series	θ_0 (degrees)	ψ_{f0} (degrees)	h (cm)	a (cm)	α (degrees)	ψ_p (degrees)	ψ_f (degrees)	H (cm)	FS
C-S1-H1	4.7	46.3	12.1	125.8	74.0	25.0	67.3	16.8	1.1
C-S1-H2	3.0	47.3	16.3	119.0	85.0	24.0	69.0	21.7	1.1
C-S1-H3	3.0	30.3	20.2	115.9	73.7	22.7	67.3	26.5	1.2
C-S1-H4	3.0	49.0	28.5	125.5	68.0	21.0	67.0	36.5	1.3
C-S1-H5	3.0	48.3	37.0	125.8	78.5	20.0	65.3	47.3	1.4
C-S1-H6	3.0	48.3	44.5	125.6	65.3	18.3	63.7	56.0	1.5
C-S1-H7	3.0	48.3	53.0	125.5	71.3	18.0	63.3	66.6	1.5
C-S2-H1	3.0	30.3	12.2	124.2	46.0	24.7	52.0	20.9	1.1
C-S2-H2	3.0	29.7	16.3	123.1	68.3	24.3	51.0	28.2	1.1
C-S2-H3	3.0	30.3	20.4	123.1	64.0	24.3	51.7	34.9	1.1
C-S2-H4	3.0	29.7	24.7	123.0	66.3	24.0	50.7	42.6	1.1
C-S2-H5	3.0	29.8	28.3	122.6	63.3	22.8	49.5	47.8	1.2
C-S2-H6	3.0	30.0	32.4	121.9	60.7	22.3	49.3	54.1	1.2
C-S2-H7	3.0	29.3	36.7	121.8	65.7	21.7	48.0	61.5	1.2

Table B-1 Results of factor safety calculation of 4×4×4 cm blocks size.   (cont.)

Series	θ_0 (degrees)	ψ_{f0} (degrees)	h (cm)	a (cm)	α (degrees)	ψ_p (degrees)	ψ_f (degrees)	H (cm)	FS
C-S2-H8	3.0	29.7	40.5	121.8	74.3	20.7	47.3	66.3	1.3
C-S3-H1	3.0	21.0	12.0	122.8	76.0	23.0	41.0	25.5	1.2
C-S3-H2	3.0	21.3	16.0	124.3	62.0	24.0	42.3	34.3	1.1
C-S3-H3	3.0	22.0	20.2	123.7	75.7	23.3	42.3	41.8	1.2
C-S3-H4	3.0	22.0	24.4	123.0	71.7	23.3	42.3	50.5	1.2
C-S3-H5	3.0	22.3	28.3	123.1	69.0	23.3	42.7	58.0	1.2
C-S3-H6	3.0	22.7	32.5	127.2	76.0	24.0	43.7	66.7	1.1

Table B-2 Results of factor safety calculation of 4×4×8 cm blocks size.

Series	θ₀ (degrees)	ψf0 (degrees)	h (cm)	a (cm)	α (degrees)	ψp (degrees)	ψf (degrees)	H (cm)	FS
R8H-S1-H1-1	3	50	12.2	132.0	39	26	73	16.0	1.05
R8H-S1-H1-2	3	49	12.2	132.0	39	27	73	16.2	1.01
R8H-S1-H1-3	3	51	12.2	131.0	39	27	75	15.9	1.00
R8H-S1-H2-1	3	50	20.2	132.0	36	26	73	26.4	1.03
R8H-S1-H2-2	3	50	20.2	131.9	39	25	72	26.3	1.08
R8H-S1-H2-3	3	50	20.2	132.0	37	26	73	26.4	1.03
R8H-S1-H3-1	3	50	28.4	132.0	39	24	71	36.7	1.12
R8H-S1-H3-2	3	50	28.4	132.0	38	25	72	36.9	1.07
R8H-S1-H3-3	3	49	28.4	132.0	38	24	70	37.1	1.12
R8H-S1-H4-1	3	50	36.3	131.9	37	24	71	46.9	1.11
R8H-S1-H4-2	3	50	36.3	132.0	37	24	71	46.9	1.11
R8H-S1-H4-3	3	51	36.3	132.0	38	24	72	46.5	1.11
R8H-S1-H4-4	3	50	40.7	107.4	87	25	72	52.9	1.06
R8H-S1-H5-1	3	49	44.7	132.0	38	24	70	58.4	1.11
R8H-S1-H5-2	3	48	44.7	132.0	42	24	69	59.0	1.11
R8H-S1-H5-3	3	50	44.7	132.0	42	24	71	57.8	1.11
R8H-S1-H7-1	3	49	48.8	107.4	87	25	71	64.1	1.06
R8H-S2-H1-1	3	30	12.0	132.1	87	24	51	20.5	1.15
R8H-S2-H1-2	3	30	12.0	124.0	87	24	51	20.5	1.15
R8H-S2-H1-3	3	31	12.0	115.3	87	27	55	20.9	1.01
R8H-S2-H2-1	3	29	16.1	115.2	87	27	53	29.3	1.00
R8H-S2-H2-2	3	30	16.1	115.0	87	26	53	28.3	1.04
R8H-S2-H2-3	3	30	16.1	115.2	87	27	54	28.7	1.00
R8H-S2-H3-1	3	30	20.4	115.2	87	25	52	35.4	1.08

Table B-2 Results of factor safety calculation of 4×4×8 cm blocks size.　(cont.)

Series	θ_0 (degrees)	ψ_{f0} (degrees)	h (cm)	a (cm)	α (degrees)	ψ_p (degrees)	ψ_f (degrees)	H (cm)	FS
R8H-S2-H3-2	3	30	20.4	115.3	87	25	52	35.4	1.08
R8H-S2-H3-3	3	29	20.4	115.3	87	25	51	36.2	1.08
R8H-S2-H4-4	3	30	24.3	115.5	87	24	51	41.6	1.12
R8H-S2-H4-5	3	30	24.3	115.3	87	25	52	42.2	1.07
R8H-S2-H4-6	3	30	24.3	115.5	87	25	52	42.2	1.07
R8H-S2-H5-1	3	30	28.3	115.2	87	24	51	48.4	1.12
R8H-S2-H5-2	3	31	28.3	115.3	87	24	52	47.5	1.12
R8H-S2-H5-3	3	30	28.3	115.5	87	24	51	48.4	1.12
R8H-S2-H6-1	3	30	36.2	115.5	87	24	51	62.0	1.12
R8H-S2-H6-2	3	29	36.2	115.2	87	24	50	63.3	1.12
R8H-S2-H6-3	3	30	36.2	115.3	87	24	51	62.0	1.12
R8H-S2-H7-1	3	29	44.6	115.4	87	23	49	76.8	1.17
R8H-S2-H7-2	3	30	45.2	115.5	87	23	50	76.3	1.17
R8H-S2-H7-3	3	30	44.6	115.3	87	23	50	75.3	1.17

Table B-3 Results of factor safety calculation of 4×4×12 cm blocks size.

Series	θ_0 (degrees)	ψ_{f0} (degrees)	h (cm)	a (cm)	α (degrees)	ψ_p (degrees)	ψ_f (degrees)	H (cm)	FS
R12H-S1-H1-1	3	49	12.1	121.0	23	26	72	16.0	1.05
R12H-S1-H1-2	3	49	12.1	120.8	22	26	72	16.0	1.05
R12H-S1-H1-3	3	49	12.1	108.6	23	26	72	16.0	1.05
R12H-S1-H2-1	3	49	16.2	121.0	22	26	72	21.4	1.04
R12H-S1-H2-2	3	49	16.2	120.8	22	26	72	21.4	1.04
R12H-S1-H2-3	3	50	16.2	121.0	22	25	72	21.1	1.08
R12H-S1-H3-1	3	49	20.2	121.0	22	26	72	26.7	1.03
R12H-S1-H3-2	3	49	20.2	108.7	22	25	71	26.6	1.08
R12H-S1-H3-3	3	49	20.2	108.6	23	25	71	26.6	1.08
R12H-S1-H4-1	3	48	24.2	108.7	23	25	70	32.2	1.07
R12H-S1-H4-2	3	49	24.3	108.6	23	26	72	32.1	1.02
R12H-S1-H4-3	3	49	24.2	108.6	23	25	71	31.8	1.07
R12H-S1-H5-1	3	48	28.4	108.7	23	26	71	38.0	1.02
R12H-S1-H5-2	3	48	28.5	108.6	22	25	70	37.9	1.07
R12H-S1-H5-3	3	48	28.2	108.6	22	26	71	37.7	1.02
R12H-S1-H6-1	3	48	70.2	120.7	87	25	70	93.29	1.05
R12H-S1-H7-1	3	49	48.6	120.7	87	25	71	63.88	1.06
R12H-S2-H1-1	3	30	12.3	108.5	39	26	53	21.6	1.05
R12H-S2-H1-2	3	30	12.3	108.6	40	26	53	21.6	1.05
R12H-S2-H1-3	3	30	12.3	108.6	40	26	53	21.6	1.05
R12H-S2-H2-1	3	30	16.2	108.6	40	26	53	28.5	1.04
R12H-S2-H2-2	3	30	16.2	108.7	40	26	53	28.5	1.04
R12H-S2-H2-3	3	30	16.2	109.0	39	26	53	28.5	1.04
R12H-S2-H3-1	3	30	20.1	108.7	40	25	52	34.9	1.08

Table B-3 Results of factor safety calculation of 4×4×12 cm blocks size. (cont.)

Series	θ_0 (degrees)	ψ_{f0} (degrees)	h (cm)	a (cm)	α (degrees)	ψ_p (degrees)	ψ_f (degrees)	H (cm)	FS
R12H-S2-H3-2	3	30	20.2	108.9	40	25	52	35.1	1.08
R12H-S2-H3-3	3	30	20.2	108.9	40	26	53	35.5	1.03
R12H-S2-H4-1	3	30	24.2	109.2	40	25	52	42.0	1.07
R12H-S2-H4-2	3	30	24.2	108.8	40	25	52	42.0	1.07
R12H-S2-H4-3	3	30	24.2	108.7	40	25	52	42.0	1.07
R12H-S2-H5-1	3	30	28.1	109.2	40	25	52	48.8	1.07
R12H-S2-H5-2	3	30	28.2	109.0	40	26	53	49.6	1.02
R12H-S2-H5-3	3	30	28.2	108.8	41	25	52	48.9	1.07
R12H-S2-H6-1	3	30	40.3	120.7	87	25	52	70.0	1.06
R12H-S2-H7-1	3	30	48.5	120.7	87	25	52	84.2	1.06
R12H-S3-H1-1	3	22	12.2	108.5	87	26	45	26.5	1.06
R12H-S3-H1-2	3	22	12.2	108.4	87	26	45	26.5	1.06
R12H-S3-H1-3	3	22	12.2	108.5	87	26	45	26.5	1.06
R12H-S3-H2-1	3	22	16.3	108.6	87	26	45	35.4	1.04
R12H-S3-H2-2	3	22	16.3	108.4	87	26	45	35.4	1.04
R12H-S3-H2-3	3	22	16.3	108.7	87	26	45	35.4	1.04
R12H-S3-H3-1	3	22	20.1	108.6	87	26	45	43.7	1.04
R12H-S3-H3-2	3	22	20.1	108.6	87	26	45	43.7	1.04
R12H-S3-H3-3	3	22	20.1	108.6	87	26	45	43.7	1.04
R12H-S3-H4-1	3	22	24.3	108.5	87	25	44	51.8	1.08
R12H-S3-H4-2	3	22	24.3	108.9	87	25	44	51.8	1.08
R12H-S3-H4-3	3	22	24.3	108.8	87	25	44	51.8	1.08
R12H-S3-H5-1	3	22	28.2	108.9	87	25	44	60.2	1.07
R12H-S3-H5-2	3	22	28.2	109.1	87	25	44	60.2	1.07

APPENDIX C

TOPPLING FAILURE ANALYSIS
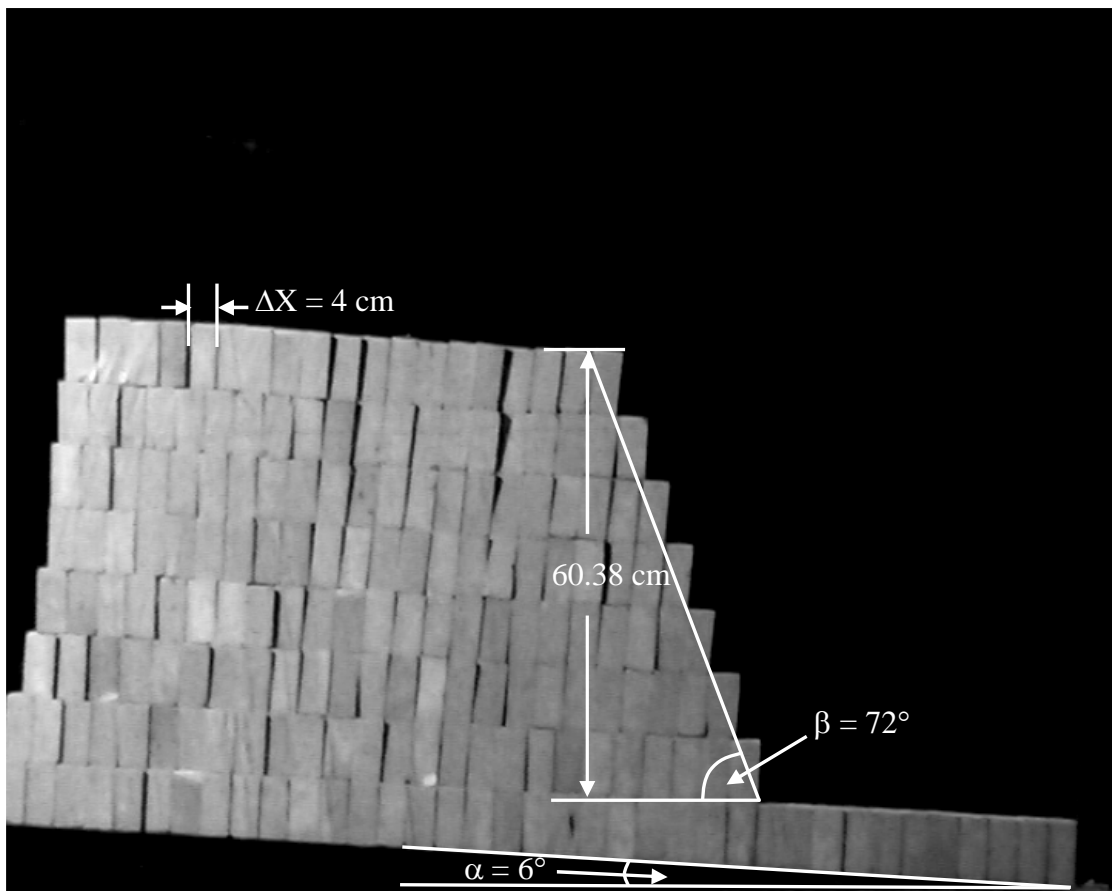
Figure C-1 Example of rock toppling failure analysis for 4×4×8 cm blocks size, rock unit weight = 23.8 kN/m^2.

Modified limit equibrium analysis of toppling can be written as:

$$P_{n,t} = \frac{(P_n M_n - P_n \Delta x \tan \phi) - (P_R L_n + P_R \Delta x \tan \phi) + \frac{y_n}{2} W_n \sin \alpha - \frac{\Delta x}{2} W_n \cos \alpha}{L_n}$$

where

$$P_d = \frac{w_n (\Delta X \cos \alpha)}{L_n}$$

and

$$P_r = \frac{w_n (y_n \sin \alpha)}{L_n}$$

Table C-1 Example of rock toppling failure of 4×4×8 cm blocks size.

n	M_n (m)	L_n (m)	Y_n (m)	P_n (N/m)	P_R (N/m)	P_nM_n	$P_n\Delta X\tan\phi$	P_d (kN/m)	P_r (kN/m)	P_nt (N/m)	Results
n(C1R1)	0	0.08	0.08	0.00	27.27	0.0	0.0	0.32	1.51	-48.87	Stable
n(C1R2)	0	0.16	0.16	0.00	56.05	0.0	0.0	1.27	3.03	-73.86	Stable
n(C1R3)	0	0.24	0.24	0.00	81.81	0.0	0.0	2.87	4.54	-95.45	Stable
n(C1R4)	0	0.32	0.32	0.00	118.16	0.0	0.0	5.09	6.06	-128.38	Stable
n(C1R5)	0	0.4	0.4	0.00	151.49	0.0	0.0	7.96	7.57	-157.91	Stable
n(C1R6)	0	0.48	0.48	0.00	186.33	0.0	0.0	11.46	9.09	-188.95	Stable
n(C1R7)	0	0.56	0.56	0.00	222.68	0.0	0.0	15.60	10.60	-221.51	Stable
n(C2R1)	0.08	0.08	0.08	0.32	25.75	0.03	0.006	0.32	1.51	-46.75	Stable
n(C2R2)	0.16	0.16	0.16	1.27	53.02	0.20	0.025	1.27	3.03	-69.34	Stable
n(C2R3)	0.24	0.24	0.24	2.87	77.26	0.69	0.056	2.87	4.54	-87.90	Stable
n(C2R4)	0.32	0.32	0.32	5.09	112.10	1.63	0.099	5.09	6.06	-117.16	Stable
n(C2R5)	0.4	0.4	0.4	7.96	143.91	3.18	0.155	7.96	7.57	-142.39	Stable
n(C2R6)	0.48	0.48	0.48	11.46	177.24	5.50	0.224	11.46	9.09	-168.50	Stable
n(C2R7)	0.56	0.56	0.56	15.60	212.08	8.74	0.304	15.60	10.60	-195.48	Stable
n(C3R1)	0.08	0.08	0.08	0.64	24.24	0.05	0.012	0.32	1.51	-44.62	Stable
n(C3R2)	0.16	0.16	0.16	2.55	49.99	0.41	0.050	1.27	3.03	-64.82	Stable
n(C3R3)	0.24	0.24	0.24	5.73	72.72	1.38	0.112	2.87	4.54	-80.36	Stable
n(C3R4)	0.32	0.32	0.32	10.19	106.04	3.26	0.199	5.09	6.06	-105.95	Stable
n(C3R5)	0.4	0.4	0.4	15.92	136.34	6.37	0.311	7.96	7.57	-126.87	Stable
n(C3R6)	0.48	0.48	0.48	22.93	168.15	11.01	0.447	11.46	9.09	-148.04	Stable
n(C3R7)	0.56	0.56	0.56	31.21	201.48	17.48	0.609	15.60	10.60	-169.45	Stable
n(C4R1)	0.08	0.08	0.08	0.96	22.72	0.08	0.019	0.32	1.51	-42.50	Stable
n(C4R2)	0.16	0.16	0.16	3.82	46.96	0.61	0.075	1.27	3.03	-60.31	Stable
n(C4R3)	0.24	0.24	0.24	8.60	68.17	2.06	0.168	2.87	4.54	-72.81	Stable

Table C-1 Example of rock toppling failure of 4×4×8 cm blocks size. (cont.)

n	M_n (m)	L_n (m)	Y_n (m)	P_n (N/m)	P_R (N/m)	P_nM_n	$P_n\Delta X\tan\phi$	P_d (kN/m)	P_r (kN/m)	P_n,t (N/m)	Results
n(C4R4)	0.32	0.32	0.32	15.28	99.98	4.89	0.298	5.09	6.06	-94.74	Stable
n(C4R5)	0.4	0.4	0.4	23.88	128.76	9.55	0.466	7.96	7.57	-111.36	Stable
n(C4R6)	0.48	0.48	0.48	34.39	159.06	16.51	0.671	11.46	9.09	-127.58	Stable
n(C4R7)	0.56	0.56	0.56	46.81	190.87	26.21	0.913	15.60	10.60	-143.41	Stable
n(C5R1)	0.08	0.08	0.08	1.27	21.21	0.10	0.025	0.32	1.51	-40.37	Stable
n(C5R2)	0.16	0.16	0.16	5.09	43.93	0.82	0.099	1.27	3.03	-55.79	Stable
n(C5R3)	0.24	0.24	0.24	11.46	63.63	2.75	0.224	2.87	4.54	-65.26	Stable
n(C5R4)	0.32	0.32	0.32	20.38	93.92	6.52	0.398	5.09	6.06	-83.52	Stable
n(C5R5)	0.4	0.4	0.4	31.84	121.19	12.74	0.621	7.96	7.57	-95.84	Stable
n(C5R6)	0.48	0.48	0.48	45.85	149.97	22.01	0.895	11.46	9.09	-107.13	Stable
n(C5R7)	0.56	0.56	0.56	62.41	180.27	34.95	1.218	15.60	10.60	-117.38	Stable
n(C6R1)	0.08	0.08	0.08	1.59	19.69	0.13	0.031	0.32	1.51	-38.25	Stable
n(C6R2)	0.16	0.16	0.16	6.37	40.90	1.02	0.124	1.27	3.03	-51.27	Stable
n(C6R3)	0.24	0.24	0.24	14.33	59.08	3.44	0.280	2.87	4.54	-57.72	Stable
n(C6R4)	0.32	0.32	0.32	25.47	87.86	8.15	0.497	5.09	6.06	-72.31	Stable
n(C6R5)	0.4	0.4	0.4	39.80	113.61	15.92	0.777	7.96	7.57	-80.33	Stable
n(C6R6)	0.48	0.48	0.48	57.32	140.88	27.51	1.118	11.46	9.09	-86.67	Stable
n(C6R7)	0.56	0.56	0.56	78.02	169.66	43.69	1.522	15.60	10.60	-91.35	Stable
n(C7R1)	0.08	0.08	0.08	1.91	18.18	0.15	0.037	0.32	1.51	-36.12	Stable
n(C7R2)	0.16	0.16	0.16	7.64	37.87	1.22	0.149	1.27	3.03	-46.75	Stable
n(C7R3)	0.24	0.24	0.24	17.20	54.54	4.13	0.335	2.87	4.54	-50.17	Stable
n(C7R4)	0.32	0.32	0.32	30.57	81.80	9.78	0.596	5.09	6.06	-61.10	Stable
n(C7R5)	0.4	0.4	0.4	47.77	106.04	19.11	0.932	7.96	7.57	-64.81	Stable

Table C-1 Example of rock toppling failure of 4×4×8 cm blocks size. (cont.)

n	M_n (m)	L_n (m)	Y_n (m)	P_n (N/m)	P_R (N/m)	P_nM_n	$P_n\Delta X\tan\phi$	P_d (kN/m)	P_r (kN/m)	P_n,t (N/m)	Results
$n_{(C7R6)}$	0.48	0.48	0.48	68.78	131.79	33.02	1.342	11.46	9.09	-66.22	Stable
$n_{(C7R7)}$	0.56	0.56	0.56	93.62	159.06	52.43	1.826	15.60	10.60	-65.32	Stable
$n_{(C8R1)}$	0.08	0.08	0.08	2.23	16.66	0.18	0.043	0.32	1.51	-34.00	Stable
$n_{(C8R2)}$	0.16	0.16	0.16	8.92	34.84	1.43	0.174	1.27	3.03	-42.24	Stable
$n_{(C8R3)}$	0.24	0.24	0.24	20.06	49.99	4.81	0.391	2.87	4.54	-42.62	Stable
$n_{(C8R4)}$	0.32	0.32	0.32	35.66	75.74	11.41	0.696	5.09	6.06	-49.88	Stable
$n_{(C8R5)}$	0.4	0.4	0.4	55.73	98.47	22.29	1.087	7.96	7.57	-49.29	Stable
$n_{(C8R6)}$	0.48	0.48	0.48	80.25	122.70	38.52	1.566	11.46	9.09	-45.76	Stable
$n_{(C8R7)}$	0.56	0.56	0.56	109.22	148.46	61.17	2.131	15.60	10.60	-39.28	Stable
$n_{(C9R1)}$	0.08	0.08	0.08	2.55	15.15	0.20	0.050	0.32	1.51	-31.87	Stable
$n_{(C9R2)}$	0.16	0.16	0.16	10.19	31.81	1.63	0.199	1.27	3.03	-37.72	Stable
$n_{(C9R3)}$	0.24	0.24	0.24	22.93	45.45	5.50	0.447	2.87	4.54	-35.08	Stable
$n_{(C9R4)}$	0.32	0.32	0.32	40.76	69.68	13.04	0.795	5.09	6.06	-38.67	Stable
$n_{(C9R5)}$	0.4	0.4	0.4	63.69	90.89	25.47	1.242	7.96	7.57	-33.78	Stable
$n_{(C9R6)}$	0.48	0.48	0.48	91.71	113.61	44.02	1.789	11.46	9.09	-25.30	Stable
$n_{(C9R7)}$	0.56	0.56	0.56	124.83	137.85	69.90	2.435	15.60	10.60	-13.25	Stable
$n_{(C10R1)}$	0.08	0.08	0.08	2.87	13.63	0.23	0.056	0.32	1.51	-29.75	Stable
$n_{(C10R2)}$	0.16	0.16	0.16	11.46	28.78	1.83	0.224	1.27	3.03	-33.20	Stable
$n_{(C10R3)}$	0.24	0.24	0.24	25.79	40.91	6.19	0.503	2.87	4.54	-27.53	Stable
$n_{(C10R4)}$	0.32	0.32	0.32	45.85	63.62	14.67	0.895	5.09	6.06	-27.46	Stable
$n_{(C10R5)}$	0.4	0.4	0.4	71.65	83.32	28.66	1.398	7.96	7.57	-18.26	Stable
$n_{(C10R6)}$	0.48	0.48	0.48	103.17	104.53	49.52	2.013	11.46	9.09	-4.85	Stable
$n_{(C10R7)}$	0.56	0.56	0.56	140.43	127.25	78.64	2.740	15.60	10.60	12.78	Toppling

Table C-1 Example of rock toppling failure of 4×4×8 cm blocks size. (cont.)

n	M_n (m)	L_n (m)	Y_n (m)	P_n (N/m)	P_R (N/m)	P_nM_n	$P_n\Delta X\tan\phi$	P_d (kN/m)	P_r (kN/m)	P_nt (N/m)	Results
n(C11R1)	0.08	0.08	0.08	3.18	12.12	0.25	0.062	0.32	1.51	-27.62	Stable
n(C11R2)	0.16	0.16	0.16	12.74	25.75	2.04	0.248	1.27	3.03	-28.68	Stable
n(C11R3)	0.24	0.24	0.24	28.66	36.36	6.88	0.559	2.87	4.54	-19.98	Stable
n(C11R4)	0.32	0.32	0.32	50.95	57.56	16.30	0.994	5.09	6.06	-16.24	Stable
n(C11R5)	0.4	0.4	0.4	79.61	75.74	31.84	1.553	7.96	7.57	-2.74	Stable
n(C11R6)	0.48	0.48	0.48	114.64	95.44	55.03	2.236	11.46	9.09	15.61	Toppling
n(C11R7)	0.56	0.56	0.56	156.03	116.64	87.38	3.044	15.60	10.60	38.82	Toppling
n(C12R1)	0.08	0.08	0.08	3.50	10.60	0.28	0.068	0.32	1.51	-25.50	Stable
n(C12R2)	0.16	0.16	0.16	14.01	22.72	2.24	0.273	1.27	3.03	-24.17	Stable
n(C12R3)	0.24	0.24	0.24	31.53	31.82	7.57	0.615	2.87	4.54	-12.43	Stable
n(C12R4)	0.32	0.32	0.32	56.04	51.51	17.93	1.093	5.09	6.06	-5.03	Stable
n(C12R5)	0.4	0.4	0.4	87.57	68.17	35.03	1.708	7.96	7.57	12.77	Toppling
n(C12R6)	0.48	0.48	0.48	126.10	86.35	60.53	2.460	11.46	9.09	36.07	Toppling
n(C12R7)	0.56	0.56	0.56	171.64	106.04	96.12	3.349	15.60	10.60	64.85	Toppling
n(C13R1)	0.08	0.08	0.08	3.82	9.09	0.31	0.075	0.32	1.51	-23.37	Stable
n(C13R2)	0.16	0.16	0.16	15.28	19.69	2.45	0.298	1.27	3.03	-19.65	Stable
n(C13R3)	0.24	0.24	0.24	34.39	27.27	8.25	0.671	2.87	4.54	-4.89	Stable
n(C13R4)	0.32	0.32	0.32	61.14	45.45	19.56	1.193	5.09	6.06	6.18	Toppling
n(C13R5)	0.4	0.4	0.4	95.53	60.59	38.21	1.864	7.96	7.57	28.29	Toppling
n(C13R6)	0.48	0.48	0.48	137.56	77.26	66.03	2.684	11.46	9.09	56.52	Toppling
n(C13R7)	0.56	0.56	0.56	187.24	95.44	104.85	3.653	15.60	10.60	90.88	Toppling
n(C14R1)	0.08	0.08	0.08	4.14	7.57	0.33	0.081	0.32	1.51	-21.25	Stable
n(C14R2)	0.16	0.16	0.16	16.56	16.66	2.65	0.323	1.27	3.03	-15.13	Stable

Table C-1 Example of rock toppling failure of 4×4×8 cm blocks size. (cont.)

n	M_n (m)	L_n (m)	Y_n (m)	P_n (N/m)	P_R (N/m)	P_nM_n	$P_n\Delta X\tan\phi$	P_d (kN/m)	P_r (kN/m)	P_n,t (N/m)	Results
n(C14R3)	0.24	0.24	0.24	37.26	22.73	8.94	0.727	2.87	4.54	2.66	Toppling
n(C14R4)	0.32	0.32	0.32	66.23	39.39	21.20	1.292	5.09	6.06	17.40	Toppling
n(C14R5)	0.4	0.4	0.4	103.49	53.02	41.40	2.019	7.96	7.57	43.80	Toppling
n(C14R6)	0.48	0.48	0.48	149.03	68.17	71.53	2.907	11.46	9.09	76.98	Toppling
n(C14R7)	0.56	0.56	0.56	202.84	84.83	113.59	3.957	15.60	10.60	116.92	Toppling
n(C15R1)	0.08	0.08	0.08	4.46	6.06	0.36	0.087	0.32	1.51	-19.12	Stable
n(C15R2)	0.16	0.16	0.16	17.83	13.63	2.85	0.348	1.27	3.03	-10.61	Stable
n(C15R3)	0.24	0.24	0.24	40.12	18.18	9.63	0.783	2.87	4.54	10.21	Toppling
n(C15R4)	0.32	0.32	0.32	71.33	33.33	22.83	1.392	5.09	6.06	28.61	Toppling
n(C15R5)	0.4	0.4	0.4	111.45	45.45	44.58	2.174	7.96	7.57	59.32	Toppling
n(C15R6)	0.48	0.48	0.48	160.49	59.08	77.04	3.131	11.46	9.09	97.43	Toppling
n(C15R7)	0.56	0.56	0.56	218.45	74.23	122.33	4.262	15.60	10.60	142.95	Toppling
n(C16R1)	0.08	0.08	0.08	4.78	4.54	0.38	0.093	0.32	1.51	-17.00	Stable
n(C16R2)	0.16	0.16	0.16	19.11	10.60	3.06	0.373	1.27	3.03	-6.10	Stable
n(C16R3)	0.24	0.24	0.24	42.99	13.64	10.32	0.839	2.87	4.54	17.75	Toppling
n(C16R4)	0.32	0.32	0.32	76.42	27.27	24.46	1.491	5.09	6.06	39.82	Toppling
n(C16R5)	0.4	0.4	0.4	119.41	37.87	47.77	2.330	7.96	7.57	74.84	Toppling
n(C16R6)	0.48	0.48	0.48	171.96	49.99	82.54	3.355	11.46	9.09	117.89	Toppling
n(C16R7)	0.56	0.56	0.56	234.05	63.62	131.07	4.566	15.60	10.60	168.98	Toppling
n(C17R1)	0.08	0.08	0.08	5.09	3.03	0.41	0.099	0.32	1.51	-14.87	Stable
n(C17R2)	0.16	0.16	0.16	20.38	7.57	3.26	0.398	1.27	3.03	-1.58	Stable
n(C17R3)	0.24	0.24	0.24	45.85	9.09	11.01	0.895	2.87	4.54	25.30	Toppling
n(C17R4)	0.32	0.32	0.32	81.52	21.21	26.09	1.590	5.09	6.06	51.03	Toppling

Table C-1 Example of rock toppling failure of 4×4×8 cm blocks size.   (cont.)

n	M_n (m)	L_n (m)	Y_n (m)	P_n (N/m)	P_R (N/m)	P_nM_n	$P_n\Delta X\tan\phi$	P_d (kN/m)	P_r (kN/m)	P_n,t (N/m)	Results
$n_{(C17R5)}$	0.4	0.4	0.4	127.37	30.30	50.95	2.485	7.96	7.57	90.35	Toppling
$n_{(C17R6)}$	0.48	0.48	0.48	183.42	40.90	88.04	3.578	11.46	9.09	138.35	Toppling
$n_{(C17R7)}$	0.56	0.56	0.56	249.65	53.02	139.81	4.871	15.60	10.60	195.02	Toppling
$n_{(C18R1)}$	0.08	0.08	0.08	5.41	1.51	0.43	0.106	0.32	1.51	-12.75	Stable
$n_{(C18R2)}$	0.16	0.16	0.16	21.65	4.54	3.46	0.422	1.27	3.03	2.94	Toppling
$n_{(C18R3)}$	0.24	0.24	0.24	48.72	9.09	11.69	0.951	2.87	4.54	27.94	Toppling
$n_{(C18R4)}$	0.32	0.32	0.32	86.61	15.15	27.72	1.690	5.09	6.06	62.25	Toppling
$n_{(C18R5)}$	0.4	0.4	0.4	135.34	22.72	54.13	2.640	7.96	7.57	105.87	Toppling
$n_{(C18R6)}$	0.48	0.48	0.48	194.88	31.81	93.54	3.802	11.46	9.09	158.80	Toppling
$n_{(C18R7)}$	0.56	0.56	0.56	265.26	42.42	148.54	5.175	15.60	10.60	221.05	Toppling
$n_{(C19R1)}$	0.08	0	0.08	5.73	0.00	0.46	0.112	0.32	1.51	-	Toppling
$n_{(C19R2)}$	0.16	0.08	0.16	22.93	1.51	3.67	0.447	1.27	3.03	16.43	Toppling
$n_{(C19R3)}$	0.24	0.16	0.24	51.59	4.54	12.38	1.006	2.87	4.54	55.50	Toppling
$n_{(C19R4)}$	0.32	0.24	0.32	91.71	9.09	29.35	1.789	5.09	6.06	100.98	Toppling
$n_{(C19R5)}$	0.4	0.32	0.40	143.30	15.15	57.32	2.796	7.96	7.57	155.52	Toppling
$n_{(C19R6)}$	0.48	0.4	0.48	206.35	22.72	99.05	4.026	11.46	9.09	219.66	Toppling
$n_{(C19R7)}$	0.56	0.48	0.56	280.86	31.81	157.28	5.479	15.60	10.60	293.57	Toppling
$n_{(C20R2)}$	0.08	0	0.08	24.20	0.00	1.94	0.472	0.32	1.51	-	Toppling
$n_{(C20R3)}$	0.16	0.08	0.16	54.45	1.51	8.71	1.062	1.27	3.03	71.79	Toppling
$n_{(C20R4)}$	0.24	0.16	0.24	96.80	4.54	23.23	1.889	2.87	4.54	117.81	Toppling
$n_{(C20R5)}$	0.32	0.24	0.32	151.26	9.09	48.40	2.951	5.09	6.06	175.53	Toppling
$n_{(C20R6)}$	0.4	0.32	0.4	217.81	15.15	87.12	4.249	7.96	7.57	244.12	Toppling
$n_{(C20R7)}$	0.48	0.4	0.48	296.46	22.72	142.30	5.784	11.46	9.09	323.40	Toppling

Table C-1 Example of rock toppling failure of 4×4×8 cm blocks size. (cont.)

n	M_n (m)	L_n (m)	Y_n (m)	P_n (N/m)	P_R (N/m)	P_nM_n	$P_n\Delta X\tan\phi$	P_d (kN/m)	P_r (kN/m)	$P_n t$ (N/m)	Results
$n_{(C21R3)}$	0.08	0	0.08	54.45	0.00	4.36	1.062	0.32	1.51	-	Toppling
$n_{(C21R4)}$	0.16	0.08	0.16	96.81	1.51	15.49	1.889	1.27	3.03	146.17	Toppling
$n_{(C21R5)}$	0.24	0.16	0.24	151.26	4.54	36.30	2.951	2.87	4.54	192.86	Toppling
$n_{(C21R6)}$	0.32	0.24	0.32	217.82	9.09	69.70	4.249	5.09	6.06	258.87	Toppling
$n_{(C21R7)}$	0.4	0.32	0.4	296.47	15.15	118.59	5.784	7.96	7.57	337.65	Toppling
$n_{(C22R4)}$	0.08	0	0.08	96.81	0.00	7.74	1.889	0.32	1.51	-	Toppling
$n_{(C22R5)}$	0.16	0.08	0.16	151.26	1.51	24.20	2.951	1.27	3.03	241.81	Toppling
$n_{(C22R6)}$	0.24	0.16	0.24	217.82	4.54	52.28	4.250	2.87	4.54	284.58	Toppling
$n_{(C22R7)}$	0.32	0.24	0.32	296.48	9.09	94.87	5.784	5.09	6.06	357.36	Toppling
$n_{(C23R5)}$	0.08	0	0.08	151.27	0.00	12.10	2.951	0.32	1.51	-	Toppling
$n_{(C23R6)}$	0.16	0.08	0.16	217.83	1.51	34.85	4.250	1.27	3.03	358.70	Toppling
$n_{(C23R7)}$	0.24	0.16	0.24	296.49	4.54	71.16	5.784	2.87	4.54	392.99	Toppling
$n_{(C24R6)}$	0.08	0	0.08	217.83	0.00	17.43	4.250	0.32	1.51	-	Toppling
$n_{(C24R7)}$	0.16	0.08	0.16	296.49	1.51	47.44	5.784	1.27	3.03	496.84	Toppling
$n_{(C25R7)}$	0.08	0	0.08	296.49	0.00	23.72	5.784	0.32	1.51	-	Toppling

Table C-2 Example of rock toppling failure of 4×4×12 cm blocks size at slope height 72 cm, ψ_f= 63°, ΔX = 4 cm, α = 5°, β = 63° and $y/\Delta X$ = 2.

n	M_n (m)	L_n (m)	Y_n (m)	P_n (N/m)	P_R (N/m)	P_nM_n	$P_n\Delta X\tan\phi$	P_d (kN/m)	P_r (kN/m)	P_n,t (N/m)	Results
n(C1R1)	0	0.12	0.12	0.00	18.97	0.0	0.0	0.72	2.27	-35.02	Stable
n(C1R2)	0	0.24	0.24	0.00	44.00	0.0	0.0	2.87	4.54	-54.58	Stable
n(C1R3)	0	0.36	0.36	0.00	75.11	0.0	0.0	6.45	6.82	-80.21	Stable
n(C1R4)	0	0.48	0.48	0.00	112.29	0.0	0.0	11.46	9.09	-111.90	Stable
n(C1R5)	0	0.6	0.6	0.00	155.53	0.0	0.0	17.91	11.36	-149.67	Stable
n(C1R6)	0	0.72	0.72	0.00	191.19	0.0	0.0	25.79	13.63	-179.49	Stable
n(C2R1)	0.12	0.12	0.12	0.72	16.69	0.09	0.014	0.72	2.27	-31.77	Stable
n(C2R2)	0.24	0.24	0.24	2.87	39.45	0.69	0.056	2.87	4.54	-47.02	Stable
n(C2R3)	0.36	0.36	0.36	6.45	68.28	2.32	0.126	6.45	6.82	-66.91	Stable
n(C2R4)	0.48	0.48	0.48	11.46	103.18	5.50	0.224	11.46	9.09	-91.43	Stable
n(C2R5)	0.6	0.6	0.6	17.91	144.15	10.75	0.349	17.91	11.36	-120.59	Stable
n(C2R6)	0.72	0.72	0.72	25.79	177.54	18.57	0.503	25.79	13.63	-140.36	Stable
n(C3R1)	0.12	0.12	0.12	1.43	14.42	0.17	0.028	0.72	2.27	-28.52	Stable
n(C3R2)	0.24	0.24	0.24	5.73	34.90	1.38	0.112	2.87	4.54	-39.47	Stable
n(C3R3)	0.36	0.36	0.36	12.90	61.45	4.64	0.252	6.45	6.82	-53.61	Stable
n(C3R4)	0.48	0.48	0.48	22.93	94.08	11.01	0.447	11.46	9.09	-70.96	Stable
n(C3R5)	0.6	0.6	0.6	35.82	132.77	21.49	0.699	17.91	11.36	-91.51	Stable
n(C3R6)	0.72	0.72	0.72	51.59	163.88	37.14	1.006	25.79	13.63	-101.24	Stable
n(C4R1)	0.12	0.12	0.12	2.15	12.14	0.26	0.042	0.72	2.27	-25.28	Stable
n(C4R2)	0.24	0.24	0.24	8.60	30.35	2.06	0.168	2.87	4.54	-31.91	Stable
n(C4R3)	0.36	0.36	0.36	19.34	54.63	6.96	0.377	6.45	6.82	-40.31	Stable

Table C-2 Example of rock toppling failure of 4×4×12 cm blocks size at slope height 72 cm, $\psi_f = 63°$, $\Delta X = 4$ cm, $\alpha = 5°$, $\beta = 63°$ and

y/ΔX = 2. (cont.)

n	M_n (m)	L_n (m)	Y_n (m)	P_n (N/m)	P_R (N/m)	P_nM_n	$P_n\Delta X\tan\phi$	P_d (kN/m)	P_r (kN/m)	P_n,t (N/m)	Results
n(C4R4)	0.48	0.48	0.48	34.39	84.97	16.51	0.671	11.46	9.09	-50.49	Stable
n(C4R5)	0.6	0.6	0.6	53.74	121.39	32.24	1.048	17.91	11.36	-62.43	Stable
n(C4R6)	0.72	0.72	0.72	77.38	150.22	55.71	1.510	25.79	13.63	-62.12	Stable
n(C5R1)	0.12	0.12	0.12	2.87	9.86	0.34	0.056	0.72	2.27	-22.03	Stable
n(C5R2)	0.24	0.24	0.24	11.46	25.80	2.75	0.224	2.87	4.54	-24.36	Stable
n(C5R3)	0.36	0.36	0.36	25.79	47.80	9.29	0.503	6.45	6.82	-27.02	Stable
n(C5R4)	0.48	0.48	0.48	45.85	75.87	22.01	0.895	11.46	9.09	-30.02	Stable
n(C5R5)	0.6	0.6	0.6	71.65	110.01	42.99	1.398	17.91	11.36	-33.35	Stable
n(C5R6)	0.72	0.72	0.72	103.17	136.57	74.28	2.013	25.79	13.63	-23.00	Stable
n(C6R1)	0.12	0.12	0.12	3.58	7.59	0.43	0.070	0.72	2.27	-18.79	Stable
n(C6R2)	0.24	0.24	0.24	14.33	21.24	3.44	0.280	2.87	4.54	-16.80	Stable
n(C6R3)	0.36	0.36	0.36	32.24	40.97	11.61	0.629	6.45	6.82	-13.72	Stable
n(C6R4)	0.48	0.48	0.48	57.32	66.77	27.51	1.118	11.46	9.09	-9.54	Stable
n(C6R5)	0.6	0.6	0.6	89.56	98.63	53.74	1.747	17.91	11.36	-4.27	Stable
n(C6R6)	0.72	0.72	0.72	128.97	122.91	92.86	2.516	25.79	13.63	16.12	Toppling
n(C7R1)	0.12	0.12	0.12	4.30	5.31	0.52	0.084	0.72	2.27	-15.54	Stable
n(C7R2)	0.24	0.24	0.24	17.20	16.69	4.13	0.335	2.87	4.54	-9.24	Stable
n(C7R3)	0.36	0.36	0.36	38.69	34.14	13.93	0.755	6.45	6.82	-0.42	Stable
n(C7R4)	0.48	0.48	0.48	68.78	57.66	33.02	1.342	11.46	9.09	10.93	Toppling
n(C7R5)	0.6	0.6	0.6	107.47	87.25	64.48	2.097	17.91	11.36	24.81	Toppling
n(C7R6)	0.72	0.72	0.72	154.76	109.25	111.43	3.019	25.79	13.63	55.24	Toppling
n(C8R1)	0.12	0.12	0.12	5.02	3.03	0.60	0.098	0.72	2.27	-12.29	Stable

Table C-2 Example of rock toppling failure of 4×4×12 cm blocks size at slope height 72 cm, ψ_f = 63°, ΔX = 4 cm, α = 5°, β = 63° and

y/ΔX = 2. (cont.)

n	M_n (m)	L_n (m)	Y_n (m)	P_n (N/m)	P_R (N/m)	P_nM_n	$P_n\Delta X \tan\phi$	P_d (kN/m)	P_r (kN/m)	P_n,t (N/m)	Results
n(C8R2)	0.24	0.24	0.24	20.06	12.14	4.81	0.391	2.87	4.54	-1.69	Stable
n(C8R3)	0.36	0.36	0.36	45.14	27.31	16.25	0.881	6.45	6.82	12.87	Stable
n(C8R4)	0.48	0.48	0.48	80.25	48.56	38.52	1.566	11.46	9.09	31.40	Toppling
n(C8R5)	0.6	0.6	0.6	125.38	75.87	75.23	2.446	17.91	11.36	53.89	Toppling
n(C8R6)	0.72	0.72	0.72	180.55	95.60	130.00	3.522	25.79	13.63	94.36	Toppling
n(C9R1)	0.12	0.12	0.08	5.73	1.52	0.69	0.112	0.32	1.51	-6.93	Stable
n(C9R2)	0.24	0.24	0.16	22.93	9.10	5.50	0.447	1.27	3.03	3.90	Toppling
n(C9R3)	0.36	0.36	0.24	51.59	22.76	18.57	1.006	2.87	4.54	20.13	Toppling
n(C9R4)	0.48	0.48	0.32	91.71	42.49	44.02	1.789	5.09	6.06	41.76	Toppling
n(C9R5)	0.6	0.6	0.4	143.30	68.28	85.98	2.796	7.96	7.57	68.78	Toppling
n(C9R6)	0.72	0.72	0.48	206.35	86.49	148.57	4.026	11.46	9.09	115.22	Toppling
n(C10R1)	0.12	0	0.08	6.45	0.00	0.77	0.126	0.32	1.51	-	Toppling
n(C10R2)	0.24	0.12	0.16	25.79	6.07	6.19	0.503	1.27	3.03	25.70	Toppling
n(C10R3)	0.36	0.24	0.24	58.03	18.21	20.89	1.132	2.87	4.54	55.65	Toppling
n(C10R4)	0.48	0.36	0.32	103.17	36.42	49.52	2.013	5.09	6.06	90.90	Toppling
n(C10R5)	0.6	0.48	0.4	161.21	60.70	96.72	3.145	7.96	7.57	132.60	Toppling
n(C10R6)	0.72	0.6	0.48	232.14	77.39	167.14	4.529	11.46	9.09	195.07	Toppling
n(C11R2)	0.12	0.12	0.16	28.66	3.03	3.44	0.559	1.27	3.03	5.84	Toppling
n(C11R3)	0.24	0.24	0.24	64.48	13.66	15.48	1.258	2.87	4.54	37.48	Toppling
n(C11R4)	0.36	0.36	0.32	114.64	30.35	41.27	2.236	5.09	6.06	73.75	Toppling
n(C11R5)	0.48	0.48	0.4	179.12	53.11	85.98	3.495	7.96	7.57	117.38	Toppling

Table C-2 Example of rock toppling failure of 4×4×12 cm blocks size at slope height 72 cm, $\psi_f = 63°$, $\Delta X = 4$ cm, $\alpha = 5°$, $\beta = 63°$ and $y/\Delta X = 2$. (cont.)

n	M_n (m)	L_n (m)	Y_n (m)	P_n (N/m)	P_R (N/m)	$P_n M_n$	$P_n \Delta X \tan \phi$	P_d (kN/m)	P_r (kN/m)	$P_{n,t}$ (N/m)	Results
n(C11R6)	0.6	0.6	0.48	257.93	68.28	154.76	5.032	11.46	9.09	183.00	Toppling
n(C12R2)	0.12	0	0.16	31.53	0.00	3.78	0.615	1.27	3.03	-	Toppling
n(C12R3)	0.24	0.12	0.24	70.93	9.10	17.02	1.384	2.87	4.54	105.76	Toppling
n(C12R4)	0.36	0.24	0.32	126.10	24.28	45.40	2.460	5.09	6.06	148.63	Toppling
n(C12R5)	0.48	0.36	0.4	197.03	45.52	94.58	3.844	7.96	7.57	205.12	Toppling
n(C12R6)	0.6	0.48	0.48	283.73	59.18	170.24	5.535	11.46	9.09	286.49	Toppling
n(C13R3)	0.12	0.12	0.24	77.38	4.55	9.29	1.510	2.87	4.54	45.52	Toppling
n(C13R4)	0.24	0.24	0.32	137.56	18.21	33.02	2.684	5.09	6.06	102.67	Toppling
(C13R5)	0.36	0.36	0.4	214.94	37.94	77.38	4.193	7.96	7.57	164.38	Toppling
n(C13R6)	0.48	0.48	0.48	309.52	50.07	148.57	6.039	11.46	9.09	249.78	Toppling
n(C14R3)	0.12	0	0.24	83.83	0.00	10.06	1.635	2.87	4.54	-	Toppling
n(C14R4)	0.24	0.12	0.32	149.03	12.14	35.77	2.907	5.09	6.06	251.68	Toppling
n(C14R5)	0.36	0.24	0.4	232.86	30.35	83.83	4.543	7.96	7.57	299.15	Toppling
n(C14R6)	0.48	0.36	0.48	335.31	40.97	160.95	6.542	11.46	9.09	392.32	Toppling
n(C15R4)	0.12	0.12	0.32	160.49	6.07	19.26	3.131	5.09	6.06	119.31	Toppling
n(C15R5)	0.24	0.24	0.4	250.77	22.76	60.18	4.892	7.96	7.57	207.38	Toppling
n(C15R6)	0.36	0.36	0.48	361.11	31.87	130.00	7.045	11.46	9.09	314.54	Toppling
n(C16R4)	0.12	0	0.32	171.96	0.00	20.63	3.355	5.09	6.06	-	Toppling
n(C16R5)	0.24	0.12	0.4	268.68	15.17	64.48	5.242	7.96	7.57	479.26	Toppling
n(C16R6)	0.36	0.24	0.48	386.90	22.76	139.28	7.548	11.46	9.09	534.18	Toppling
n(C17R5)	0.12	0.12	0.4	286.59	7.59	34.39	5.591	7.96	7.57	234.40	Toppling

Table C-2 Example of rock toppling failure of 4×4×12 cm blocks size at slope height 72 cm, $\psi_f = 63°$, $\Delta X = 4$ cm, $\alpha = 5°$, $\beta = 63°$ and $y/\Delta X = 2$. (cont.)

n	M_n (m)	L_n (m)	Y_n (m)	P_n (N/m)	P_R (N/m)	P_nM_n	$P_n\Delta X\tan\phi$	P_d (kN/m)	P_r (kN/m)	P_n,t (N/m)	Results
$n_{(C17R6)}$	0.24	0.24	0.48	412.69	13.66	99.05	8.051	11.46	9.09	374.27	Toppling
$n_{(C18R5)}$	0.12	0	0.4	304.50	0.00	36.54	5.941	7.96	7.57	-	Toppling
$n_{(C18R6)}$	0.24	0.12	0.48	438.49	4.55	105.24	8.555	11.46	9.09	820.18	Toppling
$n_{(C19R6)}$	0.12	0.12	0.12	464.28	2.28	55.71	9.058	0.72	2.27	373.19	Toppling
$n_{(C20R6)}$	0.12	0	0.12	490.07	0.00	58.81	9.561	0.72	2.27	-	Toppling

APPENDIX D

SIMULATION RESULTS OF ROCK SLOPE UNDER DYNAMIC LOAD

Table D-1 Results of slope stability analysis for 4×4×4 cm blocks size under dynamic loading.

Series	Amplitude (mm)	A (cm)	b (cm)	h (cm)	H (cm)	α (degrees)	ψ_p (degrees)	ψ_f (degrees)	W (kN/m)	K_h or a (g)	Stability*
C-S2-H2-M2-4d	23.47	151.4	61.4	44.8	67.6	85	15	40.5	11.3	0.046	F
C-S2-H2-M2-5d	23.47	151.1	57.3	44.8	62.9	80	12	38	11.1	0.033	S
C-S2-H2-M2-6d	23.47	151.1	57.3	44.8	62.9	80	12	38	11.1	0.046	F
C-S2-H2-M2-7d	23.47	151.1	57.3	44.8	62.9	80	12	38	11.1	0.067	F
C-S2-H2-M2-8d	23.47	151.3	66.3	44.5	59.0	87	10	37	11.5	0.046	S
C-S2-H2-M2-9d	23.47	151.3	66.3	44.5	59.0	87	10	37	11.5	0.067	F
C-S2-H2-M2-10d	23.47	151.1	62.1	44.6	56.9	75	8	34	11.3	0.046	S
C-S2-H2-M2-11d	23.47	151.1	62.1	44.6	56.9	75	8	34	11.3	0.067	S
C-S2-H2-M2-12d	23.47	151.1	62.0	44.6	53.3	80	6	33.5	11.3	0.046	S
C-S2-H2-M2-13d	23.47	151.1	62.0	44.6	53.3	80	6	33.5	11.3	0.067	S
C-S2-H2-M2-14d	23.47	151.3	69.5	44.7	50.6	90	4	31.5	11.7	0.046	S
C-S2-H2-M2-15d	23.47	151.3	69.5	44.7	50.6	90	4	31.5	11.7	0.067	S
C-S2-H2-M2-16d	23.47	151.3	61.4	44.7	50.6	80	4	31.5	11.3	0.119	F
C-S2-H2-M2-17d	23.47	151.1	63.7	44.8	47.8	85	2	29	11.5	0.067	S
C-S2-H2-M2-18d	23.47	151.1	59.2	44.8	47.8	85	2	29	11.2	0.119	S
C-S2-H2-M2-19d	23.47	150.3	51.2	44.8	46.3	70	1	28	10.7	0.067	S

* Notes   F = Failure

           S = Stable (No failure)

Table D-1 Results of slope stability analysis for 4×4×4 cm blocks size under dynamic loading. (cont.)

Series	Amplitude (mm)	A (cm)	b (cm)	h (cm)	H (cm)	α (degrees)	ψp (degrees)	ψf (degrees)	W (kN/m)	Kh or a (g)	Stability*
C-S2-H2-M2-16d	23.47	151.3	61.4	44.7	50.6	80	4	31.5	11.3	0.119	F
C-S2-H2-M2-17d	23.47	151.1	63.7	44.8	47.8	85	2	29	11.5	0.067	S
C-S2-H2-M2-18d	23.47	151.1	59.2	44.8	47.8	85	2	29	11.2	0.119	S
C-S2-H2-M2-19d	23.47	150.3	51.2	44.8	46.3	70	1	28	10.7	0.067	S
C-S2-H2-M2-20d	23.47	150.3	51.2	44.8	46.3	70	1	28	10.7	0.119	S
C-S2-H1-M1-1d	23.47	151.3	42.5	52.8	80.3	85	15	40	12.2	0.013	S
C-S2-H1-M1-2d	23.47	151.3	42.5	52.8	81.3	85	16	41.5	12.2	0.013	S
C-S2-H1-M1-3d	23.47	151.3	42.5	52.8	80.8	85	17	44	12.2	0.013	F
C-S2-H1-M1-4d	23.47	150.2	41.0	52.7	80.2	80	15	40	12.0	0.013	S
C-S2-H1-M1-5d	23.47	150.2	41.0	52.7	80.2	80	15	40	12.0	0.017	S
C-S2-H1-M1-6d	23.47	150.2	41.0	52.7	80.4	80	16	42	12.0	0.017	F
C-S2-H1-M1-8d	23.47	150.2	45.1	52.6	81.8	80	17	43	12.2	0.017	F
C-S2-H1-M1-9d	23.47	151.3	46.8	52.9	76.8	85	15	43	12.5	0.027	F
C-S2-H1-M1-10d	23.47	151.3	46.8	52.9	78.3	85	16	44	12.5	0.027	F
C-S2-H1-M1-11d	23.47	149.6	40.6	52.8	76.3	91	14	41	12.0	0.027	S
C-S2-H2-M1-1d	23.47	149.6	40.6	52.8	78.1	93	16	44	12.0	0.013	S
C-S2-H2-M1-2d	23.47	149.6	40.6	52.8	82.9	95	18	44.5	12.0	0.013	F

* Notes   F = Failure
            S = Stable (No failure)

Table D-1 Results of slope stability analysis for 4×4×4 cm blocks size under dynamic loading. (cont.)

Series	Amplitude (mm)	A (cm)	b (cm)	h (cm)	H (cm)	α (degrees)	ψ_p (degrees)	ψ_f (degrees)	W (kN/m)	K_h or a (g)	Stability*
C-S2-H2-M1-3d	23.47	151.1	57.8	44.9	69.3	93	17	43.5	11.2	0.013	F
C-S2-H2-M4-1d	23.47	149.6	40.6	44.9	45.7	85	1	46	10.2	0.225	F
C-S2-H2-M4-1d	23.47	147.2	59.2	44.6	49.4	80	3	28.5	11.0	0.102	S
C-S2-H2-M4-2d	23.47	147.2	59.2	44.6	51.0	80	4	29.5	11.0	0.102	S
C-S2-H2-M4-3d	23.47	147.2	59.2	44.6	52.6	80	5	30.5	11.0	0.102	S
C-S2-H2-M4-4d	23.47	147.2	59.2	44.6	54.1	80	6	31.5	11.0	0.102	F

* Notes   F = Failure

         S = Stable (No failure)

Table D-2 Results of slope stability analysis for 4×4×8 cm blocks size under dynamic loading.

Series	Amplitude (mm)	A (cm)	b (cm)	h (cm)	H (cm)	α (degrees)	ψ_p (degrees)	ψ_f (degrees)	W (kN/m)	K_h or a (g)	Stability*
R8H-S1-H2-M1-1d	23.47	148.7	107.9	44.7	55.1	80.5	16	61.5	13.6	0.013	S
R8H-S1-H2-M1-2d	23.47	148.7	107.9	44.7	56.1	82.5	18	63.5	13.6	0.013	S
R8H-S1-H2-M1-3d	23.47	148.7	107.9	44.7	57.0	84.5	20	65.5	13.6	0.013	F
R8H-S1-H2-M1-4d	23.47	148.7	107.9	44.7	57.5	85.5	21	66.5	13.6	0.013	F
R8H-S1-H2-M1-5d	23.47	145.4	104.0	44.9	55.4	82.5	18	65.5	13.3	0.017	S
R8H-S1-H2-M1-6d	23.47	145.4	104.0	44.9	55.8	83.5	19	66.5	13.3	0.017	F
R8H-S1-H2-M1-8d	23.47	145.4	104.0	44.9	56.3	84.5	20	67.5	13.3	0.017	F
R8H-S1-H2-M1-9d	23.47	148.6	107.9	44.7	55.4	80.5	18	65	13.6	0.027	F
R8H-S1-H2-M1-10d	23.47	148.6	107.9	44.7	55.8	81.5	19	66	13.6	0.027	F
R8H-S1-H2-M2-1d	23.47	145.5	104.1	44.8	54.9	90	15	60	13.3	0.033	S
R8H-S1-H2-M2-2d	23.47	145.5	104.1	44.8	56.2	90	17	61.5	13.3	0.033	F
R8H-S1-H2-M2-3d	23.47	145.5	104.1	44.8	56.4	90	17.5	62	13.3	0.033	F
R8H-S1-H2-M2-4d	23.47	148.7	107.9	44.7	54.9	90	16	62	13.6	0.046	F
R8H-S1-H2-M2-5d	23.47	148.7	107.9	44.7	53.8	90	15	62.5	13.6	0.046	F
R8H-S1-H2-M1-2d	23.47	148.7	107.9	44.7	56.1	82.5	18	63.5	13.6	0.013	S
R8H-S1-H2-M1-3d	23.47	148.7	107.9	44.7	57.0	84.5	20	65.5	13.6	0.013	F
R8H-S1-H2-M1-4d	23.47	148.7	107.9	44.7	57.5	85.5	21	66.5	13.6	0.013	F
R8H-S1-H2-M1-5d	23.47	145.4	104.0	44.9	55.4	82.5	18	65.5	13.3	0.017	S
R8H-S1-H2-M1-6d	23.47	145.4	104.0	44.9	55.8	83.5	19	66.5	13.3	0.017	F
R8H-S1-H2-M1-8d	23.47	145.4	104.0	44.9	56.3	84.5	20	67.5	13.3	0.017	F
R8H-S1-H2-M1-9d	23.47	148.6	107.9	44.7	55.4	80.5	18	65	13.6	0.027	F

* Notes   F = Failure

       S = Stable (No failure)

Table D-2 Results of slope stability analysis for 4×4×8 cm blocks size under dynamic loading. (cont.)

Series	Amplitude (mm)	A (cm)	b (cm)	h (cm)	H (cm)	α (degrees)	ψp (degrees)	ψf (degrees)	W (kN/m)	Kh or a (g)	Stability*
R8H-S1-H2-M1-10d	23.47	148.6	107.9	44.7	55.8	81.5	19	66	13.6	0.027	F
R8H-S1-H2-M2-1d	23.47	145.5	104.1	44.8	54.9	90	15	60	13.3	0.033	S
R8H-S1-H2-M2-2d	23.47	145.5	104.1	44.8	56.2	90	17	61.5	13.3	0.033	F
R8H-S1-H2-M2-3d	23.47	145.5	104.1	44.8	56.4	90	17.5	62	13.3	0.033	F
R8H-S1-H2-M2-4d	23.47	148.7	107.9	44.7	54.9	90	16	62	13.6	0.046	F
R8H-S1-H2-M2-5d	23.47	148.7	107.9	44.7	53.8	90	15	62.5	13.6	0.046	F
R8H-S1-H2-M2-6d	23.47	148.7	107.9	44.7	53.3	90	13	59	13.6	0.046	S
R8H-S1-H2-M2-7d	23.47	148.7	107.9	44.7	53.1	90	14	62	13.6	0.046	S
R8H-S1-H2-M2-8d	23.47	145.5	95.7	44.7	51.1	75	10	57.5	12.8	0.067	S
R8H-S1-H2-M2-9d	23.47	145.5	95.7	44.7	48.2	75	5	52	12.8	0.067	S
R8H-S1-H2-M2-10d	23.47	145.5	95.7	44.7	48.8	75	6	53	12.8	0.067	S
R8H-S1-H2-M2-11d	23.47	145.5	95.7	44.7	49.3	75	7	55	12.8	0.067	S
R8H-S1-H2-M2-12d	23.47	145.5	95.7	44.7	49.9	75	8	56	12.8	0.067	F
R8H-S1-H2-M2-13d	23.47	148.7	108	44.7	47.9	85	5	54	13.7	0.119	F
R8H-S1-H2-M2-14d	23.47	148.5	107.8	44.7	46.1	85	2	49	13.6	0.119	S
R8H-S1-H2-M2-15d	23.47	148.7	107.8	44.7	45.4	85	1	48	13.6	0.119	S
R8H-S1-H2-M2-16d	23.47	148.7	107.8	44.6	51.7	90	11	58	13.6	0.046	S
R8H-S1-H2-M2-17d	23.47	148.7	107.8	44.6	52.3	90	12	59	13.6	0.046	S
R8H-S1-H2-M2-18d	23.47	148.7	107.8	44.6	51.7	90	11	58	13.6	0.067	S
R8H-S1-H2-M2-19d	23.47	148.7	107.8	44.6	52.3	90	12	59	13.6	0.067	F

* Notes   F = Failure

   S = Stable (No failure)

Table D-2 Results of slope stability analysis for 4×4×8 cm blocks size under dynamic loading. (cont.)

Series	Amplitude (mm)	A (cm)	b (cm)	h (cm)	H (cm)	α (degrees)	ψ_p (degrees)	ψ_f (degrees)	W (kN/m)	K_h or a (g)	Stability*
R8H-S1-H2-M1-11d	23.47	148.7	108	44.7	55.4	90	18	65	13.7	0.017	S
R8H-S1-H2-M1-13d	23.47	148.7	107.8	44.6	51.1	90	10	57	13.6	0.046	S
R8H-S1-H2-M1-14d	23.47	148.7	107.8	44.6	51.7	90	11	58	13.6	0.046	S
R8H-S1-H2-M1-15d	23.47	148.7	107.8	44.6	52.3	90	12	59	13.6	0.046	S
R8H-S1-H2-M1-16d	23.47	148.7	107.8	44.6	52.8	90	13	60	13.6	0.046	S
R8H-S1-H2-M1-17d	23.47	148.7	107.8	44.6	53.3	90	14	61	13.6	0.046	F
R8H-S1-H2-M1-18d	23.47	148.7	107.7	44.7	54.1	85	18	68	13.6	0.027	F
R8H-S1-H2-M2-20d	23.47	148.7	107.8	44.7	49.1	85	8	60	13.6	0.067	F
R8H-S1-H2-M2-21d	23.47	148.6	107.8	44.7	46.9	85	3	49.5	13.6	0.119	F
R8H-S1-H2-M2-22d	23.47	148.6	107.8	44.7	45.4	85	1	49.5	13.6	0.119	S
R8H-S1-H2-M2-23d	23.47	148.6	107.8	44.7	46.9	85	3	49.5	13.6	0.119	S
R8H-S1-H2-M3-2d	23.47	148.7	107.9	44.7	45.3	85	1	51	13.6	0.193	F
R8H-S1-H3-M1-1d	23.47	148.7	123.5	28.5	35.3	85	18	65	9.2	0.013	S
R8H-S1-H3-M1-2d	23.47	148.7	123.5	28.5	35.9	85	20	67	9.2	0.013	F
R8H-S1-H3-M1-3d	23.47	148.5	123.7	28.2	35.4	85	19	65.5	9.1	0.013	S
R8H-S1-H3-M1-4d	23.47	148.5	123.7	28.2	35.2	90	18	64	9.1	0.017	S
R8H-S1-H3-M1-5d	23.47	148.5	123.7	28.2	35.5	90	19	65	9.1	0.017	S
R8H-S1-H3-M1-6d	23.47	145.5	119	28.3	35.9	90	20	66	8.9	0.017	F
R8H-S1-H3-M1-7d	23.47	148.5	123.6	28.3	34.5	85	16	63	9.2	0.027	S

* Notes   F = Failure

         S = Stable (No failure)

Table D-2. Results of slope stability analysis for 4×4×8 cm blocks size under dynamic loading. (cont.)

Series	Amplitude (mm)	A (cm)	b (cm)	h (cm)	H (cm)	α (degrees)	ψ_p (degrees)	ψ_f (degrees)	W (kN/m)	K_h or a (g)	Stability*
R8H-S1-H3-M1-8d	23.47	148.5	123.6	28.3	34.8	85	17	64	9.2	0.027	S
R8H-S1-H3-M1-9d	23.47	148.5	123.6	28.3	35.1	85	18	65	9.2	0.027	F
R8H-S1-H3-M1-10d	23.47	149.8	123.5	28.9	36.1	85	19	66	9.4	0.027	F
R8H-S1-H3-M1-11d	23.47	149.7	123.6	28.4	33.3	85	12	59	9.2	0.046	S
R8H-S1-H3-M1-12d	23.47	149.7	123.6	28.4	33.6	85	13	60	9.2	0.046	S
R8H-S1-H3-M1-13d	23.47	149.7	123.6	28.4	34.0	85	14	61	9.2	0.046	S
R8H-S1-H3-M1-14d	23.47	147.7	123.6	28.4	34.3	85	15	62	9.2	0.046	F
R8H-S1-H2-M2-28d	23.47	144.4	103.2	44.7	54.9	85	16	62	13.2	0.033	S
R8H-S1-H2-M2-29d	23.47	144.4	103.2	44.7	55.4	85	17	63	13.2	0.033	S
R8H-S1-H2-M2-30d	23.47	144.4	103.2	44.7	55.9	85	18	64	13.2	0.033	F
R8H-S1-H2-M2-34d	23.47	178.7	106.9	44.6	52.3	85	12	59	15.2	0.067	F
R8H-S1-H2-M2-35d	23.47	148.7	106.9	45	56.7	85	17.5	62	13.7	0.033	F
R8H-S1-H2-M4-1d	23.47	140.3	99.7	44.5	45.3	90	1	46	12.7	0.225	F

* Notes   F = Failure

S = Stable (No failure)

Table D-3 Results of slope stability analysis for 4×4×12 cm blocks size under dynamic loading.

Series	Amplitude (mm)	A (cm)	b (cm)	h (cm)	H (cm)	α (degrees)	ψ_p (degrees)	ψ_f (degrees)	W (kN/m)	K_h or a (g)	Stability*
R12H-S1-H2-M2-1d	23.47	45.3	55.5	45.3	55.5	90	15	60	13.4	0.046	S
R12H-S1-H2-M2-2d	23.47	45.3	56.0	45.3	56.0	90	16	61	13.4	0.046	S
R12H-S1-H2-M2-3d	23.47	45.3	56.6	45.3	56.6	90	17	62	13.4	0.046	S
R12H-S1-H2-M2-4d	23.47	45.3	57.1	45.3	57.1	90	18	63	13.4	0.046	F
R12H-S1-H2-M2-5d	23.47	45.3	49.6	45.3	49.6	90	6	52	13.5	0.136	S
R12H-S1-H2-M2-6d	23.47	45.3	50.3	45.3	50.3	90	7	53	13.5	0.136	F
R12H-S1-H2-M1-1d	23.47	45.2	58.4	45.2	58.4	90	21	66	13.4	0.013	S
R12H-S1-H2-M1-2d	23.47	45.2	58.8	45.2	58.8	90	22	67	13.4	0.013	F
R12H-S1-H2-M3-1d	23.47	44.5	45.3	44.5	45.3	90	1	46	12.0	0.193	F
R12H-S1-H2-M3-2d	23.47	44.3	52.2	44.3	52.2	90	12	58	13.2	0.083	S
R12H-S1-H2-M3-3d	23.47	44.5	53.0	44.5	53.0	90	13	59	13.2	0.083	F
R12H-S1-H2-M4-1d	23.47	44.1	44.9	44.1	44.9	90	1	46	13.1	0.225	F

* Notes   F = Failure

S = Stable (No failure)

APPENDIX E

TECHNICAL PUBLICATIONS

(1) SIMULATION OF PLANE SLIDING AND TOPPING FAILURE USING SCALED-DOWN ROCK SLOPE MODEL

(2) PHYSICAL MODEL SIMULATION OF JOINTED ROCK SLOPES UNDER DYNAMIC LOADS

Simulation of Plane Sliding and Toppling Failure using Scaled-Down Rock Slope Models

Kittitep Fuenkajorn and Pongsak Pangpetch
Geomechanics Research Unit, Institute of Engineering,
Suranaree University of Technology,
Muang District, Nakhon Ratchasima, Thailand 30000.
Phone (66-44) 224-443, Fax (66-44) 224-448, E-Mail: kittitep@sut.ac.th.

Abstract

A test platform was constructed for use in the simulation of failure of scaled-down rock slopes under real gravitational force. The model capability is demonstrated by simulating two-dimensional plane sliding and toppling failure of rock slopes formed by cubical and rectangular blocks of Phu Phan sandstone, under various slope heights and face angles. Results from over 200 tests suggest that the test platform can realistically simulate the two modes of failure. The factors of safety calculated by deterministic method over-estimate the actual observations of plane sliding by as much as 30%, particularly for slopes with low sliding plane angles. The observed toppling failures agree well with those determined by Hoek and Bray solution when the friction between blocks is considered in the calculation.

1. Introduction

Physical models or scaled-down models have long been used to simulate the failure behavior of rock slope in the laboratory. They have been used as teaching and research tools to reveal the two-dimensional failure process of rock slopes under various geological characteristics. They are sometimes employed to gain an understanding of a unique failure process under site-specific conditions. Perhaps the most popular and widely used model is the Goodman's friction table [1]. Bray and Goodmam [2] discuss the base friction principle that it is commonly used to reproduce the effects of gravity in two dimensional physical models of excavations in rock. They develop mathematical principles upon which analogy between gravity and base friction can be examined. The friction table has been evolved into several versions. Cement mixed with sand, plaster or wooden blocks are commonly used to form the slope models. Teme [3] has used inclinable base-friction table as a tool in modeling of excavations. It is similar to that described by Goodman [1], Hoek and Bray [4], and Hittinger [5]. Teme's machine can however be inclined to simulate various dip angles in the field, and can test rigid and non-rigid model materials. Recently numerical analyses, primarily with distinct element and finite element methods, have been employed to simulate the plane sliding and toppling failures observed from the slope models [6-8]. Comparisons of the results from the computations and observations are made to verify the representative capability of the computer modeling and to improve an understanding of the actual behavior of rock slope failure.

The friction table poses some disadvantages. The driving force inducing sliding or failure is not from true gravitational force. Instead it largely depends on the friction and velocity of the moving belt, and hence additional calibration or correction is required to reveal the actual slope behavior. A stick-slip behavior between the belt and testing materials is common problem particularly under low speeds, making the driving force by belt moving unrealistic. In addition, since the friction table is in horizontal or gently inclined, assessment of the true effect of water can not be made.

The objective of this research is to invent a test platform for use in the laboratory simulation of scaled-down rock slope models under plane sliding and toppling failures and to

compare the observed results with those calculated by the deterministic methods [4]. The main tasks involve fabrication of the test platform, preparation of rock blocks for use in slope simulation, demonstration of the physical model performance, and calculation of the slope model stability using deterministic method.

2. Test Platform
2.1 Design Requirements and Components

The functional requirements for the test platform are (1) to test slope models with a maximum height of up to 1.5 m under varied slope face angles, (2) to induce failure of slope model using real gravitational force, and (3) to allow continuous monitoring of the failure process during testing.

To meet these requirements the test platform comprises two main components: a 2.2×2.2 m test frame supported by a movable stand. The frame is hinged through steel rods in the middle to the stand (Figure 1) allowing frame rotation from horizontal position (during arranging and loading block samples) to vertical position (for testing under true gravitational force). The frame is made of four 5-cm wide C-shaped steel bars on each side linked with a steel plate at the connected corners. A custom-made 2×2 m clear acrylic sheet with 10 mm thick is placed in the front of the frame, while an aluminum plate with the same size is in the back. The clear acrylic sheet allows visual observation of the slope movement during the test. The gap between the acrylic sheet and the steel plate is 5 cm.

All gaps and connections are water-tight. They are sealed with quick-dried silicone gel. When the frame is in horizontal position, the aluminum plate in the back becomes a flat bed supporting the tested rock blocks during loading. The clear and removable acrylic sheet is installed before rotating the frame to the upright position to prevent the block samples from tipping over. The test frame can accommodate 4 cm thick rock blocks arranged with a maximum height up to 1.5 m. A minimum clearance of 0.5 cm is maintained between the front acrylic sheet and rocks
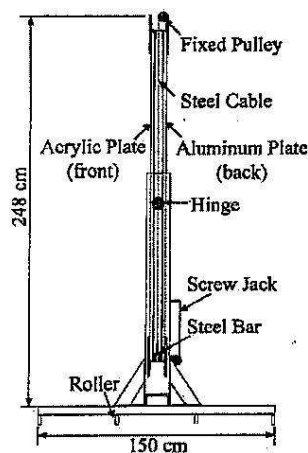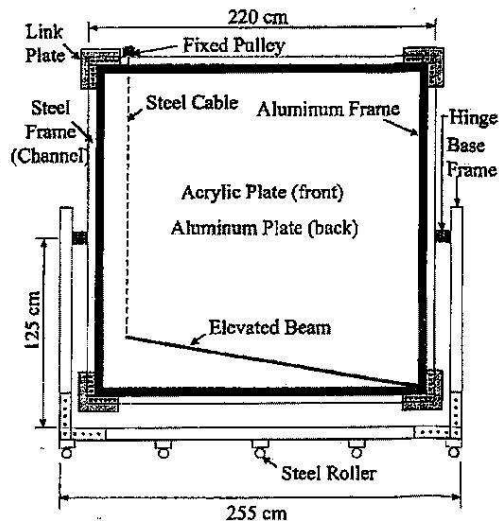
Figure 1. Schematic drawing of test platform.

and between the rear aluminum plate and the rocks to ensure that no friction is induced at these interfaces (equivalent to the release surface assumed in Hoek and Bray solution).

During the test a screw jack connecting with steel cable placing on a pulley lifts one end of a steel beam pre-installed underneath and along the slope model. Since the beam is securely hinged at the bottom near the slope toe, the entire slope model can be slowly tilted sideway toward the slope face, and eventually inducing failure (Figure 2).
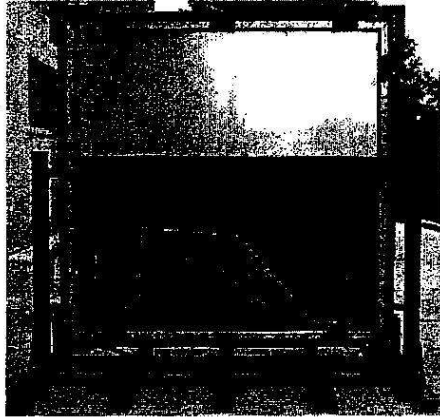
Figure 2. Example of test arrangement: Cubical blocks of Phu Phan sandstone placed in test platform.

2.2 Calculation of Slope Height

After the rock blocks have been arranged to form slope model in the test platform, the initial angle of the tilting beam, slope face and upper slope face are measured to the nearest 1 degree. Then the beam is slowly tilted toward the slope face while the video image is continuously taken. Immediately after the failure is initiated, the screw jack is secured to hold the tilting beam in-placed. The final angle of the tilting beam is measured. The slope height (H) and slope face (ψ_f) at failure can therefore be calculated ad follows (Figure 3).

$$H = \frac{h\sin(\psi_{f0} + (\psi_p - \psi_{p0}))}{\sin(\psi_{f0} - \psi_{p0})} \qquad (1)$$

$$\psi_f = \psi_{f0} + (\psi_p - \psi_{p0}) \qquad (2)$$

where: h = distance between base and top of slope model
H = height of slope at failure
ψ_{f0} = initial slope face angle
ψ_f = slope face angle at failure
ψ_{p0} = initial sliding plane angle
ψ_p = sliding plane angle at failure
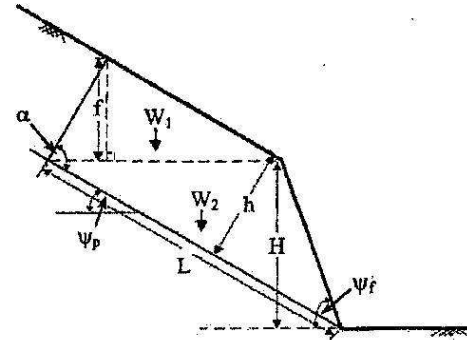
Figure 3. Parameters used for calculating height of slope model at failure.

The video recorder also provides redundant measurements of the slope angle and height immediately before and at failure. The video playbacks are also very useful to identify the location where the failure was initiated, and how it progressed.

3. Rock Block Samples

Phu Phan sandstone from Nakhon Ratchasima province was selected for use as rock samples primarily because it has highly uniform texture, density and strength. It is classified as fine-grained quartz sandstone with 72% Quartz (0.2-0.8 mm), 20% feldspar (0.1-0.8 mm), 3% mica (0.1-0.3 mm), 3% rock fragments (0.5-2mm), and 2% others (0.5-1 mm). The average density is 2.27 g/cc. To form slope models with two mutually perpendicular joint sets, cubical (4x4x4 cm) and rectangular (4x4x8 cm and 4x4x12 cm) shaped sandstone blocks were prepared. The cubical blocks were used to simulate joint sets with equal spacing, while the rectangular blocks simulated joint sets with different spacings. A total of nearly 1000 blocks of Phu Phan sandstone was prepared for rock slope failure simulation.

4. Tilt Testing

Tilt testing [4] was performed on the sandstone blocks to determine shear strength of the saw-cut surfaces. Size of the upper (sliding) block was varied to produce different contact areas ranging from 4x4, 4x8 to 4x12

cm^2. The weight of the upper block was taken into the calculation of normal load. The tests were repeated 4 times for each block size. Regression analysis on the results shows that the basic friction angle of the Phu Phan saw-cut surfaces is 26 degrees and cohesion is 0.053 kPa (Figure 4). The measured cohesion obtained here was low and agreed with the results obtained by Kemthong [9] and Kemthong and Fuenkajorn [10].

5. Simulation of Plane Sliding
5.1 Test Results

Thirty-eight plane sliding failures were simulated for dry slope models with heights
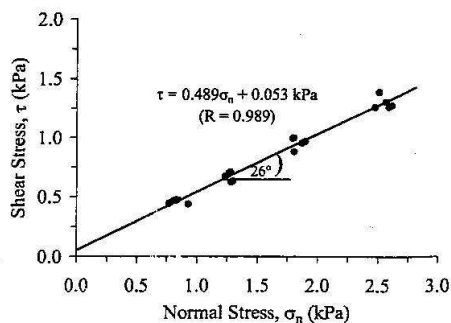
Figure 4. Results of tilt testing on bocks of Phu Phan sandstone.
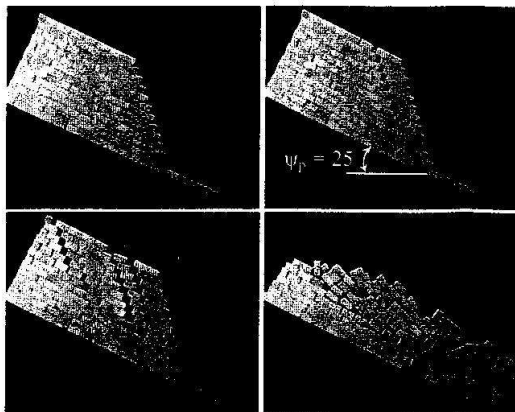
Figure 5. Simulation of sliding failure for block size 4×4×8 cm. Failure occurred at $\psi_f = 71°$.

varying from 16 to 77 cm and slope face angles from 41 to 73 degrees. Each set of slope geometry comprised sandstone blocks with the same dimension, and was simulated at least 3 times to ensure the repeatability of the results. Figure 5 shows an example of the plane sliding failure for a slope model formed by 4×4×8 cm sandstone blocks. Figure 6 shows simulation results by presenting the slope height at failure as a function of sliding plane angle. Since the measured cohesion is very low and negligible, the deterministic method simply yields the sliding plane angle equal to the friction angle of the block surfaces, as shown in the figure. The observed sliding plane angles (ψ_p) tended to be lower than those calculated by the deterministic method or lower than the basic friction angle obtained from the tilt test. This is probably due to the non-uniform distribution of the normal load and shear force on the sliding plane.

From the tested geometry the highest shear force is probably near the slope toe while the normal load largely concentrates near the middle of the sliding plane. Such non-uniform load distribution is probably similar to the actual in-situ slope conditions.

5.2 Calculation of Factor of Safety

Based on Coulomb's failure criterion a factor of safety of the sliding failure of the slope models was determined here to show the discrepancies between the observations and the calculations by the deterministic method. By assuming that the plane sliding follows Coulomb criterion, the factor of safety (F.S.) of a slope model can be derived as follows [4]:

$$FS = 2 \cdot c / \left\{ \gamma \cdot H \cdot \sin^2 \cdot \psi_p \cdot \left[a + \left(\frac{a^2}{b} \right) \right] \right\} + \frac{\tan \phi}{\tan \psi_p} \quad (3)$$

where: $a = \cot \psi_p - \cot \psi_f$
       $b = \cot (\alpha - \psi_p) + \cot \psi_p$
       c = cohesion of rock surface
       ϕ = friction angle
       γ = unit weight of rock
       α = angle of the back of slope model
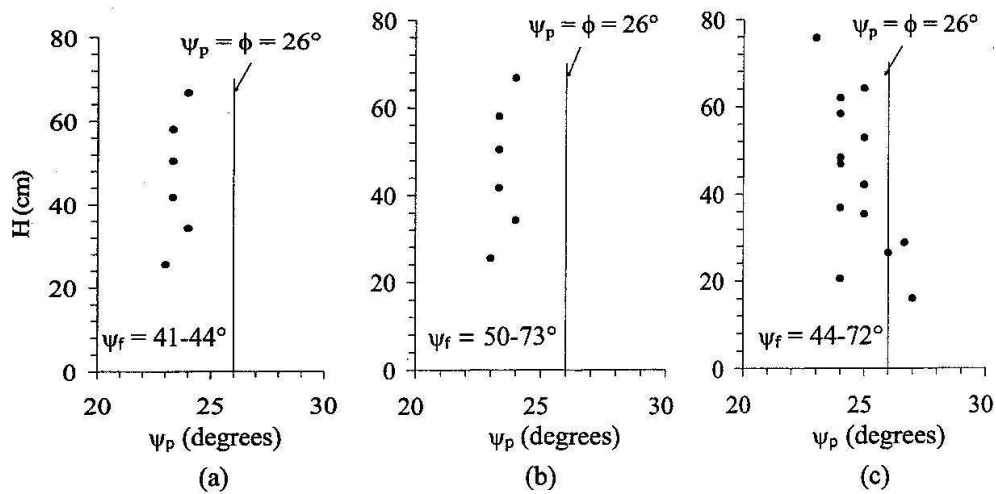
Figure 6. Sliding failure of dry slope for block size 4×4×4 cm (a), 4×4×8 (b) and 4×4×12 cm (c)

Figures 7 through 9 compare the factors of safety calculated from the model geometry at failure (using Equation 3) with the actual factor of safety observed at failure from the simulation (F.S. = 1.0). It is clear that the deterministic method by Hoek and Bray [4] over-estimate the factor of safety at failure by as high as 30% for the 4×4×4 blocks and about 10% for 4×4×12 blocks. This discrepancy is enhanced when the sliding plane angles become smaller. The calculated factor of safety seems to be insensitive to the slope face angle. The comparisons imply also that shorter blocks (4×4×4 cm) tend to slide easier than do longer ones (4×4×8 cm and 4×4×12 cm). Regardless the block dimensions, the difference between the calculated and observed factors of safety becomes insignificant for higher sliding plane angles.

6. Simulation of Toppling Failure
6.1 Test Results

Thirty seven toppling failures were simulated for all block shapes under dry condition. The slope height varies from 27 to 85 cm, and slope face from 43 to 82 degrees. Each set of slope geometry was simulated 3 times or until the results are repeatable. Figure 10 shows examples of test arrangements for toppling failure simulations with 4×4×8 cm

blocks. Figure 11 shows the results from toppling failure simulations in terms of slope height (H) as a function of the angle of the base plane on which the toppling blocks situate (ψ_p). As expected the models with a gentle slope face (ψ_f) failed at a greater slope height. At the same slope height, models with a steep slope face failed at a lower ψ_p. The slope height at failure decreases with increasing ψ_p. The dependency of this base plane angle becomes smaller for the slopes comprising taller and narrower rock blocks.
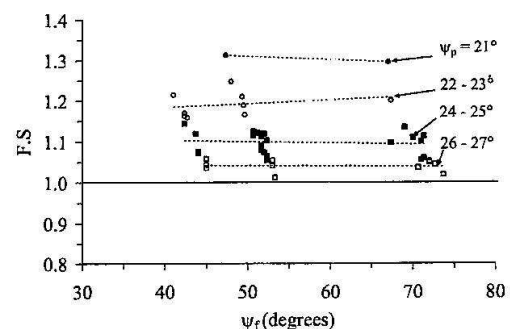
Figure 7. Factors of safety (F.S.) calculated from Eqn. (3) plotted as a function of ψ_f for block size 4×4×4 cm.
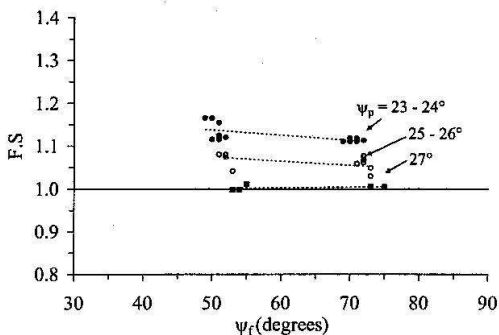
Figure 8. Factors of safety calculated from Eqn. (3) plotted as a function of ψ_f for block size 4×4×8 cm.
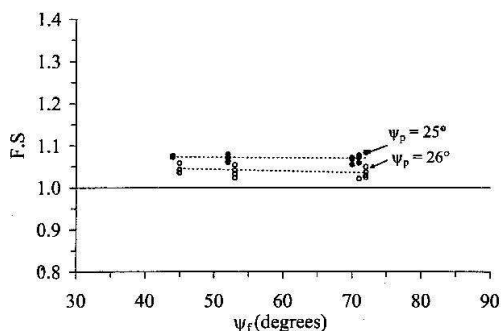
Figure 9. Factors of safety calculated from Eqn. (3) plotted as a function of ψ_f for block size 4×4×12 cm.

6.2 Toppling Failure Determined by Limit Equilibrium Analysis

Limit equilibrium analysis of toppling on a stepped base proposed by Hoek and Bray [4] can be written as:

$$P_{n-1} = \frac{P_n(M_n - \Delta x \tan\phi)}{L_n} + \frac{(W_n/2)(y_n \sin\alpha - \Delta x \cos\alpha)}{L_n} \quad (4)$$

where: P_{n-1} = force preventing toppling of the nth block
$\quad$ P_n = force inducing toppling of the nth block
$\quad$ W_n = weight of the nth block
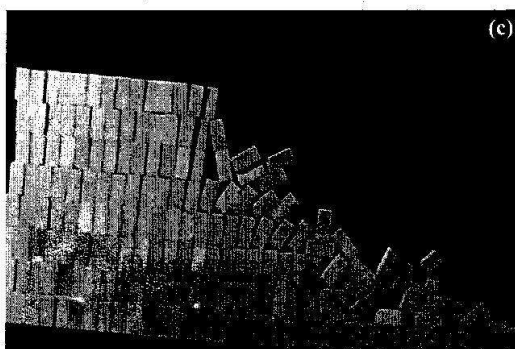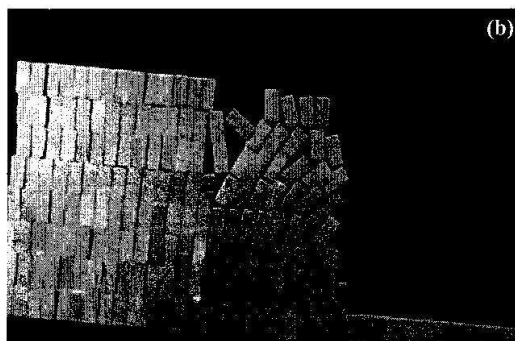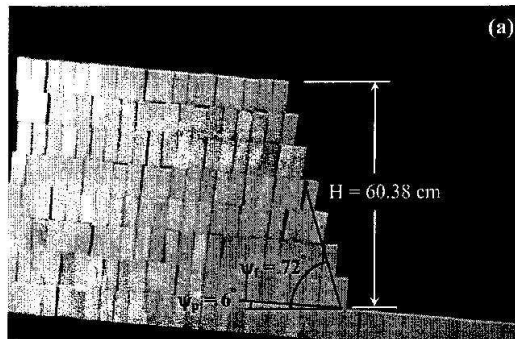
Figure 10. Simulation of toppling failure for block size 4×4×8 cm.
(a) Immediately before failure.
(b) At failure. (c) After failure.

M_n = distance between block base and the point where P_n applies
L_n = distance between block base and the point where P_{n-1} applies
Δx = width of each block
y_n = height of the nth block
α = final plane angle.
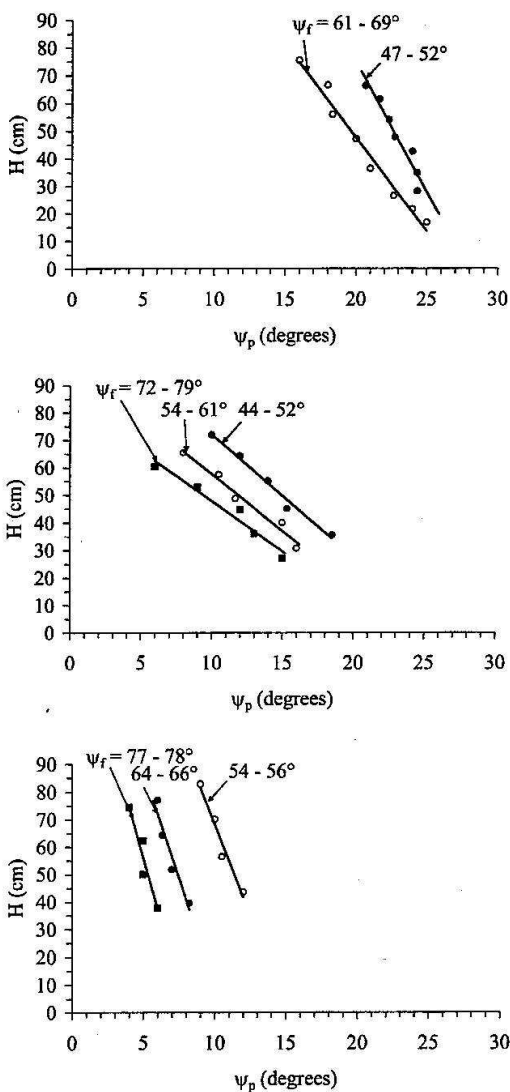
Figure 11. Results of toppling failures tested for block size 4×4×4 cm (top), 4×4×8 cm (middle), and 4×4×12 cm (bottom).

Since the slope model in this research does not have stepped base. Equation (4) requires some modification as follows.

$$P_{n,t} = \frac{c - d + \frac{y_n}{2} W_n \sin\alpha - \frac{\Delta x}{2} W_n \cos\alpha}{L_n} \qquad (5)$$

where: $c = P_n M_n - P_n \Delta x \tan\phi$

$\quad\quad\ d = P_R L_R + P_R \Delta x \tan\phi$

$\quad\quad\ P_{n,t}$ = force resisting toppling of nth block

$\quad\quad\ P_R$ = accumulated resisting force

Equation (5) is used to evaluate stability of slope and to estimate the extent of failure zone from slope toe. Figure 12 gives an example of the calculated results with the actual observations for 4×4×8 cm blocks. The test results agree well with those calculated by the equation modified from Hoek and Bray [4].

7. Discussions and Conclusions

The simulation results indicated that the deterministic method of Hoek and Bray over-estimated the stability conditions of rock slope models under the test parameters used here. This was probably due to the assumption of the uniform load and shear forces on the incipient sliding plane used in the calculation.
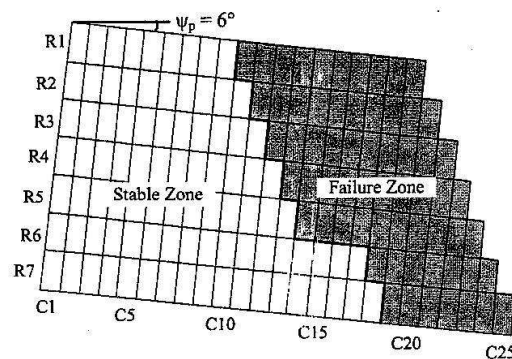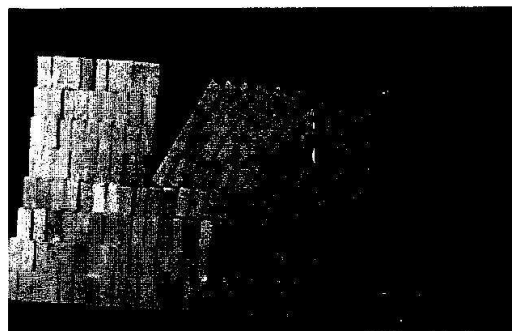
Figure 12. Observation (top) and calculation (bottom) of toppling failure for block size 4×4×8 cm. Failure occurred at $\psi_f = 72°$.

It does not however imply here that the deterministic method is entirely not conservative for plane sliding analysis. One should realize that the simulated plane sliding here is under simplified conditions, e.g., no cohesion continuous and easily detached joint planes, and truly friction free on the released surfaces.

This means that under more realistic or different test parameters and conditions the deterministic method may perform better in describing the factor of safety of the plane sliding models.

Plane sliding and block toppling failures were simulated with physical scaled-down models. Observations of the failure behavior during video playback revealed that for plane sliding the failure was initiated near the slope toe. The failure occurred at sliding plane angles (ψ_p) considerably lower than those determined from the tilt test and deterministic method, particularly for the slope models comprising shorter blocks. This was probably because the deterministic method assumes uniform normal load and shear force along the sliding plane while these loads in the slope models largely concentrate near the slope toe and virtually zero near the upper slope face. This also implies that shorter blocks (cubical blocks) slide easier than do longer ones (rectangular shaped) even though they had the same spacing (block height). For block toppling, the slope height at failure increased with decreasing the base plane angle (ψ_p) and slope face angle (ψ_f). The observed zone of instability agreed well with that determined by Hoek and Bray's method.

Acknowledgment

References

[1] R.E. Goodman, "Models of geological engineering in discontinuous rock", West Publishing Company. St Paul, Minnesota, USA, 1976.

[2] J.W. Bray and R.E. Goodman, "The theory of base friction models", International Journal of Rock Mechanics and Mining Sciences and Geomechanics Abstracts. Vol. 18, No. 6, 1981, pp. 453-468.

[3] S.C. Teme, "A kinematic modeling machine for rock slope studies", International Journal of Mining and Geological Engineering. Vol. 5, 1987, pp. 75-81.

[4] E. Hoek and J.W. Bray, "Rock slope engineering", 3rd edition, Institute of Mining and Metallurgy, London, 1981.

[5] M. Hittinger, "Numerical analysis of toppling failures in jointed rock", Ph.D. Thesis, University of California, Berkeley, USA, 1978.

[6] Y.G. Kim and H.K. Lee, "Slope stability analysis in discontinuous rocks by base friction model test and its numerical analysis", Regional Symposium on Rock Slopes, India, 1992.

[7] F. Lanoro, L. Jing, O. Stephansson and G. Barla, "D.E.M. Modeling of laboratory tests of block toppling", International Journal of Rock Mechanics and Mining Sciences. Vol. 34, No. 3-4, 1997, pp.173.

[8] Y.H. Hatzor, A.A. Arzi, Y. Zaslavsky and A. Shapira, "Dynamic stability analysis of jointed rock slopes using the DDA method: King Herod's Palace, Masada, Israel", International Journal of Rock Mechanics and Mining Sciences. Vol. 41, No. 5, 2004, pp. 813-832.

[9] R. Kemthong, "Determination of rock joint shear strength based on rock physical properties", M.Eng. Thesis, Suranaree University of Technology, Nakhon Ratchasima, 2006.

[10] R. Kemthong and K. Fuenkajorn, "Prediction of joint shear strengths of ten rock types using field-identified parameters", Proceeding of the 1st Thailand Symposium on Rock Mechanics, September 13-14, 2007, pp. 195-210.

Physical model simulation of jointed rock slopes under dynamic loads

P. Pangpetch & K. Fuenkajorn
Geomechanics Research Unit, Suranaree University of Technology, Thailand

Keywords: Plane failure, friction, sandstone, dynamic load, acceleration

ABSTRACT: Plane failures of scaled-down rock slope models have been simulated under real gravitational force and pseudo-static acceleration. The simulations involve two-dimensional plane sliding of rock slopes formed by cubical (4×4×4 cm) and rectangular (4×4×8 cm and 4×4×12 cm) blocks of sandstone, under various slope face angles with the maximum slope height up to 1 m. The sandstone blocks prepared by saw-cutting are arranged to simulate rock slopes with two mutually perpendicular joint sets. Horizontal pseudo-static acceleration of up to 0.225 g with amplitudes between 24 to 64 mm is applied. The observed sliding angles under dynamic loading are considerably lower than those calculated by the deterministic method. The discrepancy becomes larger for slope models formed by shorter sandstone blocks and under a higher acceleration. The results from the physical model simulations under dry and submerged conditions agree well with those obtained from finite difference analyses using FLAC code. The findings imply that for the smooth, open and low-cohesion joints as simulated here, assessment of rock slope stability under static and dynamic loading by using the deterministic method alone may not be conservative, particularly for the slope mass comprising joints with small spacing.

1 INTRODUCTION

Physical models or scaled-down models have long been used to simulate the failure behavior of rock slopes in the laboratory. They have been used as teaching and research tools to reveal the two-dimensional failure process of rock slopes under various geological characteristics. They are sometimes employed to gain an understanding of a unique failure process under site-specific conditions. Perhaps the most popular and widely used model is Goodman's friction table (Goodman, 1976). Bray & Goodman (1981) discuss the base friction principle that is used widely to reproduce the effects of gravity in two dimensional physical models of excavations in rock. They develop mathematical principles upon which the analogy between gravity and base friction can be examined. The friction table has later evolved into several versions (e.g. Hittinger, 1978; Teme, 1987; Kim & Lee, 1992; Lanaro et al., 1997). The slope modeling with friction table however poses some disadvantages. The driving force inducing sliding or failure is not a true gravitational force. Instead it largely depends on the friction and velocity of the moving belt, and hence additional calibration or correction is required to reveal the actual slope behavior. A stick-slip behavior between the belt and

testing materials is a common problem particularly under low speeds, making the driving force by belt moving unrealistic. Since the friction table is horizontal, or gently inclined, assessment of the true effect of water can not be made.

The objective of this research is to study rock slope failure under static and dynamic loads by means of laboratory simulation of scaled-down models. The observed results are compared with those calculated by deterministic methods and by numerical analyses. A vertical test platform has been used to host the slope models formed by cubical and prismatic blocks of Phu Phan sandstone to simulate two-dimensional plane sliding failure. The failure is induced by true gravitational force and horizontal pseudo-static acceleration of up to 0.225 g. The effect of water-submerging is investigated. Comparisons are made of the results from physical model simulations and from numerical analysis.

2   SOME PREVIOUS FINDINGS

The seismic stability of earth structures has been analyzed by a pseudo-static approach in which the effects of an earthquake are represented by constant horizontal and/or vertical accelerations (Kramer, 1996). The first explicit application of the pseudo-static approach to the analysis of seismic slope stability has been attributed to Terzaghi (1950). Giani (1992) states that a pseudo-static analysis can be carried out by using the limit equilibrium method and by schematizing the dynamic loading occurrence with a time constant force which is proportional to the mass of the potentially unstable volume of rock, according to the seismic coefficient. The database against which seismic slope stability analyses can be calibrated is much smaller as compared to the database compiled for the static condition. Kramer (1996) postulates that the analysis of the seismic stability of slopes is complicated by the need to consider the effects of (1) dynamic stresses induced by earthquake shaking, and (2) the effects of those stresses on the strength and stress-strain behavior of the slope materials.

Several approaches have been made to study the effects of dynamic loading on earth structures, ranging from actual field testing and measurements, laboratory testing to numerical simulations. Siad (2003) considers gravity and inertial forces developed in the actual rock mass by the passage of seismic waves as the external forces. It is found that the stability factor is very sensitive to variations of the horizontal seismic coefficient. The impact is smaller as the friction angle of the fractures increases. The shaking table is commonly used to simulate the dynamic load imposed on the test specimen. Maugeri et al. (2000) simulate the failure of a shallow foundation subjected to an eccentric load by the shaking table to obtain a critical horizontal acceleration coefficient of the structure. The test allows varying the peak accelerations from ±0.10 to ±0.35g. Discrete element method (DEM) is a common tool for the numerical approach to study the effect of dynamic loading on geologic structures (Hatzor et al., 2004; Li et al., 2007). The DEM is based on the discontinuity analysis which can consider anisotropic and discontinuous deformations due to joints and their orientations. They compared the effect of joints on the failure modes between DEM simulations and experimental observations. It has been found that DEM predicts a lower critical excavation height than that calculated from the limit equilibrium method.

3   TEST PLATFORM

The test platform used in this research comprises two main components: a 2.2×2.2 m vertical test frame supported by a movable stand (Pangpetch & Fuenkajorn, 2007). The frame is hinged through steel rods in the middle to the stand allowing frame rotation from horizontal

position during arranging and loading block samples to vertical position for testing under true gravitational force (Figure 1). When the frame is in horizontal position, the aluminum plate becomes a flat bed supporting the rock blocks during loading. The clear and removable acrylic sheet is installed before rotating the frame to the upright position to prevent the block samples from tipping over. It also allows visual inspection and monitoring of slope movement during the test. The test frame can accommodate 4 cm thick rock blocks arranged to a maximum height of up to 1.5 m to simulate two-dimensional jointed rock slopes. Steel grooved rollers mounted underneath the stand are used for testing under dynamic loading. The rollers will be placed on a set of steel rails equipped with a high torque motor, gear system and crank arm to induce a cyclic motion to the entire test platform. The frequency and amplitude of the horizontal pseudo-static acceleration can be controlled by adjusting the rotational diameter of the flywheel and speed of the motor.

Figure 2 shows the crank arm components used to generate the horizontal acceleration to the test frame. The acceleration at point B, represented by a, can be calculated using a set of equations given by Riley & Sturges (1993).

$$a = R\omega_{OA}^2 \cos\theta + y\omega_{AB}^2 \cos\phi - y\alpha_{AB}\sin\phi \tag{1}$$
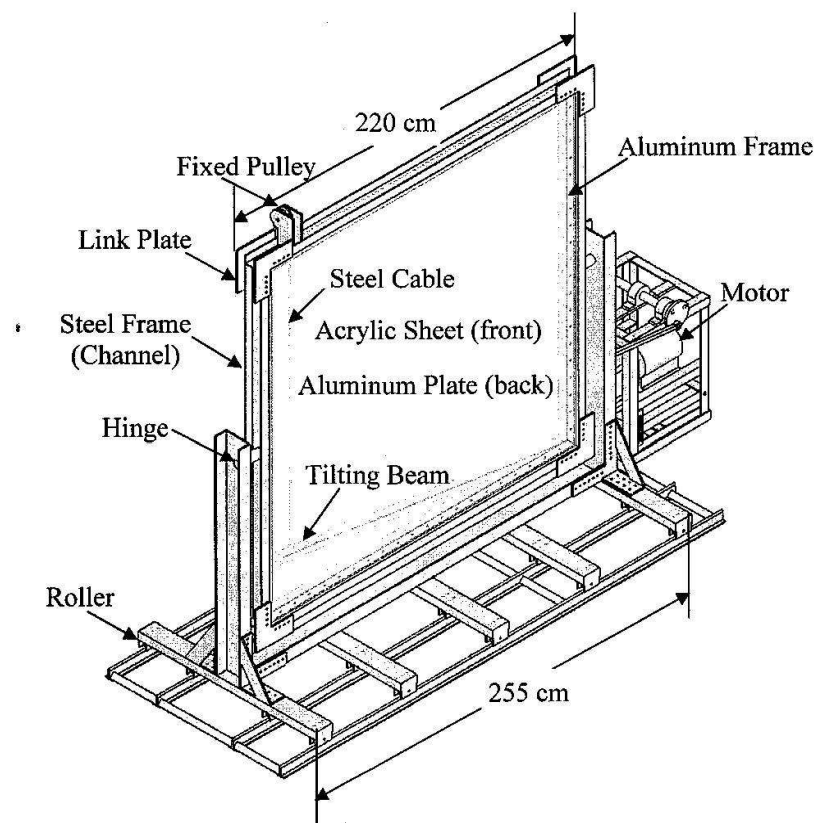
Figure 1. Schematic drawing of test platform used for physical model simulation.

Figure 2. Crank arm and flywheel used to induce dynamic loading to the test platform.

where R = radius of wheel, y = length of crack arm, ω_{OA} and ω_{AB} = angular velocity of OA and AB, θ = angle between AO and OB, α_{AB} = relationship between the acceleration of points A and B, and T = duration of flywheel rotation. The angle ϕ can be obtained from:

$$\phi = \sin^{-1}\left[\frac{R\sin\theta}{y}\right]$$

The angular velocity of OA and AB can be calculated by:

$$\omega_{OA} = \frac{2\pi}{T} ; \quad \omega_{AB} = \frac{R\omega_{OA}\cos\theta}{y\cos\phi}$$

The relationship between point A and B, and α_{AB}, is calculated by:

$$\alpha_{AB} = \frac{R\omega_{OA}^2 \sin\theta - y\omega_{AB}^2 \sin\phi}{y\cos\phi}$$

The actual rotational duration (T) is monitored for each slope model because different slope geometry and slope mass yield different weights, and hence change the speed of the test platform and the flywheel rotation.

4   ROCK SAMPLE

Phu Phan sandstone has been selected for use as rock sample here primarily because it has highly uniform texture, density and strength. It is classified as fine-grained quartz sandstone with 72% Quartz (0.2-0.8 mm), 20% feldspar (0.1-0.8 mm), 3% mica (0.1-0.3 mm), 3% rock fragments (0.5-2mm), and 2% others (0.5-1 mm). The average density is 2.27 g/cc. To form slope models with two mutually perpendicular joint sets, cubical (4x4x4 cm) and rectangular (4×4×8 cm and 4×4×12 cm) shaped sandstone blocks have been prepared by using a saw-cutting machine. The cubical blocks are used to simulate joint sets with equal spacing, while the rectangular blocks simulate joint sets with different spacing. The friction angle and cohesion of the saw-cutting surfaces of the Phu Phan sandstone determined by tilt testing are 26 degrees and 0.053 kPa (Pangpetch & Fuenkajorn, 2007). The simulated joints have their strike parallel to the slope face, and hence represent a worst case scenario for the stability condition.

5   SLOPE MODELS TESTED UNDER STATIC CONDITION

Over one hundred plane sliding failures have been simulated under dry and submerged conditions with the slope heights varying from 16 to 93 cm and slope face angles from 40 to 75 degrees. For submerged condition, the height of the water in the test models ranges from 7 to 60 cm. Each set of slope geometies is formed by sandstone blocks with the same dimension, and is simulated at least 3 times to ensure the repeatability of the results. Video records are taken during the test. Table 1 summarizes the test parameters and results for modeling under dry and submerged conditions. Pangpetch & Fuenkajorn (2007) give solutions to calculate the slope height and sliding plane angle at failure. Figures 3 and 4 show examples of the plane sliding failure for a slope model formed by 12×4 cm blocks under dry and submerged conditions. The video recorder allows examining the failure process of the slope models after the test. The failure usually initiates from the slope toe and progresses upward to the crest. A combination of plane sliding near the slope toe and toppling failure near the slope crest is often found for slope models formed by 4x4 cm blocks.

Figure 5 compares the simulation results by plotting the slope height at failure as a function of sliding plane angle. Since the measured cohesion is very low and negligible, the deterministic method simply yields the sliding plane angle equal to the friction angle of the block surfaces. The observed sliding plane angles tend to be lower than the rock friction angle. The discrepancy becomes larger for the slope models formed by shorter sandstone blocks. The sliding plane angles (ψ_p) also seem to be independent of the slope height. As expected, the observed sliding plane angles under submerged condition are lower than those under dry condition. However under the same slope conditions (e.g., slope height, face angle) the difference is less than 2-3 degrees.

6   FINITE DIFFERENCE ANALYSIS

Finite difference analyses using FLAC Slope code (Itasca, 1992) have been performed to calculate the factor of safety of some slope models. Twelve finite difference models have been constructed to represent the physical model geometry. For the dry condition, the simulations use the sliding plane angle of 25 degrees with slope heights varying from 21 to 70 cm, and slope face angles from 51 to 72 degrees. Under submerged condition the sliding angles are taken as 20 to 23 degrees, with slope heights varying from 52 to 58 cm, slope face angles from 48 to 68 degrees, and water level heights (H_w) from 30 to 69 cm. For all

Table 1. Test parameters and results of slope model simulations under dry and submerged conditions.

Block Size	No. of Testing	H (cm)	ψ_f (degrees)	ψ_p (degrees)	H_w (cm)
Dry					
4×4 cm	43	20-68	40-52	21-25	-
8×4 cm	53	16-77	49-75	23-27	-
12×4 cm	49	16-93	44-72	25-26	-
Submerged					
4×4 cm	10	36-75	40-66	20-22	13-55
8×4 cm	10	20-91	45-71	21-23	7-60
12×4 cm	11	22-70	49-69	22-24	8-54
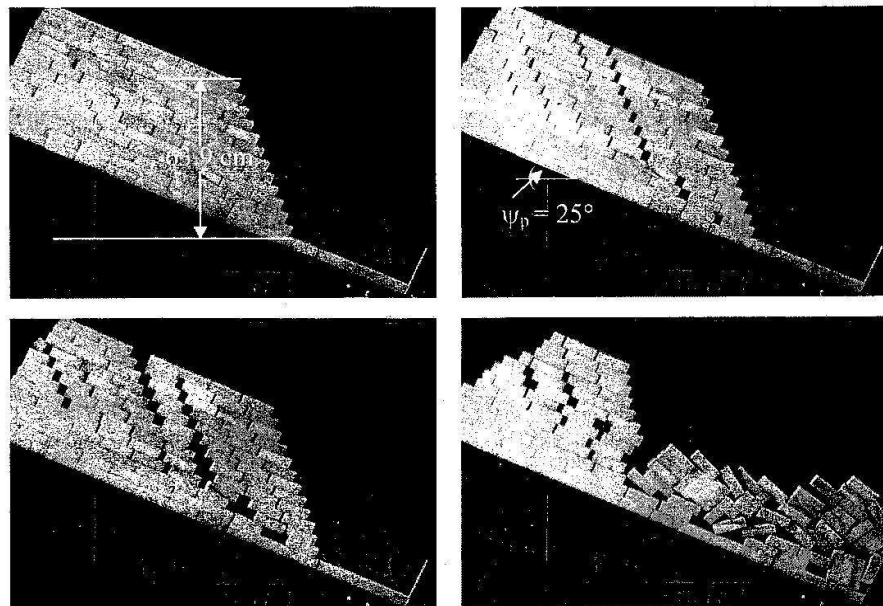
Figure 3. Simulation of sliding failure of rock slope formed by 12×4 cm blocks of sandstone under dry condition. Failure occurred at ψ_f=71°, ψ_p=25°, and H=63.9 cm.
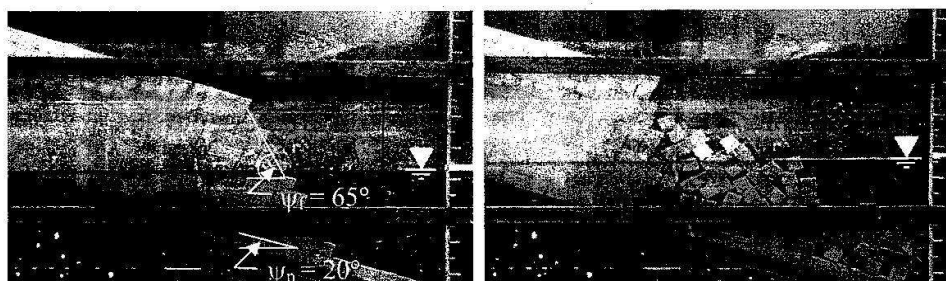
Figure 4. Example of failure of slope model formed by 4×4 cm blocks under submerged condition, showing combination of plane sliding at slope toe and toppling failure near slope crest. Failure occurred at ψ_f=65°, ψ_p=20°, H=57.3 cm, and H_w=35 cm.
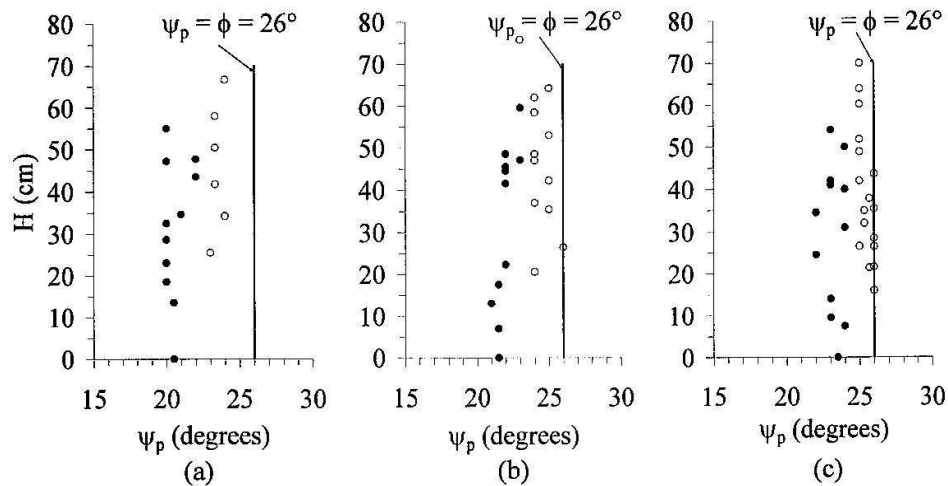
Figure 5. Slope height (H) as a function of sliding plane angle (ψ_p) for block sizes of 4×4 cm (a), 8×4 cm (b) and 12×4 cm (c). Solid points represent submerged condition.

simulations the friction angle is maintained constant at 26 degrees with cohesion equal to 0.053 kPa. The results are compared with those observed from the physical model tests. Figures 6 and 7 compare the shape of the failure zone of the numerical simulation results and the slope model observations under dry and submerged conditions. The FLAC_Slope can well predict the shape and extent of the failure zone with the factor of safety close to those observed from the tested models.

Figure 8 compares the factors of safety calculated by FLAC code and by deterministic method with those of the physical model tests for the same slope geometry under dry condition. The factor of safety of 1.0 is taken to represent the condition at which failure occurs in the slope models. Assuming that the plane sliding mechanism follows the Coulomb criterion, the deterministic method uses an equation modified from Hoek & Bray (1981) to calculate the factor of safety.

$$FS = 2 \cdot c / \left\{ \gamma \cdot H \cdot \sin^2 \cdot \psi_p \cdot \left[(\cot \psi_p - \cot \psi_f) + \left(\frac{(\cot \psi_p - \cot \psi_f)^2}{\cot(\alpha - \psi_p) + \cot \psi_p} \right) \right] \right\} + \frac{\tan \phi}{\tan \psi_p} \qquad (2)$$

where c = cohesion of rock surface, ϕ = friction angle, H = slope height, α = angle of slope back, and γ = unit weight of rock (= 23.8×10^3 kN/m^3 for Phu Phan sandstone).

The results from the three methods agree reasonably well. Very small discrepancies remain. Under dry condition, the deterministic method yields the highest factor of safety, which is about 10% greater than those observed from the test models. The factors of safety from FLAC simulations are less than 5% greater than the observations. This may be because the deterministic method assumes that the sliding block is a single and rigid mass lying on an incipient failure plane while the actual test models are a discontinuous mass formed by rock blocks. The discrepancies become even smaller for a greater slope face angle.

(a)   (b)

Figure 6.   Comparisons of FLAC simulations with physical model tests for 4×4 cm blocks (a)
and 8×4 cm blocks (b).

7   SLOPE MODELS TESTED UNDER DYNAMIC LOADING

The dynamic loading is studied by considering the effects of the horizontal pseudo-static acceleration induced by cyclic motions of the test platform in the direction parallel to the dip direction of the slope face. These cyclic motions are used to simulate the earthquake shaking. The vertical acceleration is assumed to be zero. Over one hundred plane sliding failures have been simulated with the horizontal pseudo-static accelerations between 0.013 g and 0.225 g. These accelerations are within the range tested and observed elsewhere (Kramer, 1996; Maugeri et al., 2000; Hatzor et al., 2004). The amplitude is maintained constant at 23.5 mm. The slope models have the sliding plane angles varied from 1 to 22 degrees, heights from 44 to 83 cm, and slope face angles from 28 to 68 degrees.   Table 2 summarizes the test parameters and the results.   For all slope geometries the duration for cyclic motion is

138
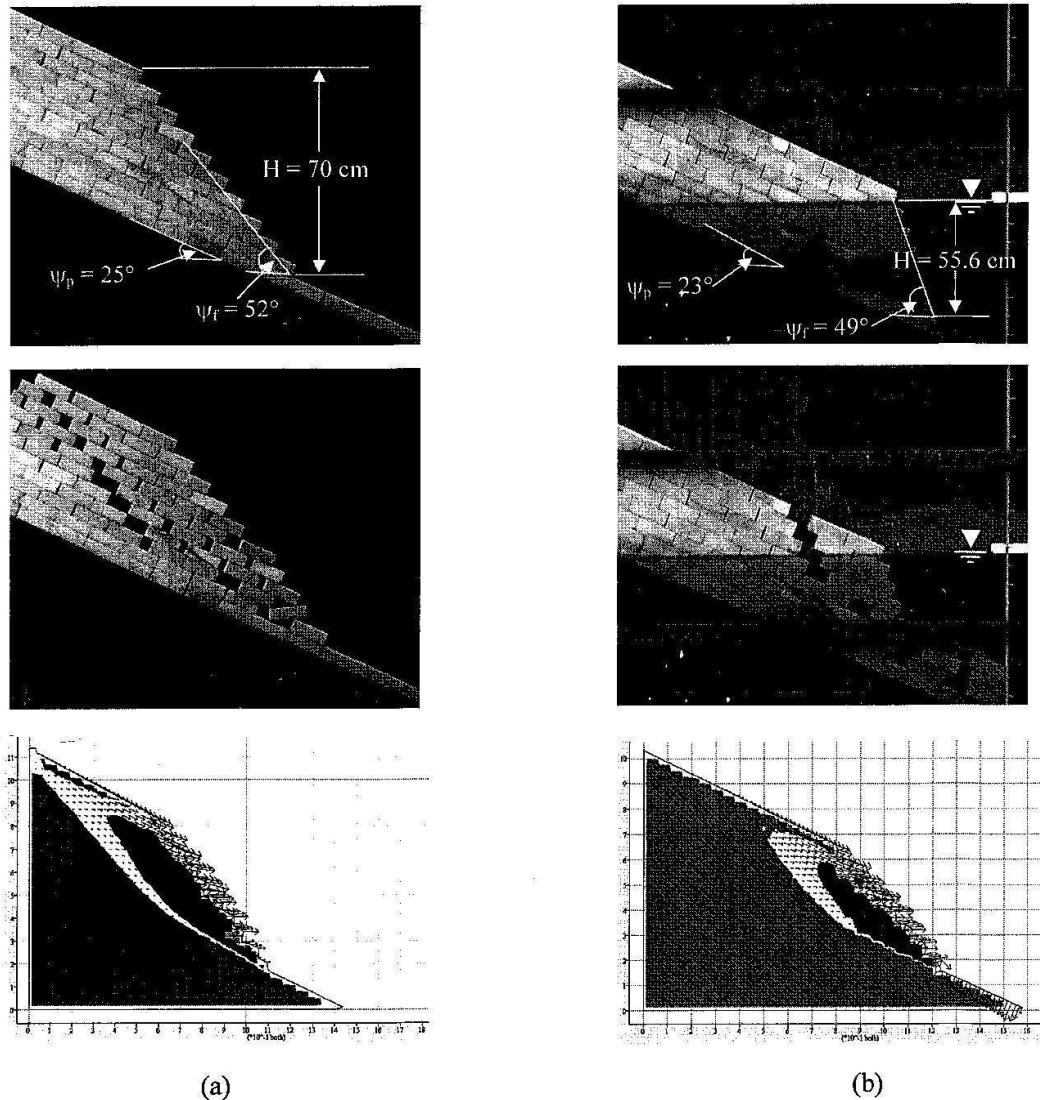
Figure 7. Comparison of FLAC simulations with physical model tests for 12×4 cm blocks under dry condition (a) and submerged condition (b).

maintained at one minute. If failure does not occur within one minute of shaking, the sliding plane angle is progressively increased by one degree interval and the test is repeated. Figure 9 shows an example of the plane sliding failure for 8x4 cm blocks. It is generally observed that under similar slope geometry and block arrangement the failure zone induced under dynamic load is more extensive than those under static loading.

To compare the test results with those calculated by the deterministic method, a closed-form solution given by Kramer (1996) is adopted here. The solution offers a simple approach to calculate the factor of safety of plane failure per unit thickness of slope mass under vertical and horizontal pseudo-static accelerations.

Physical model simulation of jointed rock slopes under dynamic loads
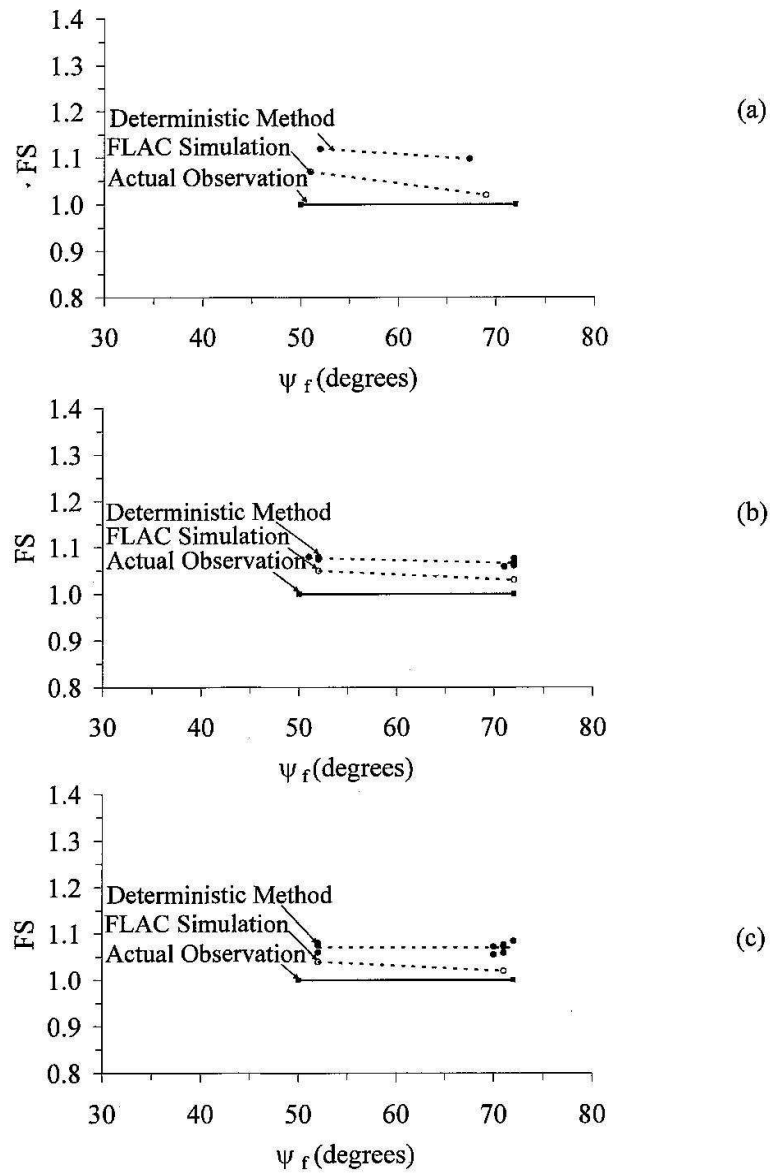
Figure 8. Factors of safety determinated for 4×4 cm blocks (a), 8×4 cm blocks (b), and 12×4 cm blocks (c) at ψ_p equal 25 degrees.

$$FS = \frac{Resisting\ force}{Driving\ force} = \frac{c \cdot 1 + [(W - F_v)\cos\psi_p - F_h \sin\psi_p]\tan\phi}{(W - F_v)\sin\psi_p + F_h \cos\psi_p}$$ (3)

$$F_h = a\ W/g = k_h W$$ (4)

$$F_v = a_v\ W/g = k_v W$$ (5)

140

Table 2. Results of rock slope stability analysis under dynamic loading with amplitude = 23.5 mm.

Block Size	No. of Tests	Frequency (Hz)	a (g)	Modified Mercalli Intensity*	H (cm)	ψ_f (degrees)	ψ_p (degrees)
4×4 cm	7	0.403	0.013	IV	69-83	40-44	15-18
	3	0.504	0.017	IV	80-82	40-43	15-17
	3	0.629	0.027	IV	76-78	41-44	14-16
	4	0.700	0.033	V	44-53	33-44	12-17
	7	0.833	0.046	V	50-77	31-41	4-15
	8	1.000	0.067	VI	46-75	28-38	1-12
	4	1.233	0.102	VI	49-54	28-32	3-6
	4	1.346	0.119	VI	46-62	28-32	1-4
	1	1.833	0.225	VII	46	46	1
8×4 cm	7	0.403	0.013	IV	55-58	61-67	16-21
	7	0.504	0.017	IV	55-56	64-68	18-20
	3	0.629	0.027	IV	54-56	63-68	18-19
	3	0.700	0.033	V	55-57	60-64	15-18
	11	0.833	0.046	V	51-55	57-63	10-16
	8	1.000	0.067	VI	48-52	52-59	10-12
	6	1.346	0.119	VI	45-48	48-54	1-5
	1	1.700	0.193	VII	45	51	1
	1	1.833	0.225	VII	45	46	1
12×4 cm	2	0.403	0.013	IV	58-59	66-67	21-22
	4	0.833	0.046	V	55-57	60-63	15-18
	2	1.117	0.083	VI	52-53	58-59	12-13
	2	1.429	0.136	VII	49-50	52-53	6-7
	1	1.700	0.193	VII	45	46	1
	1	1.833	0.225	VII	45	46	1

* Modified Mercalli Intensity from Richter (1958) and Wald et al. (1999) as:

IV = Felt indoors by many, outdoors by few during the day. At night, some awakened. Dishes, windows, doors disturbed; walls make cracking sound.

V = Felt by nearly everyone; many awakened. Some dishes, windows broken. Unstable objects overturned.

VI = Felt by all; many frightened. Some heavy furniture moved; a few instances of fallen plaster. Damage slight.

VII = Damage negligible in building of good design and construction; slight to moderate in well-built ordinary structures; considerable damage in poorly built or badly designed structures; some chimneys broken.

Where F_h and F_v = horizontal and vertical inertial forces, a = horizontal pseudo-static acceleration, a_v = vertical pseudo-static acceleration (assumed here = 0), W = weight of the failure mass, ψ_p = angle of planar failure surface, g = gravitational acceleration, l = the length of the failure plane, and k_h and k_v = dimensionless horizontal and vertical pseudo-static accelerations
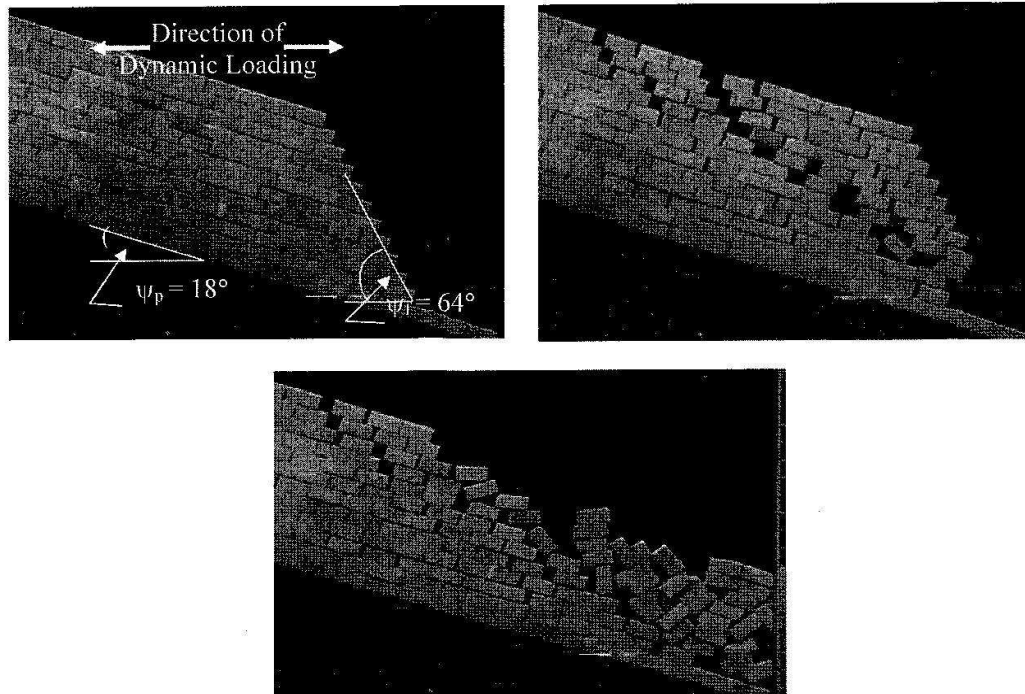
Figure 9. Simulation of sliding failure for 8×4 cm blocks at a = 0.046 g and amplitude=23.5 mm.

In relation to the earthquake phenomena Kramer (1996) postulate that the horizontal pseudo-static force decreases the factor of safety by reducing the resisting force and increasing the driving force. The vertical pseudo-static force typically has less influence on the factor of safety since it reduces (or increases, depending on its direction) both the driving force and the resisting force. As a result, the effects of vertical accelerations are frequently neglected in pseudo-static analyses resolving the forces on the potential failure mass in a direction parallel to the failure surface.

In this study the vertical pseudo-static acceleration (a_v) is assumed to be zero, subsequently the vertical inertial force (F_v) becomes zero. This assumption conforms to Kramer's conclusion above. The above equation is therefore reduced to:

$$FS = \frac{c \cdot 1 + [W \cos \psi_p - F_h \sin \psi_p] \tan \phi}{(W \sin \psi_p + F_h \cos \psi_p)} \tag{6}$$

By setting FS=1, the relationship between the acceleration, a, and the angle of the failure plane, ψ_p, can be developed. Under this condition the acceleration required to induce plane failure for a rock slope decreases with increasing failure plane angle (Figures 10 and 11). Figure 10 shows how the acceleration decreases with increasing the failure plane angle under various joint cohesions with a constant friction angle of 26 degrees. The joint cohesion is equal to zero in Figure 11 while the friction angles vary from 15 to 35 degrees.
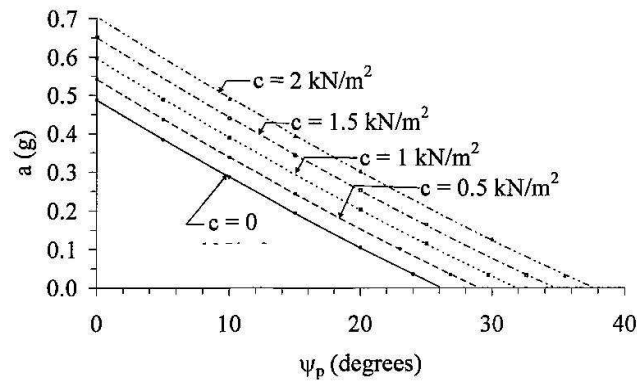
Figure 10. Pseudo-static acceleration (a) that induces plane failure as a function of sliding plane angle (ψ_p) for various joint cohesions, for $\phi = 26°$
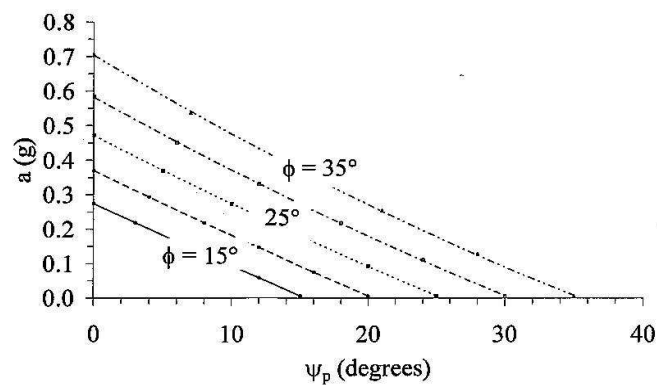
Figure 11. Pseudo-static acceleration (a) that induces plane failure as a function of sliding plane angle (ψ_p) for various joint friction angles, for cohesion = 0.

Results of the test models under dynamic loading are plotted in terms of the acceleration as a function of the sliding plane angle in Figure 12. A failure envelope (line separating the stable and failure conditions) can be drawn from the test results for each block size, and is compared with the results from the deterministic method using FS=1. It is clearly shown that the deterministic method significantly over-estimates the actual observations. Under the same sliding plane angle the deterministic solution gives the acceleration at failure at more than twice of those observed from the test models. This is probably because the deterministic method assumes a rigid and continuous mass of rock above the incipient sliding plane while the slope models are formed by discrete rock blocks. The deterministic method also assumes that all relevant forces pass through the centroid of the sliding mass. The presence of interaction forces between the blocks in the slope model could enhance the shape effect of the individual blocks above the sliding plane. This behavior may be better demonstrated by a discrete element analysis that can incorporate the effect of dynamic loading. The discrepancy between deterministic method and test models becomes greater for a lower sliding plane angle, and particularly for the slope models formed by short blocks (4×4 cm). In addition the acceleration required to fail slope models with the shorter blocks tends to be lower than those with longer ones (8×4 cm and 12×4 cm).
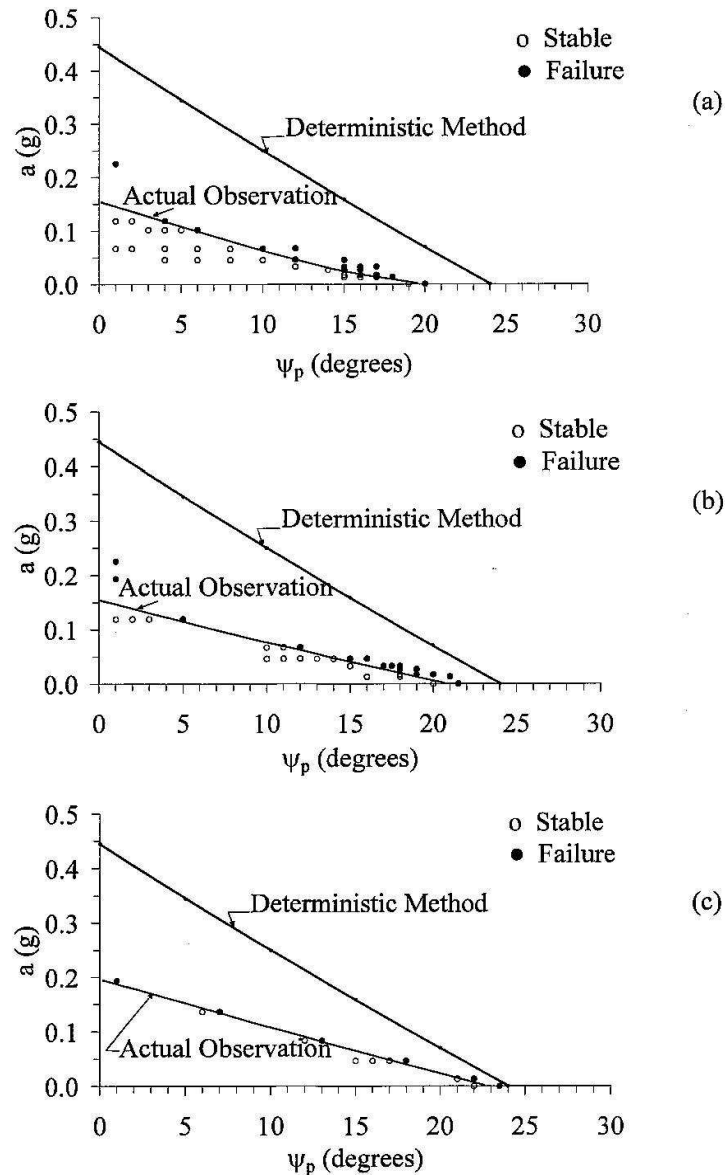
Figure 12. Pseudo-static acceleration (a) as a function of sliding plane angle (ψ_p) at failure for 4×4 cm (a), 8×4 cm (b), and 12×4 cm (c) blocks.

8 DISCUSSIONS AND CONCLUSIONS

It is recognized that the joints simulated in the slope models here are very smooth and clean with low cohesion and friction angle, which may not truly represent most actual rock joints found in in-situ rock slopes. Nevertheless the comparisons of the test results with the deterministic solutions (by Hoek & Bray, 1981) and computer simulations (FLAC_Slope code) under the same test parameters (e.g., joint properties and slope characteristics) have revealed significant implications. Under static condition the deterministic method and

computer simulation over-estimate the factor of safety for the plane sliding failure by about 5 to 10%, particularly for the slope models with shorter blocks. This is probably due to the impacts of the block spacing, block shape and interaction forces between the discrete blocks in the sliding mass. This implies that stability analysis by assuming that the sliding mass is continuous as used by the deterministic method may not be conservative, particularly for slope masses with short-spaced joints compared to the slope height.

The discrepancy between the deterministic method and the test results under dynamic loading is highly significant. The deterministic solution proposed by Kramer (1996) over-estimates the acceleration at failure by more than twice those observed from the test models. The discrepancy however reduces for slope models formed by larger sandstone blocks and under a greater sliding plane angle. This is again probably due to the assumption of the continuous mass imposed by the deterministic method. These findings indicate that under dynamic loading plane sliding analysis using the simple deterministic method for rock slopes with small joint spacing compared to the slope height will give a non-conservative result. In addition, the deterministic approach for stability analysis of low-angled sliding planes under dynamic loading may be inappropriate. In this case an additional physical model testing or discrete element analysis that is capable of dynamic simulation should be performed.

The physical models tested here have a narrow range of the size and shape of the rock blocks used to simulate the joint spacing in the test frame. Additional test results obtained from slope models with larger blocks, probably up to 20×20 cm, and with smaller blocks, 2×2 cm, would provide a clearer indication of the effect of joint spacing on slope stability. Studying the impact of joint roughness determined from the physical test models is also desirable. It would reveal the adequacy or inadequacy of the deterministic methods and the sensitivity of the induced acceleration to the joint roughness. This may be experimentally assessed by using cast cement blocks with various degrees of pre-defined roughness on the surfaces.

ACKNOWLEDGEMENT

REFERENCES

Bray, J.W. & Goodman, R.E., 1981. The theory of base friction models. *International Journal of Rock Mechanics and Mining Science and Geomechanics.* 18(6): 453-468.

Giani, G.P., 1992. *Rock Slope Stability Analysis.* A.A. Balkema. Rotterdam, The Netherlands.

Goodman, R.E., 1976. *Models of geological engineering in discontinuous rock.* West Publishing Company. St Paul, Minnesota, USA.

Hatzor, Y.H., Arzi, A.A., Zaslavsky, Y. & Shapira, A., 2004. Dynamic stability analysis of jointed rock slopes using the DDA method: King Herod's Palace, Masada, Israel. *International Journal of Rock Mechanics and Mining Sciences.* 41(5): 813-832.

Hittinger, M., 1978. *Numerical analysis of toppling failures in jointed rock,* Ph.D. Thesis, University of California, Berkeley, USA.

Hoek, E. & Bray, J.W., 1981. *Rock slope engineering.* 3rd edition, Institute of Mining and Metallurgy, London.

Itasca, 1992. *User manual for FLAC-fast Langrangian analysis of continua, version 3.0.* Itasca Consulting Group Inc., Minneapolis, MN.

Physical model simulation of jointed rock slopes under dynamic loads

Kim, Y.G. & Lee, H.K., 1992. Slope stability analysis in discontinuous rocks by base friction model test and its numerical analysis. *Regional Symposium on Rock Slopes*. Coal India Limited, India. pp. 195-201.

Kramer, S. L, 1996. *Geotechnical earthquake engineering*. New Jersey: Prentice Hall. pp. 423-463.

Lanaro, F., Jing, L., Stephansson, O. & Barla, G., 1997. D.E.M. Modeling of laboratory tests of block toppling. *International Journal of Rock Mechanics and Mining Sciences*. 34(3-4): 173.

Li, S.H., Wang, J.G., Liu, B.S. & Dong, D.P., 2007. Analysis of critical excavation depth for a jointed rock slope using a Face-to-Face discrete element method. *Rock Mech. Rock Engng.* 40(4): 331-348.

Maugeri, M., Musumeci, G., Novita, D. & Taylor, C.A., 2000. Shaking table test of failure of a shallow foundation subjected to an eccentric load. *Soil Dynamics and Earthquake Engineering*. 20: 435-444.

Pangpetch, P. & Fuenkajorn, K., 2007. Simulation of rock slope failure using physical model. In *Proceedings of the First Thailand Symposium on Rock Mechanics*. Suranaree University of Technology, Nakhon Ratchasima. pp. 227-243.

Richter, C., 1958. *Elementary Seismology*. W.H. Freeman and Co., San Francisco. pp. 136-138.

Riley, W.F. & Sturges, L.D., 1993. *Engineering Mechanics Dynamics*. John Wiley & Sons, Inc. pp. 89-103.

Siad, L., 2003, Seismic stability analysis of fracture rock slopes by yield design theory. *Soil and Earthquake Engineering*. 23: 203-212.

Teme, S.C., 1987. A kinematic modeling machine for rock slope studies. *International Journal of Mining and Geological Engineering*. 5: 75-81.

Terzaghi, K., 1950. Mechanisms of landslides. In *Application of Geology to Engineering Practice. Geol. Soc. of America*, New York, Berkey, pp. 83-123.

Wald, D.A., Quitoriano, V., Heaton, T.H. & Kanamori, H., 1999. Relationships between peak ground acceleration, peak ground velocity, and modified Mercalli intensity in California. *Earthquake Spectra*. 15: 557-564.

BIOGRAPHY

Mr. Pongsak Pangpetch was born on February 4, 1982 in Chiangrai province, Thailand. He received his Bachelor's Degree in Engineering (Geotechnology) from Suranaree University of Technology in 2006. For his post-graduate, he continued to study with a Master's degree in the Geological Engineering Program, Institute of Engineering, Suranaree university of Technology. During graduation, 2006-2009, he was a part time worker in position of research assistant at the Geomechanics Research Unit, Institute of Engineering, Suranaree University of Technology. He has published four technical papers related to rock mechanics as; In 2007, *"Simulation of Rock Slope Failure using Physical Model"* in the proceeding of the first Thailand symposium on rock mechanics, Nakhon Ratchasima, Thailand. In 2008, *"Simulation of Plane Sliding and Toppling Failure using Scaled-Down Rock Slope Models"* in research and development journal of the engineering institute of Thailand, Vol. 19, No. 3. And in 2009, he has published two technical papers as *"Simulation of Dynamic Loading on Rock Slope Stability on Rock Slope Stability using Physical Model"* in EIT-JSCE joint international symposium monitoring and modelling in geo-engineering. Bangkok, Thailand and *"Physical Model Simulation of Jointed Rock Slopes under Dynamic Loads"* in the proceeding of the second Thailand symposium on rock mechanics. Chonburi, Thailand. For his work, he is a good knowledge in geomechanics theory and practice.